Study on homodimer of glucocorticoid receptor and transcriptional regulation in single-cell level using fluorescence correlation spectroscopy and microwells.

（蛍光相関分光法とマイクロウェルを用いた
シングルセルにおけるグルココルチコイド
受容体の二量体と転写制御に関する研究）

Sho Oasa

（大浅　翔）

A dissertation for the degree of

Doctor of Life Science

Hokkaido University

March, 2016

Contents

Abbreviations

APD: Avalanche Photodiode

CPP: Counts per particle

Dex: Dexamethasone

EGFP: Enhanced green fluorescent protein

ESS: Equivalent-single-cell lysate solution

FCS: Fluorescence correlation spectroscopy

FCCS: Fluorescence cross-correlation spectroscopy

GR: Glucocorticoid receptor

hGRE: half glucocorticoid response element

HRP: Horseradish peroxidase

IpGRE: Imperfect palindrome glucocorticoid response element

LSM: Laser scanning microscopy

LRS: Lowest relative standard deviation

mKO2: monomeric Kusabira-Orange 2

OAD: One-component anomalous diffusion fitting

OND: One-component normal diffusion fitting

PDMS: Polydimethylsiloxane

PpGRE: Perfect palindrome glucocorticoid response element

R6G: Rhodamine 6G

SDS: Sodium Dodecyl Sulfate

TagRFP675: Tag red fluorescent protein 675

TND: Two-component normal diffusion fitting

Chapter 1

Introduction

1.1 Glucocorticoid receptor α

The human glucocortiocid receptor α (GR) is a ligand-induced transcription factors which belongs to a nuclear receptor superfamily that relates with several processes such as immune response and metabolism [1, 2]. The GR possesses three main domains, transactiavtion domain at N-terminal region, DNA-binding domain (DBD) at central region and ligand-binding domain (LBD) at C-terminal region (Fig. 1-1). The N-terminal region contains the activation function-1 (AF-1) motif which relates with the basal transcriptional machinery via modifications such as phosphorylation. The DBD have two zinc finger motifs and is essential domain for homodimerization as well as DNA binding. The C-terminal region contains the LBD, a nuclear localization signal (NLS) and an activation function-2 (AF-2) which interacts with cofactors [3-5].

Unliganded GR predominantly localizes in the cytoplasm as complexes with molecular chaperones. The molecular chaperones maintain the conformation of LBD for high affinity of ligand [6-8]. The ligand binding induces dissociation of chaperoning complex and then, translocation into the nucleus (Fig. 1-2). In the nucleus, the activated GR regulates specifically transcription of target genes by monomeric and homodimeric mechanisms [9-12]. A direct binding of GR to glucocorticoid response element (GRE) induces specifically transactiavtion and transrepression of target genes (Fig. 1-2 A and B) [13, 14]. In contrast, the activated GR have also functions to regulate transcription of target gene through an indirect binding of monomers to other transcription factors, such as NF-κB [15]. Therefore, the

activated GR monomer modulates the transcriptional activity of other transcription factors without a direct binding to DNA (Fig. 1-2 C).

X-ray crystallography analysis indicated that two DNA-binding domains homodimerize on the palindromic GRE [16]. Moreover, the homodimer of GR have a higher affinity to palindromic GRE than monomeric GR [17]. Therefore, these previous reports suggested that GR homodimerization is essential process for transactivation of target genes. However, there are no correlation between homodimerization of GR and transcriptional activity using Number and Brightness analysis and quantitative real-time PCR of bulk measurement [18]. The quantitative relationship between homodimer formation and transcriptional activity of target genes is still unclear. In this thesis, I describe the quantitative relationship between the concentration of homodimeric GR and transcriptional activity in single-cell level using a combination method of fluorescence correlation spectroscopy (FCS) and polydimethylsiloxane (PDMS) chip of microwells (FCS-microwell system).

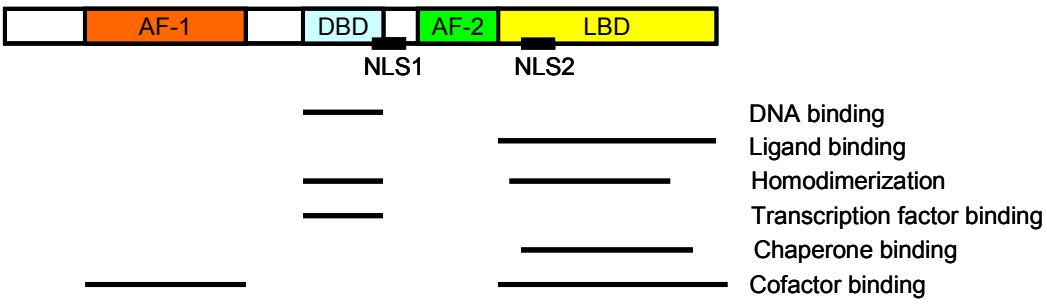

Fig. 1-1 Schematic drawing of the domains of human glucocorticoid receptor α (GR)

Full length of GR was composed by 777 amino acid residues. The each domain of GR is shown as following: activation function-1 (AF-1), DNA-binding domain (DBD), ligand binding domain (LBD), activation function-2 (AF-2) and two nuclear localization signals (NLS1 and NLS2). The functions of each domain are shown in the diagram.

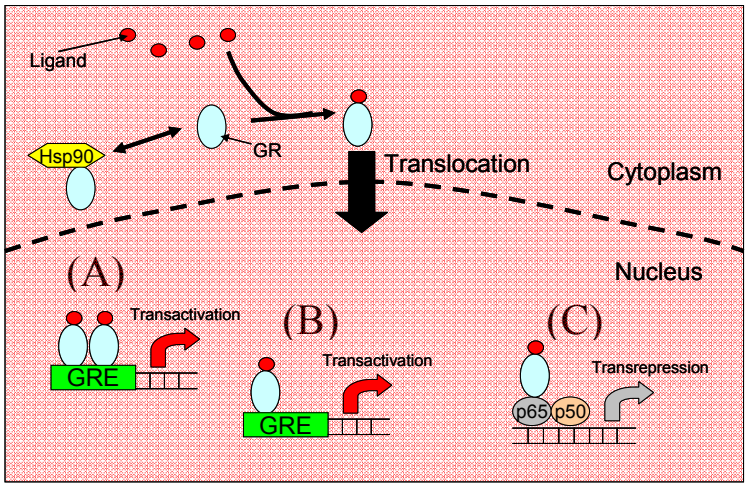

Fig. 1-2 Schematic diagram of transcriptional regulation by GR

GR localizes in the cytoplasm without ligand activation. After ligand binding, GR translocates into nucleus. The activated GR regulates transactivation and transrepression by some pathways: **(A)** Transactivation by homodimeric GR, **(B)** Transactivation by monomeric GR, **(C)** Transrepression through an interaction of GR to other transcription factor, such as NF-κB

1.2 Fluorescence correlation spectroscopy

Fluorescence correlation spectroscopy (FCS) is a method based on an observation of fluorescent-intensity fluctuation which is the result of fluorescent-molecule diffusion in and out of observation area (Fig. 1-3). The autocorrelation function ($G(\tau)$) was calculated from a fluorescent-intensity fluctuation. This autocorrelation function gives two important parameters, number of molecules (N) and diffusion time (τ_D) in observation area [19, 20]. The concentration and diffusion constant of fluorescently-labeled particles were calculated from these parameters. FCS technique can be applied to determine the absolute concentration and the molecular weight and size of fluorescent particles. Therefore, there are many applications to investigate molecular interactions *in vitro* and in living cells [21-23]. Moreover, the particle brightness which calculated by division of average fluorescent intensity to number of molecules is affected by homooligomeric state of fluorescently-labeled particles, such as

homodimer. Therefore, FCS revealed the homooligomeric and heterooligomeric state of fluorescently-labeled proteins from particle brightness and diffusion time, respectively [24].

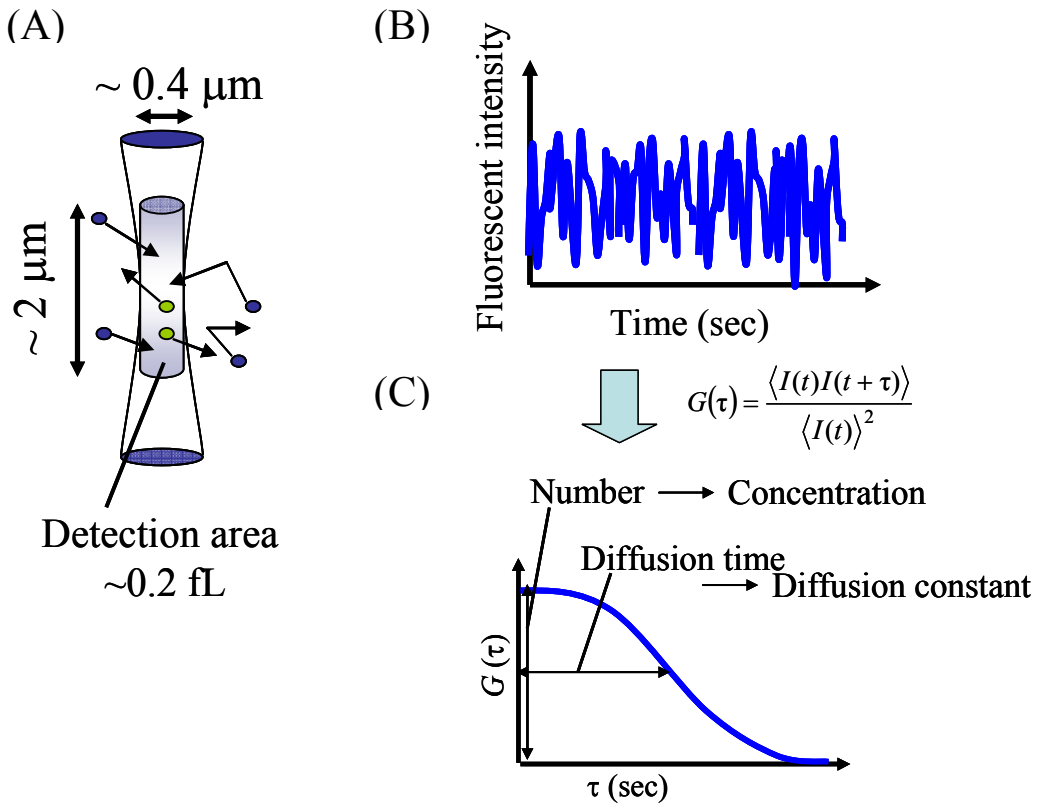

Fig. 1-3 Schematic diagram of FCS

(A) Schematic diagram of observation area of FCS. **(B)** Fluctuation of fluorescence intensity over time. **(C)** Autocorrelation function ($G(\tau)$)

1.3 Bulk measurement and single-cell measurement

The protein expression level and protein states have quantified using biochemical methods, such as electrophoresis and enzyme-linked immuno-sorbent assay (ELISA) (Fig. 1-4 A). However, these methods only quantified the average information from several cells. For GR study, the expression level, homodimerization and transcriptional activity are averaged by number of cells (Fig. 1-4 B). The homodimerization of GR and transcriptional activity are heterogenous between single cells with different expression level of GR. Therefore,

single-cell method is needed to determine the relationship between the amount of homodimeric GR and transcriptional activity without any average processes.

The microwell system can achieve the single-cell measurement. The poydimethylsiloxane (PDMS) chip of microwells is 60 μm in diameter and 40 μm in depth with a volume of 113 pL (Fig. 1-5). The microwell provides a stable condition for isolating protein molecules extracted from single cell [25]. There are no fluid exchange between individual microwells without any insulation material used at the interface between the coverslip and the microwells.

In this thesis, FCS was combined with mcirowell system toward single-cell measurements (FCS-microwell system). FCS-microwell system was used to determine the concentration of enhanced green fluorescent protein (EGFP)-fused glucocorticoid receptor (EGFP-GR) and fluorescent reporter for transcriptional activity in single-cell level. In chapter 2, the feasibility of FCS-microwell system was confirmed. In chapter 3 and 4, the dissociation constant for homodimerization of EGFP-GR was determined. In chapter 5, the relationship between the concentration of homodimeric EGFP-GR and transcriptional activity was determined.

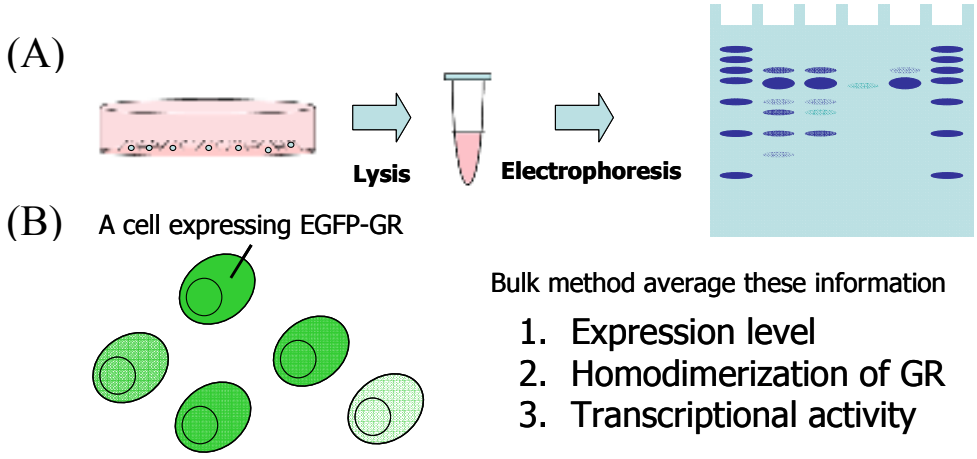

Fig. 1-5 Conventional protein quantification using bulk measurement

(A) Schematic diagram of bulk measurement **(B)** The bulk measurement average the single-cell information.

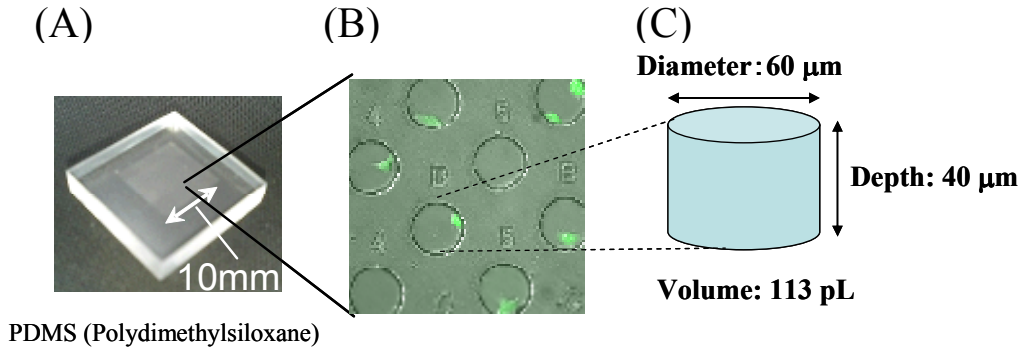

Fig. 1-5 Microwells

(A) An overview of PDMS chip **(B)** An enlagerd image of microwells on PDMS chip. EGFP-expressing cells were cultured in microwells. **(C)** A size of microwells.

1.4 Fluorescence cross-correlation spectroscopy

Dual color fluorescence cross-correlation spectroscopy (FCCS), which is the extension of FCS is a powerful technique to determine the molecular interaction between two species labeled by two spectrally distinct fluorescent molecules [26-28]. FCCS can detect the coincidence of two different-color fluorescent molecules in an observation area (Fig. 1-6). FCCS is used widely to determine the dissociation constant of protein-protein or protein-DNA interaction *in vitro* and *in vivo* [29, 30].

In this thesis, FCCS was used to determine the dissociation constant for homodimerization of GR in chapter 4 and the dissociation constant between EGFP-GR and Alexa647-labeled GRE in the chapter 5.

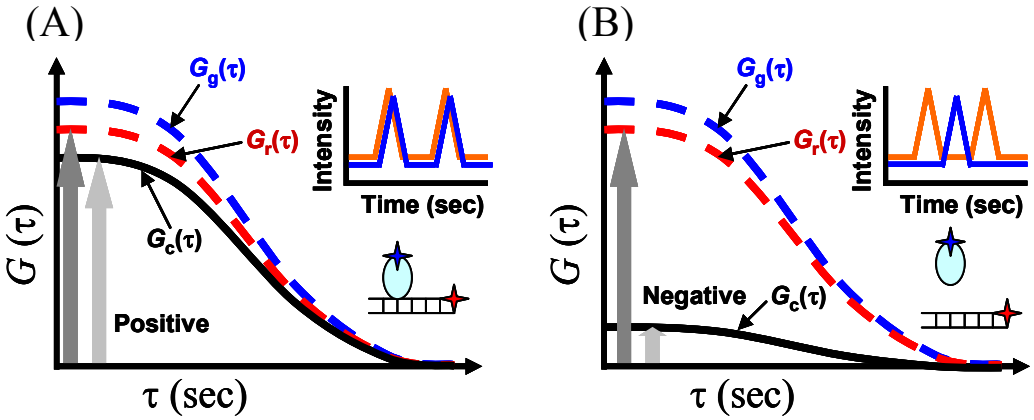

Fig. 1-6 Schematic drawing of FCCS

A positive cross-correlation function ($G_c(\tau)$: Black solid line) is observed **(A)** or not observed **(B)** with or without binding of target molecules labeled by two-color fluorescent molecules. $G_g(\tau)$: autocorrelation function of green channel (Blue dashed line), $G_r(\tau)$: autocorrelation function of red channel (Red dashed line), respectively.

Chapter 2

The feasibility of FCS-microwell system toward single-cell measurements

2.1 Introduction

Fluorescence correlation spectroscopy (FCS) is a powerful technique to determine the absolute concentration of fluorescent molecules [19, 20]. Moreover, the microwell system provides a stable condition for isolating proteins from single cell [25]. The FCS-microwell system, in which FCS and microwell system is combined, is useful tool to determine the concentration of fluorescently-labeled proteins from single cell [24]. The most common fluorescent protein for FCS is enhanced green fluorescent protein (EGFP) *in vitro* and *in vivo*. However, the feasibility of FCS-microwell system is unknown.

In this chapter, to verify the feasibility of FCS-microwell system, two kinds of experiments was performed. First of all, EGFP dilution system was measured using FCS-microwell system to show the lower limit for determination of the EGFP concentration. Second, the cell volume of EGFP-expressing cells was quantified by FCS-micrwell sytem and Z-stack image method, and compared between both methods to confirm complete lysis of the single cell in microwells and that there was no leakage from the microwell system.

2.2 Materials and methods

2.2.1 Chemicals

The components of the lysis buffer were 80% Celytic M Cell Lysis Reagent (Sigma-Aldrich), 1% Protease inhibitor cocktail (Sigma-Aldrich), 10 mM $MgCl_2$, 0.1% SDS, and 200 U/mL Benzonase nuclease (Sigma-Aldrich).

2.2.2 Single-cell method combining FCS and microwells

The microwells were 60 μm in diameter and 40 μm in depth with a volume of 113 pL. Each microwell was denoted by a number and a letter to determine the positions of microwells of interest and find them easily after biological treatment such as a ligand for GR. The polydimethylsiloxane (PDMS) chip with microwells was originally designed and ordered to Fluidware Technologies Inc., Tokyo, Japan. The microwells and coverslips (No. S1: Matsunami Glass, Tokyo, Japan) were treated with N101 blocking reagent (Nippon Oil and Fats, Tokyo, Japan) to prevent adsorption of proteins.

Schematic diagrams of the FCS-microwell system are shown in Fig. 2-1. The PDMS chip was attached to a glass stick with double-sided tape (Nitoms, Tokyo, Japan) and the chip was pressed onto a coverslip in opti-MEM (Fig. 2-1 A, left). After pressing the PDMS chip onto the coverslip, the position (a number and a letter) of the microwells in which single cell was cultured were noted down (Fig. 2-1 A, right). The medium on the coverslip was changed to lysis buffer and the protein extracted from each cell was kept in the microwell after cell lysis, following which FCS measurements were carried out in each microwell (Fig. 2-1 B, right).

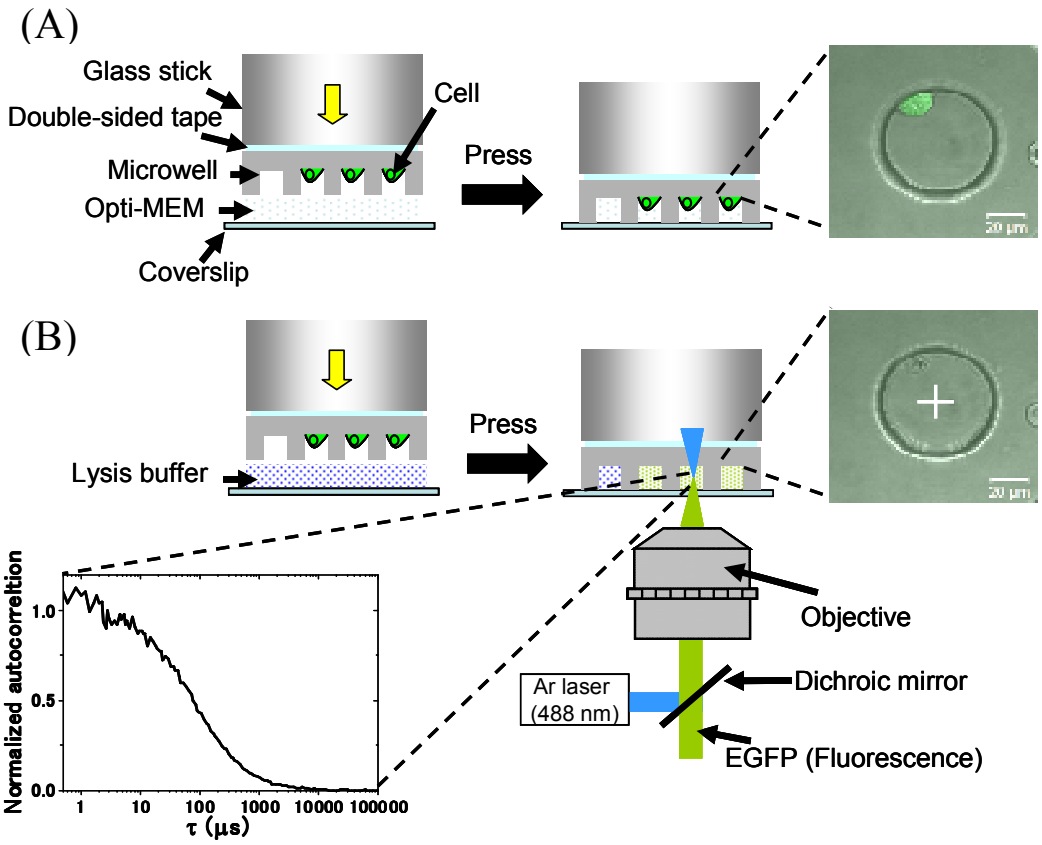

Fig. 2-1 Schematic diagram of FCS-microwell system.

(A) Schematic diagram of the single-cell isolation and an isolated single cell in a microwell.

(B) The lysis step for single cell and FCS measurements (Scale bar: 20 μm).

2.2.3 Cell culture and transfection in microwells

HeLa cells were cultured in Dulbecco's Modified Eagle's Medium (DMEM, Sigma-Aldrich) supplemented with 10% fetal bovine serum (FBS) at 37°C with 5% CO_2. To culture the HeLa cells, the microwells on the PDMS chips were washed using a detergent water, which were then evaporated in a glass vacuum dryer to remove the water from the microwells. After evaporation, the cell culture medium containing the HeLa cell suspension

was poured onto the PDMS chip in a 60 mm dish and incubated for 4 hours at 37^{O}C.

HeLa cells on 35 mm dishes were transfected using Optifect reagent (Invitrogen). After replacement of the culture medium on dishes with fresh medium, 0.1 μg of plasmid-encoded EGFP was mixed with 1.5 μL Optifect in opti-MEM and added to the cell culture dishes. After 24 hours incubation at 37^{O}C with 5% CO_2, the transfected HeLa cells were trypsinized and transferred to the microwells on the PDMS chips.

2.2.4 LSM imaging and FCS measurements

LSM imaging and FCS measurements were performed using an LSM510-ConfoCor2 (Carl Zeiss, Jena, Germany) equipped with an Ar ion laser, water immersion objective (C-Apochromat, 40X, 1.2 N.A., Corr; Carl Zeiss, Jena, Germany), a photomultiplier for LSM imaging and an avalanche photodiode detector (APD) for FCS measurements (Fig. 2-2). The pinhole diameter was adjusted to 70 μm, EGFP was exicited at 488 nm and the EGFP fluorescent signals were detected above 505 nm for LSM imaging and at 505-550 nm for FCS measurements. FCS measurements were carried out five times for 10 seconds.

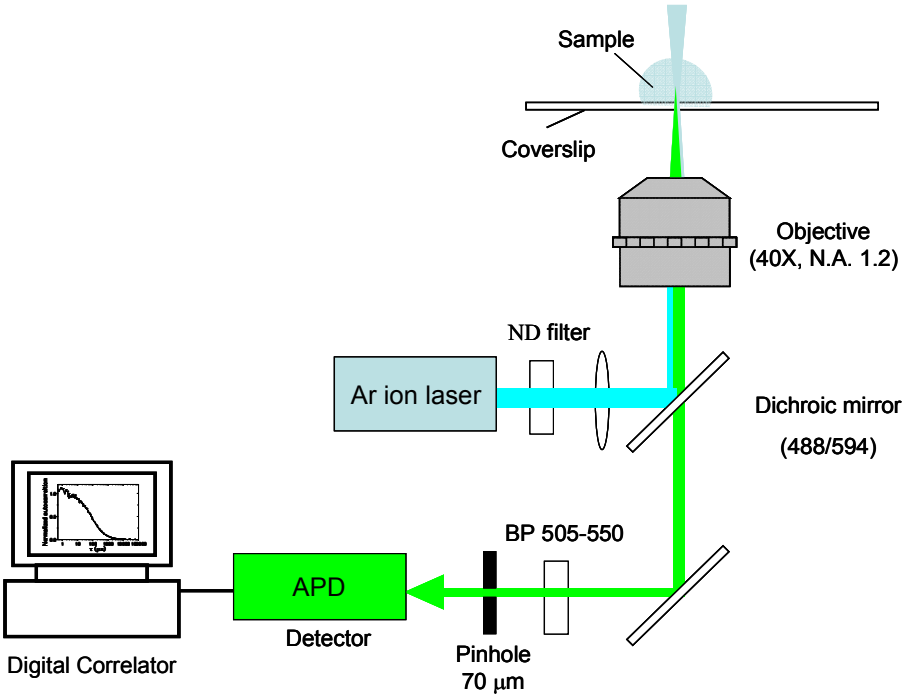

Fig. 2-2 Optical setup for FCS

The Ar ion laser (488 nm) was used for the excitation of EGFP. The fluorescence passed through the band pass filter of 505-550 nm and 70 μm pinhole for EGFP. The avalanche photodiode detector was connected to the digital correlator.

2.2.5 Data analysis of FCS measurements

Data obtained from FCS measurements were calculated with AIM software (Carl Zeiss, Jena, Germany). The autocorrelation function, $G(\tau)$ was defined as follows:

$$G(\tau) = \frac{\langle I(t)I(t+\tau)\rangle}{\langle I(t)\rangle^2} \qquad \text{- (2-1)}$$

where τ shows the delay time, I is fluorescent intensity and $G(\tau)$ denotes the autocorrelation function, respectively. The obtained autocorrelation functions were fitted using a one-component model as follows:

$$G(\tau) = 1 + \left(1 + \frac{F_{\text{triplet}} e^{-\frac{\tau}{\tau_{\text{triplet}}}}}{1 - F_{\text{triplet}}}\right) \cdot \frac{1}{N}\left(1 + \frac{\tau}{\tau_D}\right)^{-1} \cdot \left(1 + \frac{1}{s^2}\frac{\tau}{\tau_D}\right)^{-\frac{1}{2}} \quad \text{- (2-2)}$$

where F_{triplet} is the average fraction of triplet state molecules, τ_{triplet} is the average relaxation time and τ_D is the average diffusion time of molecules. The diffusion constant of molecules was calculated from the diffusion constant of a standard molecule, rhodamine 6G (D_{R6G}; 414 $\mu m^2/s$) [31] and the ratio of diffusion times τ_{R6G} and τ_D. N is the average number of fluorescent molecules in the effective observation volume (V_{eff}) defined by 3D Gaussian volume elements with lateral radius w_0 and axial radius z_0. s shows the structure parameter representing the ratio of w_0 to z_0 ($s = z_0/w_0$). w_0 and z_0 were determined by calibration measurement of R6G.

$$w_0 = \sqrt{4 D_{\text{R6G}} \cdot \tau_{\text{R6G}}} \quad \text{-(2-3)}$$

$$s = \frac{z_0}{w_0} \quad \text{-(2-4)}$$

The effective observation volume was calculated using the following equation.

$$V_{\text{eff}} = \pi^{\frac{3}{2}} \cdot w_0^2 \cdot z_0 \quad \text{-(2-5)}$$

The fitting models of a one-component with normal or anomalous diffusion and two-component with normal diffusion for FCS measurement in the cells that expressed EGFP were compared (Fig. 2-3). There were no significant differences in the chi square values between the autocorrelation function and fitting curves and number of molecules, even if EGFP was present in the cell. Moreover, the number of molecules (N) was not different in the models and this indicates estimated dissociation constant is the same among these models. Therefore, the fitting model of a one-component with normal diffusion was selected for fitting to all data. To remove the effect of background fluorescence on the obtained N_{meas}, the

corrected N (N_{corr}) was calculated as follows [32, 33]:

$$N_{corr} = \frac{N_{meas} \cdot (I_{meas} - I_B)^2}{(I_{meas})^2} \quad \text{-(2-6)}$$

Where N_{meas} is the number of molecules obtained from FCS measurements, I_{meas} is the measured average fluorescent intensity and I_B is the background average fluorescent intensity from FCS measurement of a non-transfected HeLa cell lysate.

The concentration of fluorescent molecules ([C_{corr}]) was calculated from the effective observation volume (V_{eff}), corrected number of molecules (N_{corr}) and Avogadro's number (N_A) as given below.

$$[C_{corr}] = \frac{N_{corr}}{V_{eff} \cdot N_A} \quad \text{-(2-7)}$$

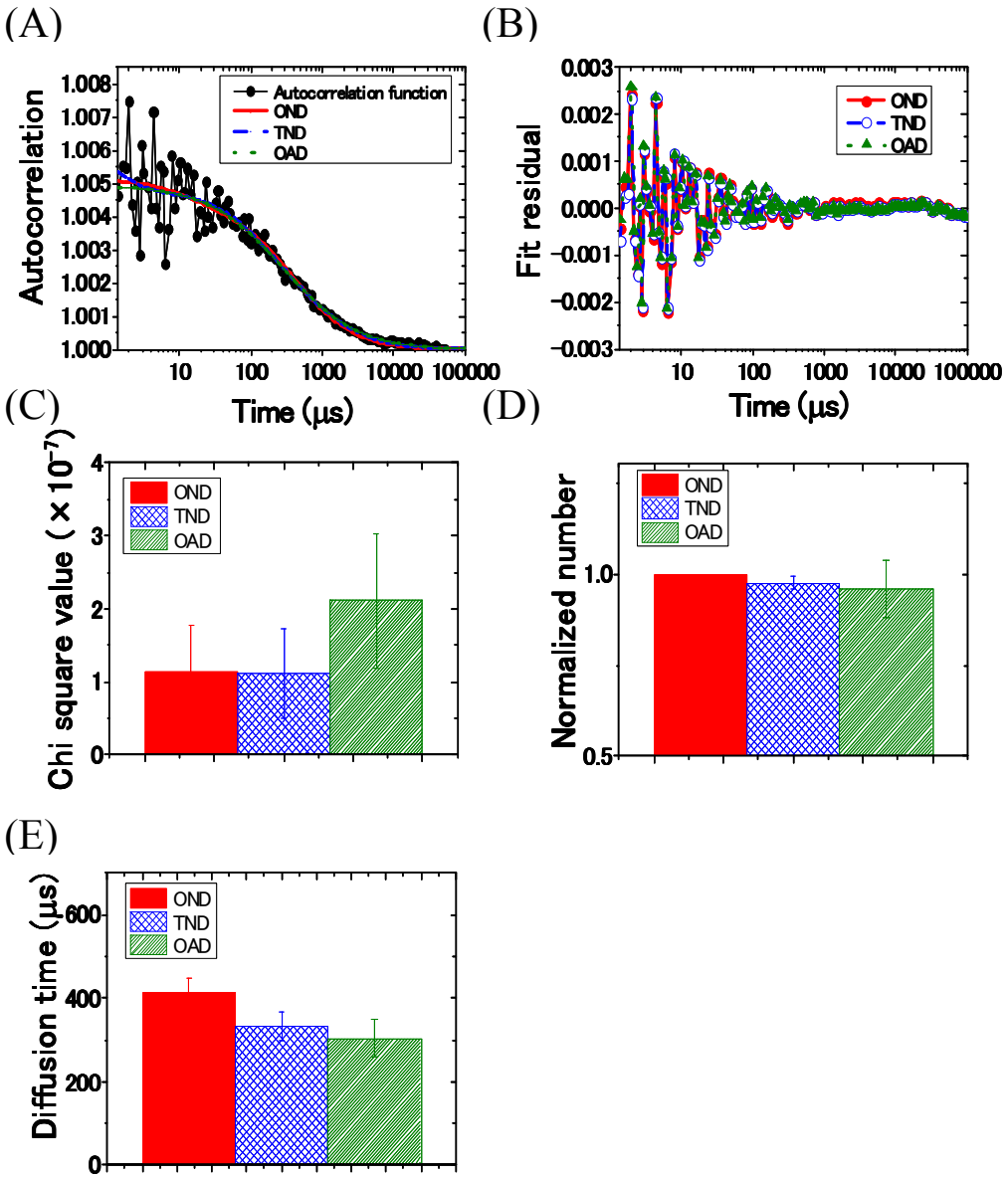

Fig. 2-3 Comparison of fitting models to cellular EGFP measurement

The fitting models between one-component with normal diffusion (OND), two-component with normal diffusion (TND) and one-component with anomalous diffusion (OAD) were compared in EGFP measurement in living HeLa cells. **(A)** Typical autocorrelation function and fitting curves. Black plots: Autocorrelation function, Red line: Fitting curve of OND, Blue dashed line: Fitting curve of TND, Green dotted line: Fitting curve of OAD. **(B)** Fit residuals. Red line with filled circle: Fitting curve of OND, Blue dashed line with open circle:

Fitting curve of TND, Green dotted line with filled triangle: Fitting curve of OAD. **(C)** The chi square value of the autocorrelation function and fitting curves. **(D)** The number of molecules. **(E)** The diffusion time. The diffusion time of the first component is shown for TND because almost all fractions were in the first component (above 90%). The data number was 3 for calculation of the average value and standard deviation of each fitting model. Fitted red bar: OND, Meshed blue bar: TND, Shaded green bar: OAD.

2.2.6 Determination of the lower limit of the EGFP concentration by FCS

EGFP was expressed in Escherichia coli (BL21 [DE3]) and purified using a Ni affinity column (GE healthcare). An equivalent-single-cell-lysate solution (ESS), defined as which contained the same concentration of endogenous protein extracted from a single cell in a microwell (single cell in 113 pL), was prepared to measure the background fluorescence. The number of cells was estimated using a cell counter, and then the volume of the lysis buffer was calculated by multiplying of number of cells by the microwell volume (113 pL).

EGFP diluted with ESS was measured by FCS in three microwells and the counts per particle (CPP) in which the average fluorescent intensity was divided by the number of molecules (*N*), were obtained for different concentrations of EGFP. For the same laser intensity, the average number of molecules and the average fluorescent intensity are linearly related. Therefore, the measured CPP should be constant if the fluorescent intensity and the number of EGFP molecules are correctly determined. The CPP value with the lowest relative standard deviation (LRS) determined from five independent measurements yielded an expected CPP_{LRS} value of 8.71 kHz (blue dashed line in Fig. 2-5 A). The total deviation between CPP_{LRS} and measured CPP value (X^2) was calculated for each EGFP concentration according to the following equation:

$$X_j^2 = \sum_{i=1}^{5} \frac{(\mathrm{CPP_{LRS}} - CPP_{j,i})^2}{\mathrm{CPP_{LRS}}} \qquad \text{-(2-8)}$$

where i = 1 - 5 denotes independent measurements for the same concentration (j). Hence, X^2 shows the sum of the squared deviation normalized to CPP_{LRS}. If the total deviation between CPP_{LRS} and the measured CPP value (X^2) is smaller than 9.488 (P = 0.05 and the degree-of-freedom = 4), the average CPP value is statistically similar to CPP_{LRS} (Fig. 2-5 B). The statistically similar point at the lowest concentration of EGFP was defined as the lower limit for determination of the EGFP concentration (Fig. 2-5C).

2.2.7 Comparison of cell volume measurements between the Z-stack imaging method and FCS-microwell system

To confirm whether the extracted EGFP was conserved in the microwells, the cell volumes calculated from the Z-stack image of LSM ($V_{cell\text{-}z}$) and FCS-microwell system ($V_{cell\text{-}F}$) were compared. An optical slice of 512×512 pixels in the Z-stack image was acquired. The fluorescence-detected voxel number in the Z-stack image was counted using Image J software (NIH) and the cell volume from Z-stack image ($V_{cell\text{-}Z}$) was calculated by multiplying the voxel number by the size (0.2 μm×0.2 μm×0.87 μm) used in the objective (C-Apochromat, 40X, 1.2N.A., Corr).

Moreover, cell volume could be calculated using the FCS-microwell system. If the EGFP-containing lysate remains in the microwell after cell lysis, the total concentration of EGFP in the single cell before lysis and that in the microwell after lysis can be represented by the following equation.

$$[C_{cell,corr}] \cdot V_{cell\text{-}F} = [C_{m,corr}] \cdot V_m \qquad \text{-(2-9)}$$

where $V_{cell\text{-}Z}$ and V_m are the volumes of the cell from the FCS-microwell system and

microwell (113 pL), respectively. The EGFP concentration at the inside of the cell before lysis ([$C_{cell,corr}$]) and that in the microwell after lysis ($C_{m,corr}$) were obtained by FCS measurement at the inside of the HeLa cell before cell lysis and in the microwell after cell lysis in the same microwell, respectively. The cell volume was calculated using the following equation:

$$V_{\text{cell-F}} = \frac{\left[C_{\text{m, corr}}\right] \cdot \text{Vm}}{\left[C_{\text{cell, corr}}\right]} \qquad \text{-(2-10)}$$

2.3 Results

2.3.1 Lower limit for determination of EGFP concentration

Toward quantification of the number of EGFP-tagged target proteins in single-cell level, FCS measurements were performed with equivalent-single-cell lysate solution (ESS)-diluted EGFP in the microwell for a determination of the lower limit of the EGFP concentration. FCS measurements were performed in three microwells and similar autocorrelation functions and fit residuals were obtained for all three (Fig. 2-4).

To clarify the lower limit for determination of the EGFP concentration, counts per particle (CPP_{EGFP}) was calculated, because CPP_{EGFP} should be constant when the EGFP fluorescent intensity and number of molecules are measured correctly. Without background correction, the CPP_{EGFP} was reduced with the decrease of EGFP concentration (Fig. 2-5 A). In contrast, the CPP_{EGFP} was constant until the concentration of 0.17 nM with background correction. The total deviation between CPP_{LRS} (8.71 kHz) and the measured CPP (X^2 in equation (2-8)) was calculated for each concentration (Fig. 2-5 B). When the total deviation was lower than the dashed blue line (9.488; P = 0.05 and degree-of-freedom = 4), CPP_{EGFP} was similar to CPP_{LRS} (Fig. 2-5 A). The lower limits of the concentrations of EGFP without and with background correction were 2.5 nM and 0.17 nM, respectively, as shown by the black arrows in Fig. 2-5 C. These results indicated that the EGFP concentration from 0.17 to 1741 nM could be quantified by using the FCS-microwell system with background correction.

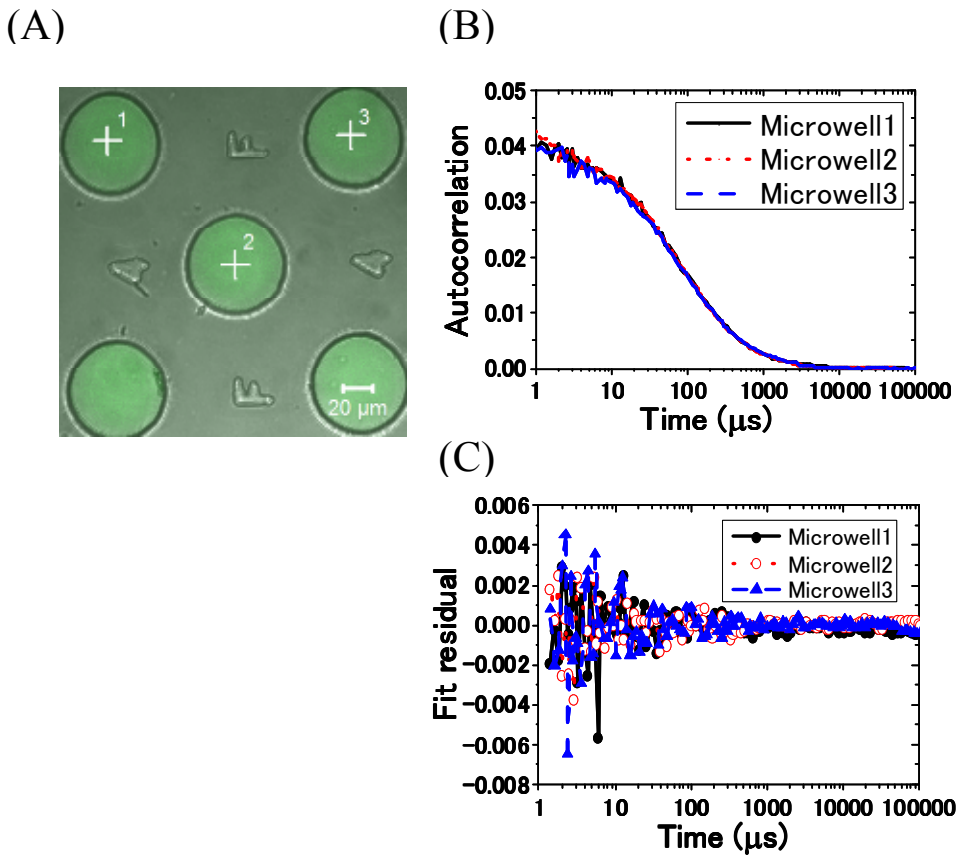

Fig. 2-4 FCS measurement of EGFP solution in microwell

(A) Fluorescent image of microwells with 200 nM recombinant EGFP. White cross: FCS measurement point. (Scale bar: 20 μm) **(B, C)** Autocorrelation function and fit residuals at position 1, 2 and 3 in the fluorescent image. Black solid line: microwell 1, Red dotted line: microwell 2, Blue dashed line: microwell 3.

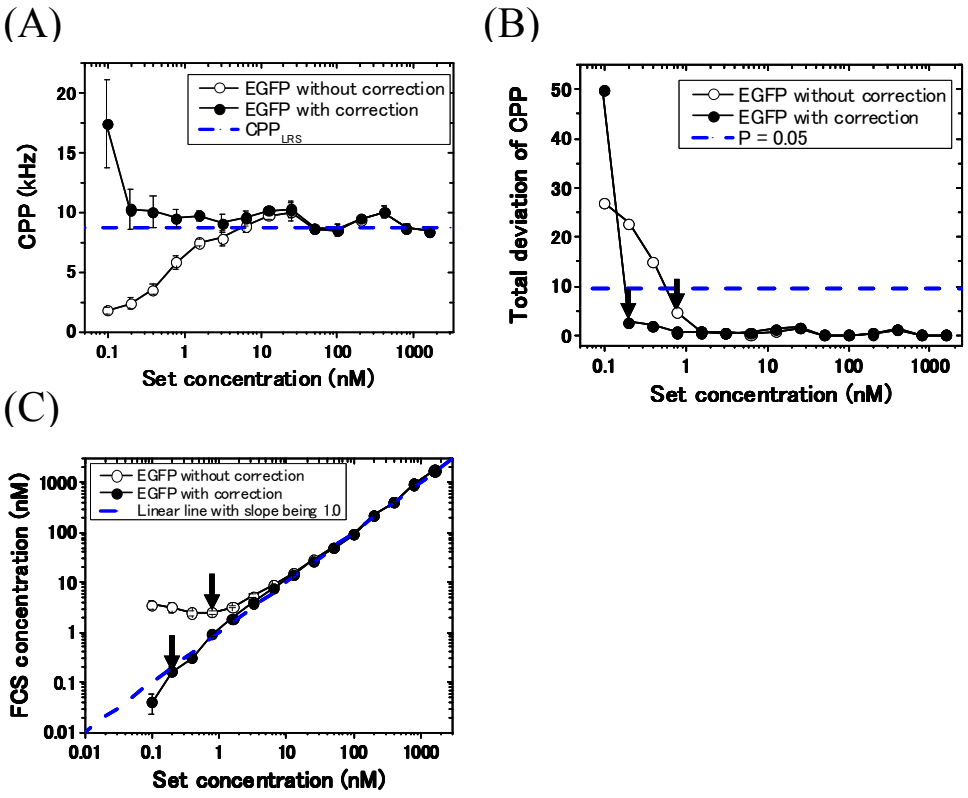

Fig. 2-5 Lower limit for determination of the EGFP concentration

(A) CPP with and without background correction of FCS-obtained data at each concentration. The average value and standard deviation were calculated from five measurements. Open symbol: Without background correction, Filled symbol: With background correction, Blue dashed line: CPP_{LRS} (8.71 kHz). **(B)** Total deviation of CPP between 5 data determinations and CPP_{LRS} in (B) at each concentration. Open symbol: Without background correction, Filled symbol: With background correction, Blue dashed line (9.488): P = 0.05 and degree-of-freedom = 4, Black arrow: Lower limit for determination of EGFP concentration. **(C)** FCS-obtained EGFP concentration at each concentration. The average value and standard deviation were calculated from five measurements. Open symbol: Without background correction, Filled symbol: With background correction, Blue dashed line: Linear line with slope being 1.0, Black arrow: Lower limit for determination of EGFP concentrations: 2.5 nM and 0.17 nM without and with background correction, respectively.

2.3.2 Comparison of cell volume between FCS-microwell system and Z-stack image method

The cell volumes obtained from Z-stack image and the FCS-microwell system were compared. Typical images of an EGFP-experssing HeLa cell are shown in Fig. 2-6 A, and autocorrelation functions and fit residuals before and after cell lysis in Fig. 2-6 B. Scatter plots were obtained and linear fitting with Deming regression (Y = 1.2X - 0.7; Slope; 1.2±0.3, Intercept; -0.7±1.2) was performed for all single-cell data obtained from Z-stack image method and the FCS-microwell system method (Fig. 2-7). The cell volumes calculated by both methods agreed well with each other because the plot was on a line with a slope of almost 1.0. This indicated complete lysis of the cell in microwells and that there was no leakage from the microwell system as well as that the concentration of EGFP in the microwells after lysis could be determined correctly.

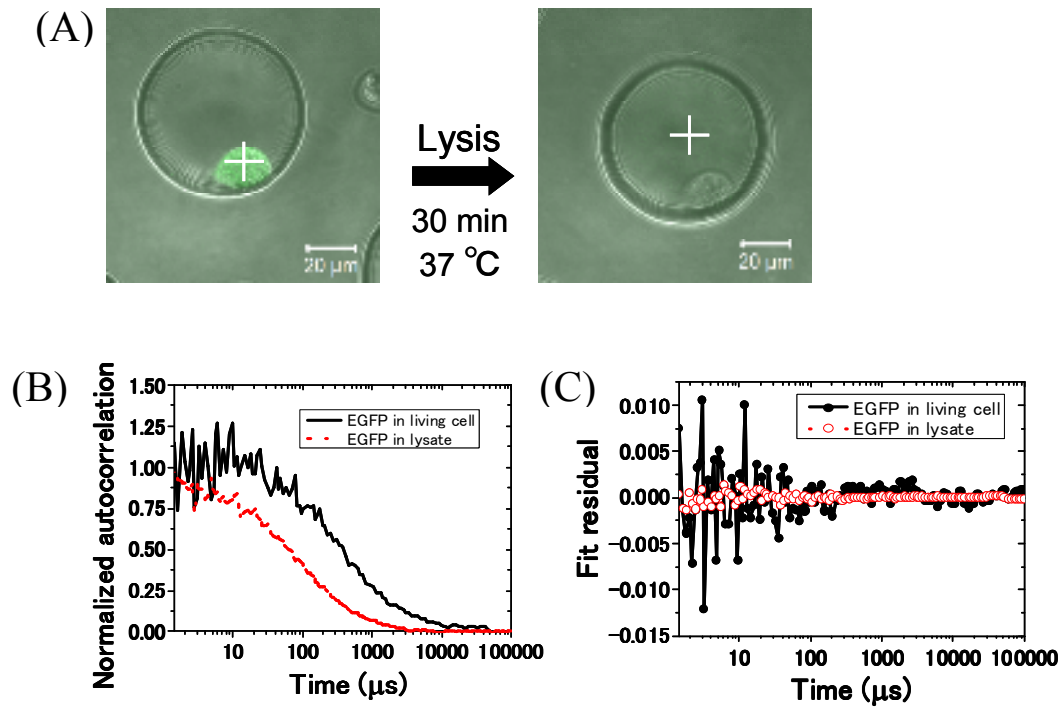

Fig. 2-6 Typical FCS data for a calculation of cell volume

(A) Typical images of EGFP-expressing single cell in microwell before and after cell lysis. White cross: FCS measurement position (Scale bar, 20 μm). **(B)** Typical autocorrelation functions and fit residuals determined by FCS measurement in living HeLa cell and lysate. Black solid line: EGFP in living cell, Red dotted line: EGFP in lysate.

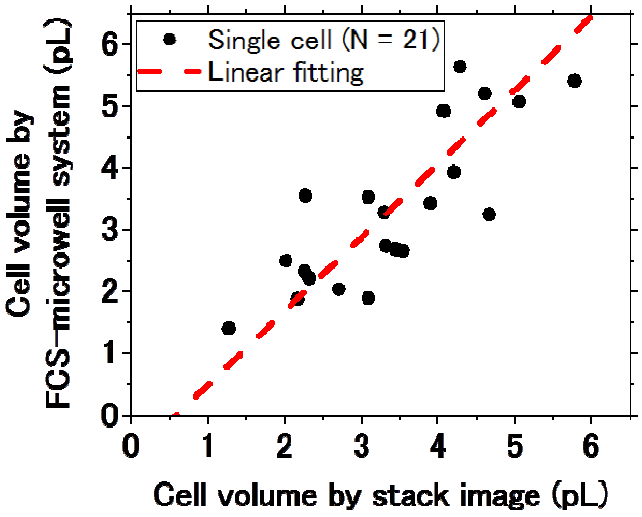

Fig. 2-7 Comparison of cell volume between FCS-microwell system and Z-stack image method

Cell volume determined using the FCS-microwell system ($V_{cell\text{-}F}$) and Z-stack image method ($V_{cell\text{-}Z}$). Data number was 21. Filled symbol: Single-cell data, Red dashed line: Linear fitting with Deming regression: Y = 1.2X - 0.7 (Slope: 1.2±0.3, Intercept: -0.7±1.2)

2.4 Discussion

The aim of this study was to confirm the feasibility of the FCS-microwell system toward single-cell measurement. FCS widely used for protein dynamics fused fluorescent proteins in single living cells [22, 23]. However, the total amount of functional proteins fused fluorescent proteins is difficult to quantify in living cells because of photobleaching of fluorescent proteins and their heterogenous distribution. In contrast, the FCS-microwell system can be used to isolate the cell lysate from single cell and total amount of functional protein can be determined without photobleaching. The quantitative range of the EGFP concentration was from 0.17 nM to 1741 nM with background correction (Fig. 2-5 C). Considered with average cell volume of HeLa cell in Fig. 2-7, FCS-microwell system could quantify the amounts of

functional proteins fused EGFP from 6.4 nM to 65.6 μM concentrations in single cell. However, it should be noted that this limitation was defined under the condition of 5 measurements for 10 seconds and that the excitation with lower laser power may enable the quantification in the higher concentration region above 1741 nM in microwell. Moreover, the cell volume result in Fig. 2-7 indicated that there was no leakage of cell lysate from microwell system after cell lysis. We conclude that FCS-microwell system can employ to determine the concentration of EGFP-fused functional protein from single cell.

Moreover, the cell volumes determined by the Z-stack image method and FCS-microwell system method were in good agreement (Fig. 2-7). The FCS-microwell system is easier to use for estimation of cell volume than the Z-stack image method because only FCS measurements in the cell before cell lysis and in the microwell after cell lysis are required.

Chapter 3

Determination of dissociation constant for homodimerization of glucocorticoid receptor with endogenous expression using FCS-microwell system

3.1 Introduction

The human glucocorticoid receptor α (GR) is a ligand-induced transcription factor which belongs to the nuclear receptor superfamily [1, 2]. It is well-known that liganded GRs homodimerize and transactivate several target genes in the nucleus [9-15]. Therefore, its homodimerization property is important for the control of the GR transactivation. However, the dissociation constant of GR homodimerization remains controversial [34, 35]. One report indicated that the *in vitro* dissociation constant of GR homodimerization was 3.9 nM and concluded that almost all GRs homodimerize in the absence of specific binding to GRE [34]. In contrast, another report indicated that the dissociation constant of GR homodimerization was above 100 μM and that GRs homodimerize on the specific binding to GRE [35].

To address this controversial question, the *in vitro* dissociation constant for homodimerization of GR in single-cell level was determined using FCS-microwell system. Therefore, enhanced green fluorescent protein (EGFP) fused glucocorticoid receptor (GR) was transiently expressed in the cells. The apparent particle brightness of EGFP-GR is

affected by the fraction of monomeric and homodimeric EGFP-GR. The ratio of the homodimer to monomer of EGFP-GR was calculated using the particle brightness obtained by FCS measurement, following which concentration of homodimeric EGFP-GR was calculated. Fitting bimolecular reaction model to the concentration of homodimeric EGFP-GR, the dissociation constant for homodimerization was determined. Moreover, the diffusion constant of EGFP-GR was compared with theoretical value of diffusion constant calculated from molecular weight of EGFP-GR to reveal the complex formation with endogenous interacting proteins.

3.2 Materials and methods

3.2.1 Constructs and chemicals

The expression vectors for enhanced green fluorescent protein (EGFP) fused with wild type of human glucocorticoid receptor α (EGFP-GR) and tandem dimer of EGFP were described previously [36, 37]. A synthetic ligand of GR, dexamethasone (Dex), was purchased from Sigma-Aldrich. Dex was used at a concentration of 0.5 μM in opti-MEM (GIBCO) for activation of GR. The components of the lysis buffer were 80% CelLytic M Cell Lysis Reagent (Sigma-Aldrich), 1% Protease Inhibitor Cocktail (Sigma-Aldrich), 10 mM $MgCl_2$, 0.1% SDS and 200 U/mL Benzonase nuclease (Sigma-Aldrich).

3.2.2 Cell culture and transfection in microwells

HeLa cells were cultured in Dulbecco's Modified Eagle's Medium (DMEM, Sigma-Aldrich) supplemented with 10% fetal bovine serum (FBS) at 37^{o}C with 5% CO_2. After transfection of EGFP-GR, DMEM with charcoal-stripped 10% FBS was used as the culture medium to prevent activation of GR by endogenous ligands in FBS. To culture the HeLa cells, the microwells on the PDMS chips were washed using a detergent water, which

was then evaporated in a glass vacuum dryer to remove the water from the microwells. After evaporation, the cell culture medium containing the HeLa cell suspension was poured onto the PDMS chip in a 60 mm dishes and incubated for 4 hours at 37^{O}C.

The plasmid encoded EGFP, tandem dimer of EGFP or EGFP-GR were transfected to HeLa cells on 35 mm dishes using Optifect reagent (Invitrogen). After replacement of the culture medium on dishes with fresh medium, the plasmid of 0.1 μg of EGFP, 0.1 μg of tandem dimer of EGFP or 3.0 μg of EGFP-GR was mixed with Optifect in opti-MEM and added to the cell culture dishes. After 24 hours incubation at 37^{O}C with 5% CO_2, the transfected HeLa cells were trypsinized and transferred to the microwells on the PDMS chips.

3.2.3 Western blotting analysis for expression level of exogenous EGFP-GR and endogenous GR in HeLa cell

The endogenous GR is expressed in HeLa cells. To estimate the amount of exogenous EGFP-GR and endogenous GR in HeLa cells, western blottings were performed (Fig. 3-3). The transfected HeLa cells were collected by cell scraper with PBS. The EGFP-GR was extracted from HeLa cells by lysis buffer. The cell lysates were centrifuged (15000 rpm at 4^{O} C) for 10 min and the whole cell lysates were collected. The lysates were solubilized with 4X Laemmli sample buffer (NacalaiTesque), heat denatured at 95^{O}C for 5 min, electrophhoresed on 7.5% polyacrylamide precast gel (ePAGEL, ATTO) for 90 min at 20 mA, and then transferred onto a PVDF membrane (Bio-Rad Laboratories, Hercules, CA) at 15V for 150 min on ice. Membranes were blocked 1 hr in 5% skim milk and washed three times in PBST buffer (137 mM NaCl, 2.7 mM KCl, 10 mM Na_2HPO_4, 2 mM KH_2PO_4, pH 7.4 and 0.05% Tween 20) at room temperature. The membranes were blotted incubated with a polyclonal anti-GR antibody (ab3579, abcam) at 4^{O}C overnight in Can Get Signal solution 1 (TOYOBO), subsequently horseradish peroxidase (HRP)-conjugated anti-mouse antibody (Jackson

ImmunoResearch) in Can Get Signal solution 2 (TOYOBO) for 1 hr at room temperature. To identify the amount of α-tubulin in lanes as inner control, the membranes were blotted with anti-α-tubulin antibody (upstate cell signaling solutions) in Can Get Signal solution 1, then HRP-conjugated anti-rabbit antibody (Jackson ImmunoResearch) in Can Get Signal solution 2. After being washed three times with PBST, all blots were visualized with the ECL kit (GE Healthcare) and ImageQuant LAS4000-mini (Fuji film).

The amount ratio of exogenous EGFP-GR and endogenous GR ($R_{\text{EGFP-GR, endoGR}}$) was estimated as follows:

$$R_{\text{EGFP - GR, endoGR}} = \frac{I_{\text{EGFP - GR}}}{I_{\text{endoGR}} \times TE} \qquad \text{-(3-1)}$$

where, $I_{\text{EGFP-GR}}$ is band intensity of EGFP-GR normalized that of α-tubulin, I_{endoGR} is band intensity of endogenous GR normalized that of α-tubulin and TE show the transfection efficiency of EGFP-GR ($TE = 0.34 \pm 0.08$) estimated from LSM images, because EGFP-GR was not expressed in all HeLa cells by transient transfection. All intensities of bands were quantified by ImageJ (NIH).

3.2.4 Single-cell method to detect the homodimer of GR

Schematic diagrams of the FCS-microwell system are shown in Fig. 3-1. The PDMS chip was attached to a glass stick with double-sided tape (Nitoms, Tokyo, Japan), pressed onto a coverslip in dexamethasone (Dex) with opti-MEM and incubated at 37°C for 20 min to activate EGFP-GR (Fig. 3-1 A, left). After 20 min incubation of the PDMS chip, the position (a number and a letter) of the microwells in which single cell was cultured were noted down (Fig. 3-1 A, right). The medium on the coverslip was changed to lysis buffer and the protein extracted from each cell was kept in the microwell after cell lysis, following which FCS measurements were carried out in each microwell (Fig. 3-1 B, right).

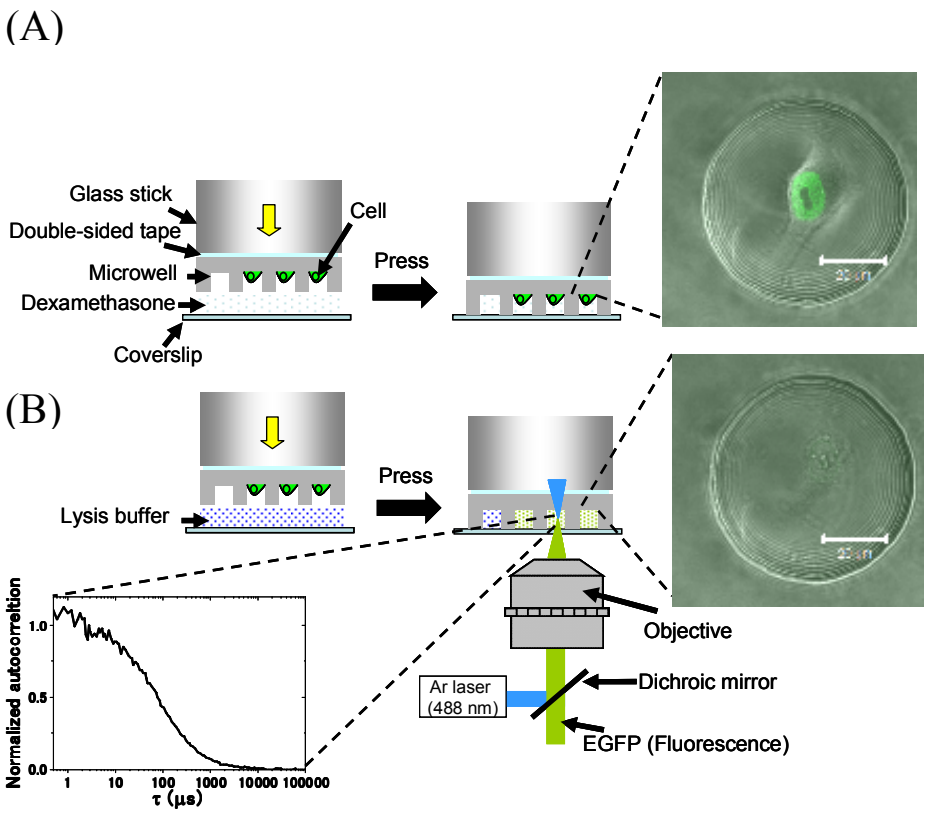

Fig. 3-1 Schematic diagram of FCS-microwell system to detect homodimerization of GR. **(A)** Schematic diagram of the single-cell isolation and 20 min incubation with Dex in a microwell. **(B)** The lysis step for single cell and FCS measurements (Scale bar: 20 μm).

3.2.5 LSM imaging and FCS measurements

LSM imaging and FCS measurements were performed using an LSM510-ConfoCor2 (Carl Zeiss, Jena, Germany) equipped with an Ar ion laser, water immersion objective (C-Apochromat, 40X, 1.2N.A., Corr, Carl Zeiss, Jena, Germany), a photomultiplier for LSM imaging and an avalanche photodiode detector for FCS measurements.

The optical setup for LSM imaging and FCS measurement was same as described at 2. 2. 3 of materials and methods in the chapter 2.

3.2.6 Data analysis and determination of dissociation constant of EGFP-GR in homodimerization

The data analysis of FCS measurements was same as described at 2.2.4 of materials and methods in chapter 2.

The dissociation constant K_d for homodimerization of EGFP-GR was determined using the following equations:

$$[\mathrm{D}] = \frac{K_d + 4[\mathrm{M}_0] - \sqrt{(K_d + 4[\mathrm{M}_0])^2 - 16[\mathrm{M}_0]^2}}{8} \quad \text{-(3-2)}$$

$$[\mathrm{M}_0] = [\mathrm{M}] + 2[\mathrm{D}] \quad \text{-(3-3)}$$

where $[M_0]$ is the total concentration of EGFP-GR in the microwell, and [M] and [D] are the concentration of monomeric and homodimeric EGFP-GR, respectively.

To obtain the [M] and [D], the monomeric fraction F_m and homodimeric fraction F_d (F_m+F_d = 1) of EGFP-GR were calculated using equations (3-4), (3-5) and (3-6) [38]. FCS measurement can be used to obtain the apprarent number of molecules and brightness, which is defined as the counts per particle (CPP). When monomeric and homodimeric EGFP-GR are contained in the lysate, the apparent CPP ($CPP_{\mathrm{EGFP\text{-}GR,app}}$) is obtained as shown by the following equation [38].

$$CPP_{\mathrm{EGFP\text{-}GR,\,app}} = \frac{F_m \cdot \eta_m{}^2 + F_d \cdot \eta_d{}^2}{F_m \cdot \eta_m + F_d \cdot \eta_d} \quad \text{-(3-4)}$$

where η_m and η_d are the CPP of monomeric and homodimeric EGFP-GR, respectively. If the CPP of the tandem dimer of EGFP is twice that of EGFP (Fig. 3-2), the CPP of homodimeric EGFP-GR (η_d) will be twice the CPP of monomeric EGFP-GR (η_m), which is the same as that of EGFP (CPP_{EGFP}).

$$\eta_m = CPP_{\mathrm{EGFP}} \quad \text{-(3-5)}$$

$$\eta_d = 2 \cdot CPP_{\mathrm{EGFP}} \quad \text{-(3-6)}$$

By using equations (3-4), (3-5) and (3-6), the fractions of monomeric and homodimeric EGFP-GR (F_m and F_d) were shown as equations (3-7) and (3-8).

$$Fm = \frac{4 - 2R}{3 - R} \quad \text{-(3-7)}$$

$$Fd = \frac{R - 1}{3 - R} \quad \text{-(3-8)}$$

where,

$$R = \frac{CPP_{\text{EGFP -GR, app}}}{CPP_{\text{EGFP}}} \quad \text{-(3-9)}$$

3.3 Results

3.3.1 Comparison of CPP between EGFP and tandem dimer of EGFP

To confirm the homodimeric EGFP-GR was detected using FCS-microwell system, the CPP of tandem dimer of EGFP was measured. The CPP of the tandem dimer of EGFP (22.9±6.7 kHz) was twice higher than that of EGFP (11.3±1.5 kHz) (Fig. 3-2). This indicated that the CPP of homodimeric EGFP-GR can be shown as twice CPP of EGFP in equation (3-6).

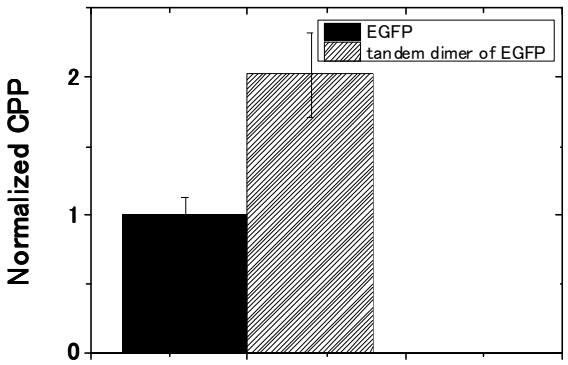

Fig. 3-2 Comparison of CPP between EGFP and tandem dimer of EGFP

The CPP of EGFP and the tandem dimer of EGFP were measured by FCS using whole HeLa cell lysate. The CPP of EGFP and the tandem dimer of EGFP were 11.3±1.5 kHz and 22.9± 6.7 kHz, respectively. The average value and standard deviation were calculated from five independent experiments. Filled bar: EGFP, Shaded bar: tandem dimer of EGFP.

3.3.2 Determination of dissociation constant of EGFP-GR in homodimerization from HeLa cell

To determine dissociation constant for homodimerization of GR, EGFP-GR was transiently expressed in HeLa cells. However, the endogenous GR is expressed in HeLa cells and there is the possibility of a pseudo dimer between EGFP-GR and endogenous GR. This pseudo dimer detected as monomeric EGFP-GR in FCS measurements. Therefore, the expression levels of exogenous EGFP-GR and endogenous GR in HeLa cells were estimated using western blotting. The bands of EGFP-GR, endogenous GR and α-tubulin were shown in Fig. 3-3 A. The EGFP-GR and endogenous GR were observed with transfection of EGFP-GR, in contrast only endogenous GR was observed without transfection of EGFP-GR. By using the band intensity and equation (3-2), the ratio of expression levels of EGFP-GR and endogenous GR was analyzed and the expression level of EGFP-GR was found to be

7.07-folds higher than that of endogenous GR in living HeLa cell (Fig. 3-3 B). This indicated that EGFP-GR was over-expressed, compared with endogenous GR in HeLa cells.

The amount of homodimeric EGFP-GR was determined using the FCS-microwell system. Typical images of a HeLa cell expressing EGFP or EGFP-GR were shown in Fig. 3-4 C. EGFP-GR localized in the nucleus after addition of dexamethasone (Dex), but not EGFP and EGFP-GR in absence of Dex. The extraction efficiency of EGFP-GR was 90% and reached a plateau at 90 min after cell lysis treatment (Fig. 3-5). FCS measurements were performed in microwells after 90 min cell-lysis treatment and typical autocorrelation functions and fit residuals of EGFP and EGFP-GR in the absence and presence of Dex are shown in Fig. 3-6. The CPP was considered for distinguishing the fractions of monomeric and homodimeric EGFP-GR because the change of CPP between monomeric and homodimeric EGFP-GR is more sensitive than that of the diffusion time of EGFP-GR. The normalized CPP increased with the increase in the total concentration of EGFP-GR in the presence of Dex. On the other hand, it was constant in the absence of Dex (Fig. 3-7 A). The homodimeric fraction of EGFP-GR was calculated from the normalized CPP using equation (3-8) (Fig. 3-7 B). Next, the concentration of homodimeric EGFP-GR was calculated using the homodimeric fraction and EGFP-GR concentration from FCS measurements. The data were fitted by the bimolecular reaction model (equation (3-2)) using the curve fitting based on the non-linear least-squares in whole range. The dissociation constant for homodimerization of GR was determined to be 49.6±7.27 nM (Fig. 3-7 C, Blue dashed line). In order to small number of data points at higher concentration, the data were fitted by the different method, the weighted non-linear least-squares in whole range. The weighting factor of the each data point for fitting was the inverse of the number of data points within the window of ±2.5 nM from each data point. However, the dissociation constant which was obtained to be 34.3±5.37 was similar to that by least-squares fitting in whole range (Fig. 3-8).

Next, the data points in the 0 to 50 nM range were fitted by least-squares fitting. The

maximum amount of endogenous GR in COS-1 is 61 nM based on the previously reported 111000 molecules per cell (1420 fmol/mg) [39] and our finding of a 3 pL of average cell volume. Moreover, 16200 fmol/mg in cytotrophoblasts [40] was calculated to be 701 nM using the same method. The range above a total EGFP-GR concentration of 50 nM in the microwell was ignored in this fitting model because the 50 nM total concentration of EGFP-GR corresponded to a 1.5 μM concentration in a cell seemed to be overexpression compared with the endogenous concentration of GR. The dissociation constant for homodimerization of EGFP-GR was determined to be 107±19 and 49.6±7.27 nM using the least-squares fitting in the range of 0 to 50 nM and whole range, respectively (Fig. 3-7 C). The dissociation constant suggested that all GRs did not consist of a homodimer but that there was equilibrium between the monomer and homodimer forms in both fitting.

Moreover, the diffusion constants determined from the autocorrelation function of FCS measurements were lower than the theoretical diffusion constant calculated from the molecular weight of homodimeric EGFP-GR (240 kDa) (Fig. 3-9). These results suggested that EGFP-GR formed not only a monomer-dimer equivalent state, but also a large-molecular-weight complex with endogenous interacting proteins. This lower diffusion constant might originate from GR-DNA complexes but this probability is small because a nuclease (Benzonase) was present in the extraction buffer.

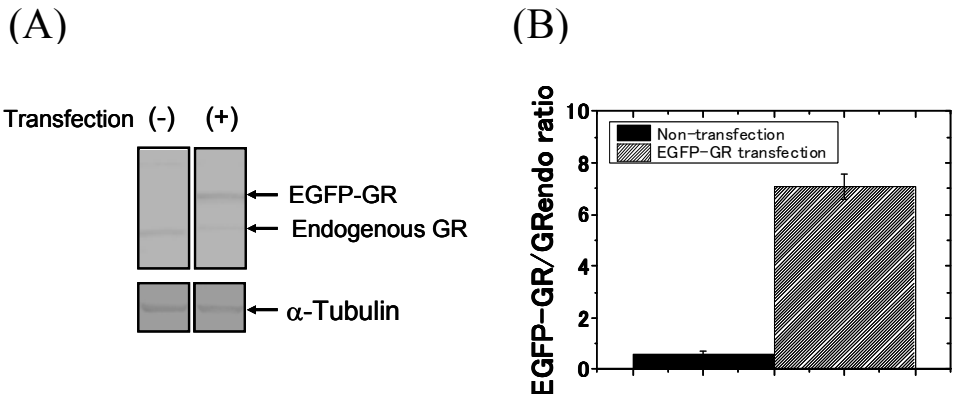

Fig. 3-3 Comparison of the amounts of exogenous EGFP-GR and endogenous GR

(A) The images of bands that originated from the exogenous EGFP-GR and endogenous GR or α-tubulin were cropped from the membranes blotted using an anti-GR or anti-α-tubulin antibody. **(B)** The ratio of the amounts of exogenous EGFP-GR and endogenous GR were 0.56 ± 0.14 and 7.07 ± 0.47 in nontransfected cells and EGFP-GR expressing cells, respectively. The average and standard deviation were calculated from three-independent experiments. Solid bar: nontransfected HeLa cells, Shaded bar: EGFP-GR-expressing HeLa cells.

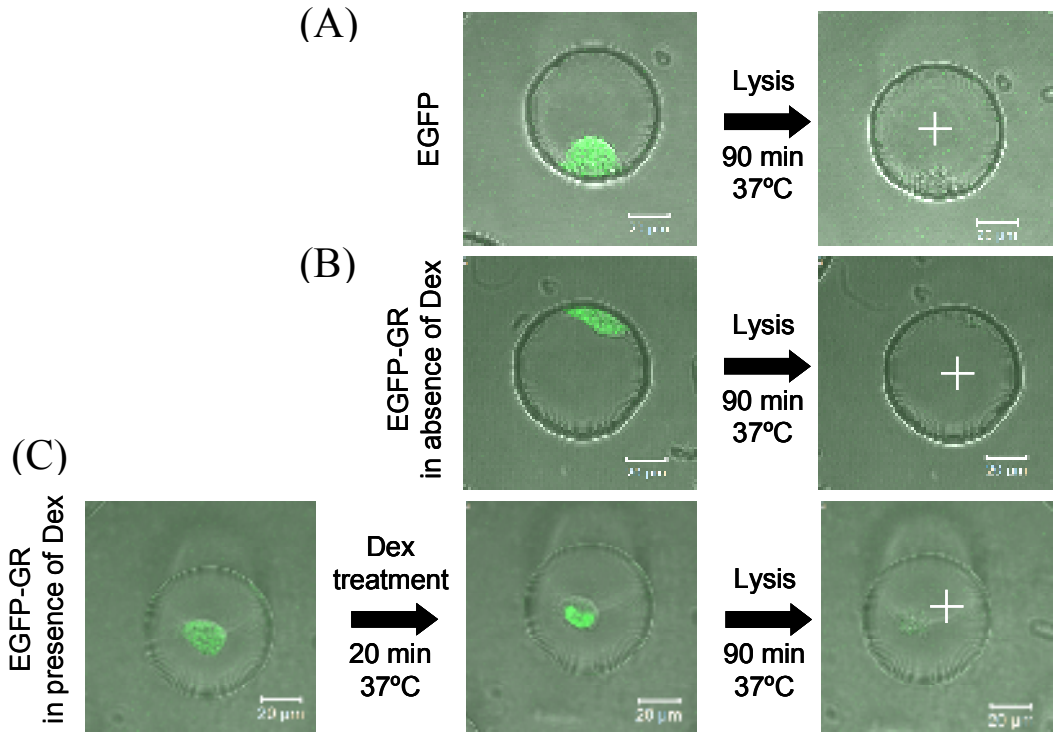

Fig. 3-4 Comparison of localization of EGFP-GR in the absence and presence of Dex

Typical images of EGFP, EGFP-GR in the absence and the presence of Dex. **(A)** EGFP, **(B)** EGFP-GR in the absence of Dex, **(C)** EGFP-GR in the presence of Dex. EGFP-GR in the presence of Dex only localized in the nucleus. White cross: FCS measurement point, Scale bar: 20 μm.

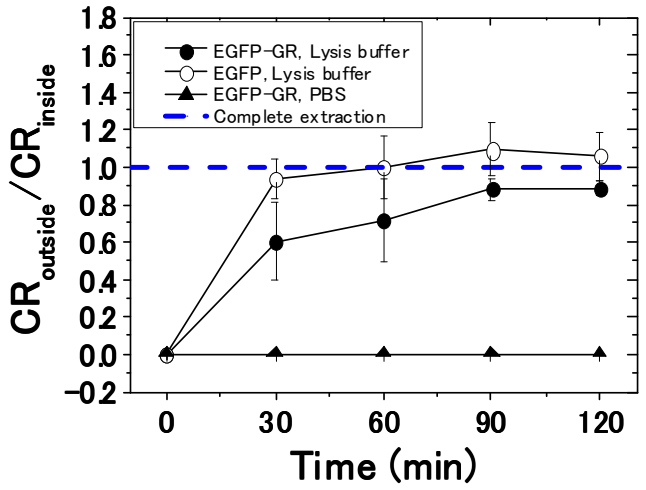

Fig. 3-5 The efficiency of EGFP-GR extraction into lysis buffer

The ratio of fluorescent intensity (Count rate: CR) between inside and outside of the cell was measured by FCS after cell lysis. If all EGFP and EGFP-GR molecules are extracted from the cell, the ratio of CR at inside of the cell to that at outside of the cell reaches to 1.0 (Blue dashed line). Open circles indicate the extraction of EGFP by lysis buffer as a positive control and filled triangles show the extraction of EGFP-GR by PBS as a negative control. Filled circles show the extraction of EGFP-GR by lysis buffer. These results suggested that 90 min lysis was an effective extraction time. Data number was 10 for calculation of the average value and standard deviation.

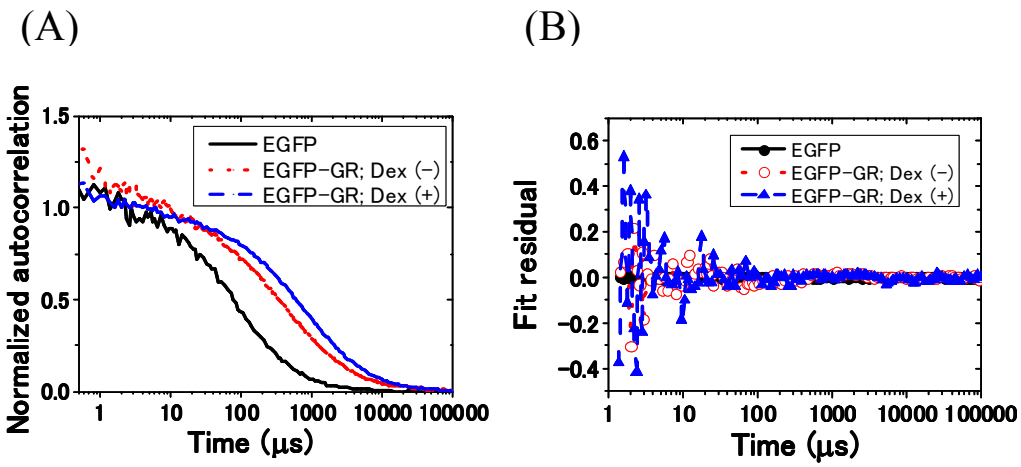

Fig. 3-6 Comparison of normalized autocorrelation functions of EGFP and EGFP-GR in the absence and the presence of Dex

Typical normalized autocorrelation functions **(A)** and fit residuals **(B)** of EGFP and EGFP-GR with and without Dex treatment. Black solid line: EGFP, Red dotted line: EGFP-GR without Dex treatment, Blue dashed line: EGFP-GR with Dex treatment.

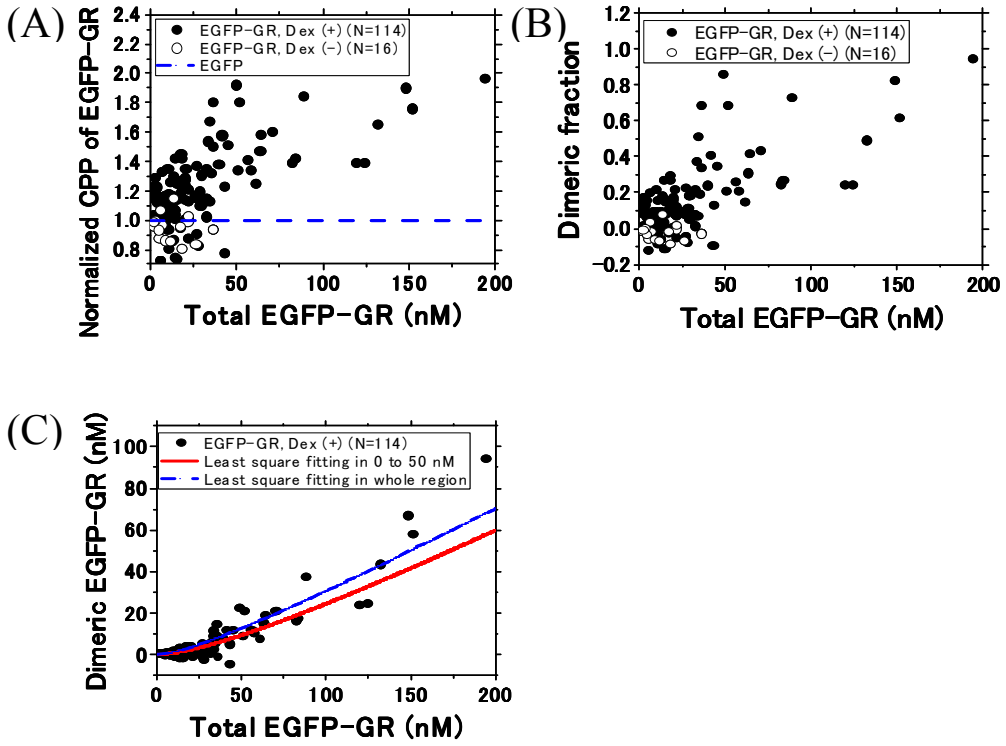

Fig. 3-7 Determination of dissociation constant for homodimerization of EGFP-GR from HeLa cells

(A) CPP of EGFP-GR normalized by CPP of EGFP. Data numbers were 16 and 114 in the absence and the presence of Dex, respectively. Open symbol: EGFP-GR in the absence of Dex treatment, Filled symbol: EGFP-GR in the presence of Dex treatment. Blue dashed line: EGFP **(B)** Dimeric fractions of EGFP-GR in the absence and the presence of Dex after cell lysis were calculated by equation (3-8) and normalized CPP of EGFP-GR. Open symbol: EGFP-GR in the absence of Dex treatment, Filled symbol: EGFP-GR in the presence of Dex treatment. The number of data was 16 and 114 in the absence and the presence of Dex, respectively. **(C)** Determination of the dissociation constant in EGFP-GR homodimerization (K_d: 49.6±7.27 nM and 107±19 nM) in the least-squares fitting in whole range and 0 to 50 nM range, respectively. Filled symbol: EGFP-GR in the presence of Dex treatment, Red solid line: least-squares fitting in the region of 0 to 50 nM, Blue dashed line: least-squares fitting in whole region by equation (3-2) in materials and methods. Data number was 114.

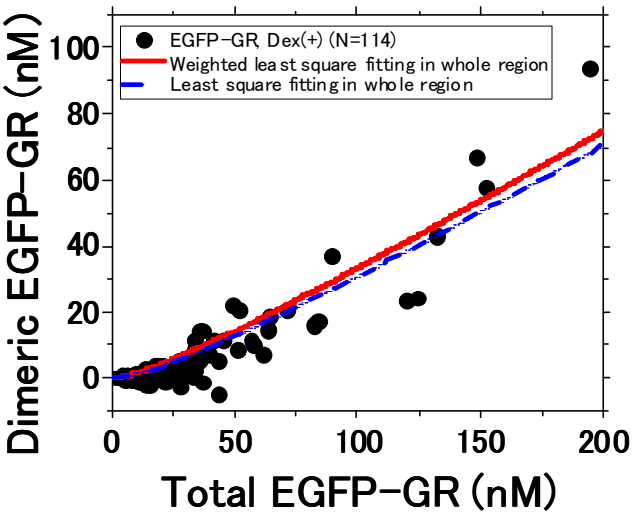

Fig. 3-8 Comparison of fitting methods for the dissociation constant of homodimerization of EGFP-GR

The fitting methods between least-squares fitting and weighted least-squares fitting in whole range were compared to determine the dissociation constant for homodimerization of EGFP-GR. The weighting factor of the each data point for fitting was the inverse of the number of data points within window ±2.5 nM from each data point. The similar dissociation constant was obtained by the other windows from ±1 (K_d: 40.6±6.1 nM) to ± 5 nM (K_d: 29.6±4.8 nM) (data not shown). Black filled symbol: EGFP-GR in the presence of Dex, Red solid line: Weighted least-squares fitting in whole region, Blue dashed line: Least-squares fitting in whole region. Data number was 114.

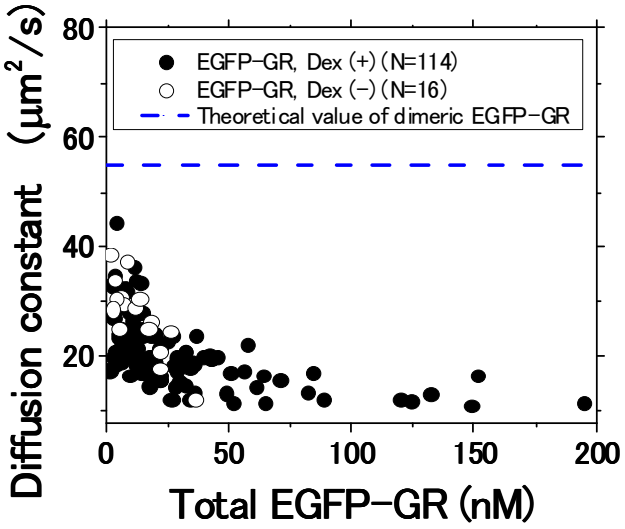

Fig. 3-9 Complex formation of EGFP-GR with endogenous interacting proteins in the absence and the presence of Dex

Diffusion constant of EGFP-GR with and without Dex treatment. Data numbers were 16 and 114 in the absence and the presence of Dex, respectively. Open symbol: EGFP-GR without Dex treatment, Filled symbol: EGFP-GR with Dex treatment, Blue dashed line: Theoretical diffusion constant of homodimeric EGFP-GR calculated by molecular weight (240 kDa).

3.4 Discussion

Fluorescence correlation spectroscopy (FCS) is widely used to investigate the dynamic properties of fluorescently-labeled proteins in living cells [22, 23]. However, it was difficult to determine the concentration of fluorescently-labeled proteins in living cells, because of heterogenous distribution and photobleacing of fluorescent proteins. FCS-microwell system could determine the concentration of homodimeric EGFP-GR and dissociation constant using bimolecular reaction model equation. In this chapter, on the basis of the concentration of EGFP-GR in the microwell using FCS-microwell system, the dissociation constant of GR homodimerization determined to be 49.6 nM and 107 nM with two different fitting concentration range (Fig. 3-7 C). There is two-fold difference between these dissociation

constants. This result may indicate the different form of GR homodimerization at 0 to 50 nM and above 50 nM concentration range. On consideration with endogenous concentration of GR in the cell, the dissociation constant of 107 nM might be more effective to the homodimerization of GR in the cell. Moreover, the dissociation constant for homodimerzation of GR suggested that GR homodimerized partially in the absence of GRE because our experiments were performed without addition of GRE-containing oligonucleotides and with lysis buffer containing Benzonase nuclease.

The diffusion constant showed that GR formed a large complex than homodimeric GR (Fig. 3-9). Previous studies have reported proteins interacting with GR such as Hsp90 and cofactors [6-8, 11, 41]. However, the regulatory proteins for homodimerization of GR remain unknown. We speculate that the detected large complex contains interacting proteins and that these proteins regulate homodimerization of GR in the living cell.

In this work, single-cell measurement was performed for homodiemrization of GR and complex formation in single cells. The variance of the CPP and diffusion constant from single cell were focused on to examine the heterogeneity of homodimerization and complex formation in single cells. The relative standard deviation of the normalized CPP and diffusion constant of EGFP-GR were calculated to be in the ranges from 0 to 10 nM, 10 nM to 20 nM and 20 to 30 nM (Fig. 3-10). These values were higher than those of the relative standard deviation of EGFP, corresponding to the measurement error (Fig. 3-10). These results suggested that the homodimerization and complex formation of EGFP-GR were heterogenous in single cells. This may show that single-cell methods are needed for understanding the functions of GR.

Here, the FCS-microwell system was used to determine the monomer and dimer concentrations at the single-cell level. This system could be revealed the relationship between the amount of homodimeric GR and its transcriptional activity in single-cell level. In addition to GR homodimer formation, the heterodimers of EGFP-GR and other nuclear receptors (like MR: Mineralocorticoid receptor) should be considered in biological systems in future.

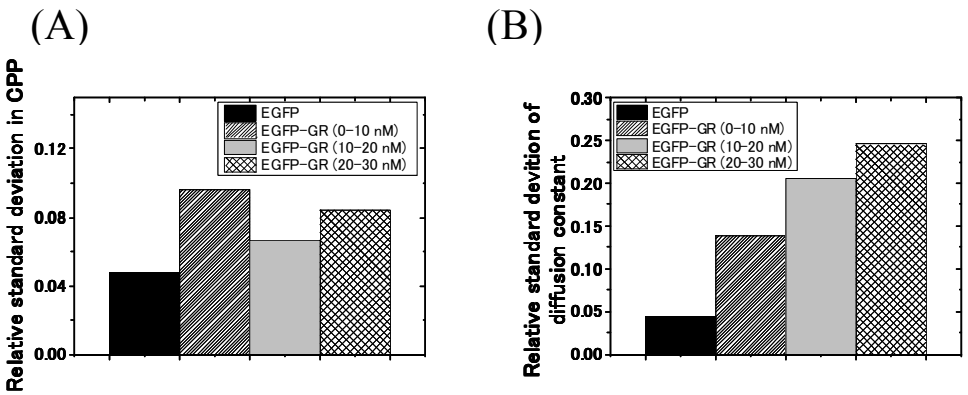

Fig. 3-10 The heterogeneity of homodimerization and complex formation

(A) Relative standard deviations of normalized CPPs of EGFP and EGFP-GR. **(B)** Relative standard deviations of diffusion constants of EGFP and EGFP-GR. The relative standard deviations of EGFP-GR with different concentrations of EGFP-GR, 0 to 10 nM, 10 to 20 nM and 20 to 30 nM were calculated from the average values and standard deviations of CPP and the diffusion constant in microwells obtained from single-cell data shown in Fig. 3-7 A and Fig. 3-9. Filled black bar: EGFP, Shaded bar: EGFP-GR (0-10 nM), Filled gray bar: EGFP-GR (10-20 nM), Meshed bar: EGFP-GR (20-30 nM). Number of data was 5.

Chapter 4

Determination of the dissociation constant for homodimerization of glucocorticoid receptor without endogenous expression using FCS-microwell system

4.1 Introduction

The human glucocorticoid receptor α (GR) is a ligand-induced transcription factor which belongs to the nuclear receptor superfamily [1, 2]. It is well-known that liganded GRs homodimerize and transactivate several target genes in the nucleus as described in chapter 1 and 3 [9-15]. Therefore, its homodimerization property is important for the control of the GR transactivation. The HeLa cells have the expression of endogenous GR (Fig. 3-3). This endogenous GR may cause the error of the concentration of homodimeric EGFP-GR in order to forming the pseudo dimer between EGFP-GR and endogenous GR. In contrast, U2OS cells have no expression of endogenous GR. Therefore, the dissociation constant for homodimerization of EGFP-GR was determined in U2OS cells using FCS-microwell system without any effects of endogenous GR. Moreover, it has identified that GRs formed a homodimer via a surface at DNA-binding domain. A point mutation of A458T inhibited the homodimerization of GR. The homodimerization deficient mutant (A458T) was used as a negative control for homodimerization of GR.

Some earlier studies suggested homodimerization of GR on specific binding of GR to GRE via monomeric GR binding with allosteric effect, in which first monomer of GR accelerates binding of the second monomer [35, 42-45]. However, preformed homodimer [17, 34, 45-48] preferentially binds to GRE rather than homodimeric GR arising from sequential binding of the monomeric GR [17]. The necessity of DNA binding of GR for its homodimerization and its large complex formation with endogenous interacting proteins still remains unclear. To address this question, the dissociation constant for homodimerization of DNA-binding deficient mutant (C421G) was determined using FCS-microwell system.

In this chapter, the dissociation constant for homodimerization of GR was determined in WT with and without Dex and mutants with Dex. The diffusion constant analysis revealed the complex formation of WT, DNA-binding deficient mutant and homodimerization-deficient mutant. Moreover, EGFP-GR and tandem-dimer mCherry-GR (mCh_2-GR) were transiently co-expressed in U2OS cells. A combination method of fluorescence cross-correlation spectroscopy (FCCS) and microwell system (FCCS-microwell system) determined the dissociation constant for the homodimerization of GR.

4.2 Materials and methods

4.2.1 Constructs and chemicals

The expression vectors for EGFP-GR_{WT}, their mutants and tandem dimer of EGFP was described previously [22, 36, 37]. The expression vectors for tandem dimer of mCherry (mCh_2), mCh_2 fused with GR (mCh_2-GR) and mCh_2 fused EGFP was described in doctoral thesis by Manisha. Dex was used at a concentration of 0.5 µM in opti-MEM (GIBCO) for activation of GR. The components of the lysis buffer were 80% CelLytic M Cell Lysis Reagent (Sigma-Aldrich), 1% Protease Inhibitor Cocktail (Sigma-Aldrich), 10 mM $MgCl_2$, 0.1% SDS and 200 U/mL Benzonase nuclease (Sigma-Aldrich).

4.2.2 Cell culture and transfection in microwells

U2OS cells were cultured in McCoy's 5A modified medium (GIBCO) supplemented with charcoal-stripped 10% FBS at 37^{O}C with 5% CO_2. To culture the U2OS cells, the microwells on the PDMS chips were washed using a detergent water, which was then evaporated in a glass vacuum dryer to remove the water from the microwells. After evaporation, the cell culture medium containing the U2OS cell suspension was poured onto the PDMS chip in a 6-well plate dish and incubated for 4 hours at 37^{O}C.

For FCS measurments, the plasmid encoded 0.1 μg EGFP and 4.9 μg empty vector or 5 μg EGFP-GRs were transfected to U2OS cells on 6-well plate dishes using Lipofectamin 2000 reagent (Invitrogen). For FCCS measurements, the plasmids encoded a set of 0.1 μg EGFP, 0.1 μg mCh_2 and 4.8 μg empty vector, 0.1 μg EGFP-mCh_2 and 4.9 μg empty vector or 2 μg EGFP-GR and 3 μg mCh_2-GR were transfected to U2OS cells on 6-well plate dishes using ViaFact (Promega). After replacement of the culture medium on dishes with fresh medium, the plasmids were mixed with Lipofectaimin 2000 or ViaFact in opti-MEM and added to the cell culture dishes. After 6 hours incubation at 37^{O}C with 5% CO_2, the medium on the dishes was changed to fresh one and the U2OS cells was incubated continuously at 37^{O}C with 5% CO_2 for 18 hours. The transfected U2OS cells were trypsinized and transferred to the microwells on the PDMS chips.

4.2.3 Single-cell method to detect the homodimer of GR

The PDMS chip was attached to a glass stick with double-sided tape (Nitoms, Tokyo, Japan) and the chip was pressed onto a coverslip in dexamethasone (Dex) with opti-MEM and incubated at 37^{O}C for 20 min to activate EGFP-GR. After 20 min incubation of the PDMS chip, the position (a number and a letter) of the microwells in which single cell was cultured were noted down. The medium on the coverslip was changed to lysis buffer and the protein

extracted from each cell was kept in the microwell after cell lysis, following which FCS or FCCS measurements were carried out in each microwell. The detailed method was described in the chapter 3.

4.2.4 LSM imaging and FCS measurements

LSM imaging and FCS measurements of EGFP and EGFP-GR were performed using an LSM510-ConfoCor2 (Carl Zeiss, Jena, Germany) equipped with an Ar ion laser, water immersion objective (C-Apochromat, 40X, 1.2N.A., Corr, Carl Zeiss, Jena, Germany), a photomultiplier for LSM imaging and an avalanche photodiode detector for FCS measurements. The optical setup for LSM imaging and FCS measurement was same as described at 2. 2. 3 of materials and methods in the chapter 2.

4.2.5 LSM imaging and FCCS measurements

LSM imaging and FCCS measurements were performed using LSM510-Confocor3 (Carl Zeiss, Jena, Germany) equipped with an Ar ion laser, He-Ne laser, water immersion objective (C-Apochromat, 40X, 1.2N.A., Corr, Carl Zeiss, Jena, Germany), two photomultipliers for LSM imaging and two avalanche photodiode detectors for FCCS measurements (Fig. 4-1). EGFP was excited at the 488 nm laser and mCherry was excited at the 594 nm laser. The pinhole diameter was adjusted to 70 μm. The emission signals were split by a dichroic mirror (600 nm beam splitter) and detected at 505-550 nm for EGFP and 615-680 nm for mCherry for LSM imaging and at 505-540 nm for EGFP and 615-680 nm for mCherry for FCCS measurements. FCCS measurements were performed 10 times with durations of 5 seconds.

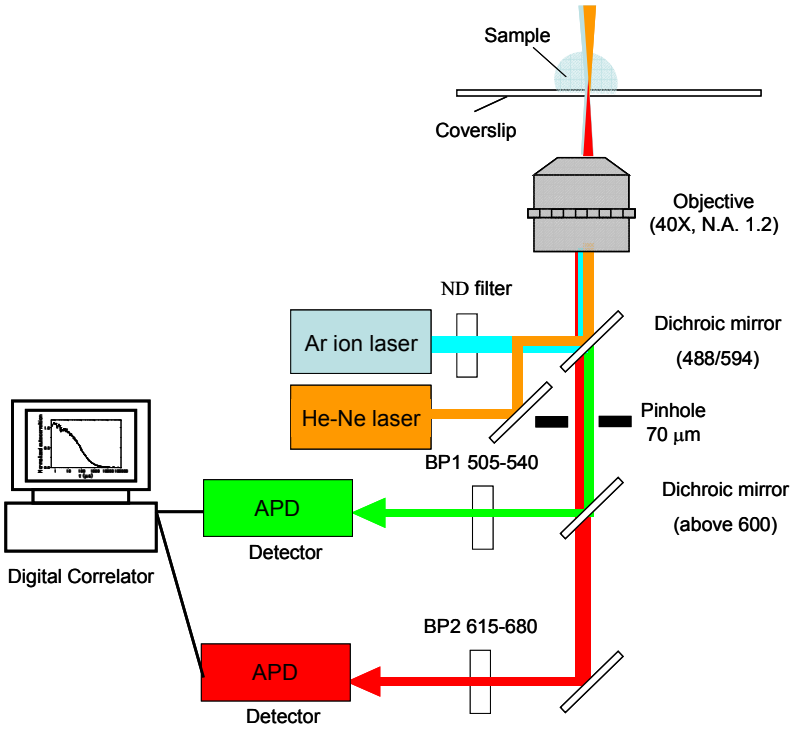

Fig. 4-1 Optical setup for FCCS measurements

The continuous-wave Ar ion laser (488 nm) and He-Ne laser (594 nm) were used for the excitation of EGFP and mCherry, respectively. Dichroic mirror represents 600 nm beam splitter. BP1 and BP2 represent the band pass filter 505-540 nm for EGFP and 615-680 nm for mCherry, respectively. The fluorescence was detected at 505-540 nm for EGFP and at 615-680 nm for mCherry. Two detectors were connected to the digital correlator.

4.2.6 Data analysis and determination of dissociation constant of EGFP-GR in homodimerization

The data analysis of FCS measurements was same as described at 2.2.4 of materials and

methods in chapter 2.

The dissociation constant K_d for homodimerization of EGFP-GR was determined using the following equations:

$$[D] = \frac{K_d + 4[M_0] - \sqrt{(K_d + 4[M_0])^2 - 16[M_0]^2}}{8} \quad \text{-(4-1)}$$

$$[M_0] = [M] + 2[D] \quad \text{-(4-2)}$$

where $[M_0]$ is the total concentration of EGFP-GR in the microwell, and [M] and [D] are the concentration of monomeric and homodimeric EGFP-GR, respectively.

To obtain the [M] and [D], the monomeric fraction F_m and homodimeric fraction F_d (F_m+F_d = 1) of EGFP-GR were calculated using equations (4-3), (4-4) and (4-5) [38]. FCS measurement can be used to obtain the apprarent number of molecules and brightness, which is defined as the counts per particle (CPP). When monomeric and homodimeric EGFP-GR are contained in the lysate, the apparent CPP ($CPP_{EGFP\text{-}GR,app}$) is obtained as shown by the following equation [38].

$$CPP_{EGFP\text{-}GR,app} = \frac{F_m \cdot \eta_m{}^2 + F_d \cdot \eta_d{}^2}{F_m \cdot \eta_m + F_d \cdot \eta_d} \quad \text{-(4-3)}$$

where η_m and η_d are the CPP of monomeric and homodimeric EGFP-GR, respectively. If the CPP of the tandem dimer of EGFP is twice that of EGFP (Fig. 3-2), the CPP of homodimeric EGFP-GR (η_d) will be twice the CPP of monomeric EGFP-GR (η_m), which is the same as that of EGFP (CPP_{EGFP}).

$$\eta_m = CPP_{EGFP} \quad \text{-(4-4)}$$

$$\eta_d = 2 \cdot CPP_{EGFP} \quad \text{-(4-5)}$$

By using equations (4-3), (4-4) and (4-5), the fractions of monomeric and homodimeric EGFP-GR (F_m and F_d) were shown as equations (4-6) and (4-7).

$$F_m = \frac{4 - 2R}{3 - R} \quad \text{-(4-6)}$$

$$F_d = \frac{R - 1}{3 - R} \quad \text{-(4-7)}$$

where,

$$R = \frac{CPP_{\text{EGFP -GR, app}}}{CPP_{\text{EGFP}}} \quad \text{-(4-8)}$$

4.2.7 FCCS data analysis and determination of dissociation constant of EGFP-GR in homodimerization

Data acquired from FCCS were calculated with AIM software (Carl Zeiss, Jena, Germany). The autocorrelation functions from green and red channels, $G_G(\tau)$, $G_R(\tau)$ and the cross-correlation function $G_C(\tau)$ were calculated as follows:

$$G_G(\tau) = \frac{\langle I_G(t) I_G(t+\tau) \rangle}{\langle I_G(t) \rangle^2} \quad \text{-(4-9)}$$

$$G_R(\tau) = \frac{\langle I_R(t) I_R(t+\tau) \rangle}{\langle I_R(t) \rangle^2} \quad \text{-(4-10)}$$

$$G_C(\tau) = \frac{\langle I_G(t) I_R(t+\tau) \rangle}{\langle I_G(t) \rangle \cdot \langle I_R(t) \rangle} \quad \text{-(4-11)}$$

where τ denotes the delay time, I_G is the fluorescent intensity of the green channel, I_R is the fluorescent intensity of the red channel and $G_G(\tau)$, $G_R(\tau)$ and $G_C(\tau)$ denote the autocorrelation functions of green, red and cross-correlation function, respectively. The

acquired auto- and cross-correlations were fitted using one-component model as follows:

$$G_{\text{auto}}(\tau) = 1 + \left(1 + \frac{F_{\text{triplet}} e^{-\frac{\tau}{\tau_{\text{triplet}}}}}{1 - F_{\text{triplet}}}\right) \cdot \frac{1}{N}\left(1 + \frac{\tau}{\tau_D}\right)^{-1} \cdot \left(1 + \frac{1}{s^2}\frac{\tau}{\tau_D}\right)^{-\frac{1}{2}} \quad \text{-(4-12)}$$

$$G_{\text{cross}}(\tau) = 1 + \frac{1}{N}\left(1 + \frac{\tau}{\tau_D}\right)^{-1} \cdot \left(1 + \frac{1}{s^2}\frac{\tau}{\tau_D}\right)^{-\frac{1}{2}} \quad \text{-(4-13)}$$

where F_{triplet} is the average fraction of triplet state molecules, τ_{triplet} is the average relaxation time and τ_D is the average diffusion time of molecules. N is the average number of fluorescent particles in the effective observation volume defined by lateral radius w_0 and axial radius z_0 of the confocal volume element, and s is the structural parameter ($s = z_0/w_0$). The values of $w_{0,i}$ and $z_{0,i}$ ($i = G$ or R) are determined from the diffusion constant of the rhodamine 6G (R6G: 414 μm^2/s [31]) and Alexa 594 (370 μm^2/s [49])used as standard fluorescent dyes, respectively.

$$w_{0,i} = \sqrt{4D \cdot \tau_{\text{D},i}} \quad \text{-(4-14)}$$

$$s_i = \frac{z_{0,i}}{w_{0,i}} \quad \text{-(4-15)}$$

The effective volume ($V_{\text{eff},i}$) are calculated as following:

$$V_{\text{eff},i} = \pi^{\frac{3}{2}} \cdot w_{0,i}^2 \cdot z_{0,i} \quad \text{-(4-16)}$$

$$V_{\text{eff, C}} = \left(\frac{\pi}{2}\right)^{\frac{3}{2}} \cdot (\omega_{0,G}^2 + \omega_{0,R}^2)(z_{0,G}^2 + z_{0,R}^2)^{\frac{1}{2}} \quad \text{-(4-17)}$$

The average number of green fluorescent particles (N_{G}), red fluorescent particles (N_{R}) and particles that have both green and red fluorescence (N_{C}) are give by

$$N_{\mathrm{G}} = \frac{1}{G_{\mathrm{G}}(0) - 1} \qquad \text{-(4-18)}$$

$$N_{\mathrm{R}} = \frac{1}{G_{\mathrm{R}}(0) - 1} \qquad \text{-(4-19)}$$

$$N_{\mathrm{C}} = \frac{G_{\mathrm{C}}(0) - 1}{(G_{\mathrm{G}}(0) - 1) \cdot (G_{\mathrm{R}}(0) - 1)} \qquad \text{-(4-20)}$$

To remove the effect of background fluorescence on the obtained N_{meas}, the corrected N (N_{corr}) was calculated as follows [32, 33]:

$$N_{i,\mathrm{corr}} = \frac{N_{i,\mathrm{meas}} \cdot (I_{i,\mathrm{meas}} - I_{i,\mathrm{B}})^2}{(I_{i,\mathrm{meas}})^2} \qquad \text{-(4-21)}$$

Where $N_{i,\,\mathrm{meas}}$ is tha average numbers of green or red fluorescent particles obtained from each autocorrelation function and fitting analysis (i = G or R). $I_{i,\,\mathrm{meas}}$ is the average intensity of green or red fluorescent particles during FCCS measurement (i = G or R). $I_{i,\,\mathrm{B}}$ was the average background intensity of green or red fluorescence obtained from FCCS measurments of non-transfected U2OS cell lysate (i = G or R). To use the corrected number of molecules for green and red particles from equation (4-21), the apparent number of cross was corrected as following equation:

$$N_{\mathrm{C,corr}} = (G_{\mathrm{C,meas}}(0) - 1) \cdot N_{\mathrm{G,corr}} \cdot N_{\mathrm{R,corr}} \qquad \text{-(4-22)}$$

Diffusion constants of the samples was calculated from the diffusion constant of a standard molecule, R6G (D_{R6G}; 414 $\mu m^2/s$ [31]) and the ratio of diffusion times τ_{R6G} and τ_{D} in green fluorescent particles. In case of red fluorescent particles, diffusion constants of the samples was calculated from the diffusion constant of a standard molecule, Alexa594 (D_{Alexa594}; 370 $\mu m^2/s$ [49]) and the ratio of diffusion times τ_{Alexa594} and τ_{D}. The concentration of each fluorescent protein was calculated with the use of N_A (Avogadro's number) as give below:

$$\left[C_{i,\mathrm{corr}}\right] = \frac{N_{i,\mathrm{corr}}}{V_{i,\mathrm{eff}} \cdot \mathrm{N_A}} \quad \text{-(4-23)}$$

$$\left[C_{\mathrm{C,corr}}\right] = \frac{N_{\mathrm{C,corr}}}{V_{\mathrm{C,eff}} \cdot \mathrm{N_A}} \quad \text{-(4-24)}$$

where, i = G or R

The dissociation constant for homodimerization of GR was determined using following equation:

$$K_{\mathrm{d}} = \frac{\left[G_{\mathrm{free}}\right] \cdot \left[R_{\mathrm{free}}\right]}{\left[Complex\right]} \quad \text{-(4-25)}$$

The $[G_{\mathrm{free}}]$ and $[R_{\mathrm{free}}]$ for homodimerization of GR were calculated following equations

$$\left[G_{\mathrm{free}}\right] = \left[C_{\mathrm{G,corr}}\right] - 2 \times \left[C_{\mathrm{C,corr}}\right] \quad \text{-(4-26)}$$

$$\left[R_{\mathrm{free}}\right] = \left[C_{\mathrm{R,corr}}\right] - 2 \times \left[C_{\mathrm{C,corr}}\right] \quad \text{-(4-27)}$$

$$\left[Complex\right] = \left[C_{\mathrm{C,corr}}\right] \quad \text{-(4-28)}$$

The concentrations of the unbound EGFP or tandem dimer of mCherry fusion proteins $[G_{\mathrm{free}}]$ or $[R_{\mathrm{free}}]$ were calculated by the subtraction of two times the concentration of the complex $[Complex]$ from the total concentration of the EGFP or tandem dimer of mCherry fusion proteins, $[C_{G,\mathrm{corr}}]$ or $[C_{R,\mathrm{corr}}]$. Figure 4.2 shows the possible interaction of EGFP or tandem dimer of mCherry fusion GR (EGFP-GR or mCh_2-GR) as homodimer. Therefore, (EGFP-GR-mCh_2-GR) and (EGFP-GR-EGFP-GR) were expected to be the same concentration that is calculated from the $[C_{C,\mathrm{corr}}]$ value in equation (4-26), and (EGFP-GR-mCh_2-GR) and (mCh_2-GR-mCh_2-GR) were expected to be the same concentration that is calculated from the $[C_{C,\mathrm{corr}}]$ value in equation (4-27). A scatter plot of the products of concentrations of free molecules against the concentration of the complex was generated with a least-squares linear fitting and the dissociation constant was calculated from

the slope the regression line [29].

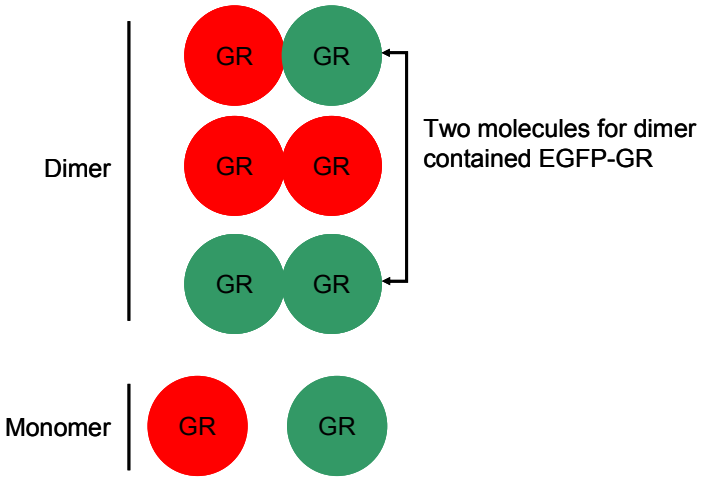

Fig. 4-2 Possible homodimer formation of EGFP-GR and mCh_2-GR

A heterodimer of EGFP-GR and mCh_2-GR only was detected by FCCS measurements. However, EGFP-GR interacts with EGFP-GR as homodimer. Considering this molecule, twice concentration of GR dimer contained in EGFP-GR was existed.

4.3 Results

4.3.1 Determination of dissociation constant of EGFP-GR in homodimerization from U2OS cell

EGFP-fused GR_{WT} and mutants (C421G: DNA-binding deficiency, A458T: Homodimerization deficiency) were transiently expressed in U2OS cells. The concentration of homodimeric EGFP-GR was determined using the FCS-microwell system. Typical images of a U2OS cell expressing EGFP or EGFP-GR_{WT}, EGFP-GR_{C421G}, EGFP-GR_{A458T} were shown in Fig. 4-3. EGFP-GR_{WT} and mutants localized in the nucleus after the addition of dexamethasone (Dex), but not EGFP and EGFP-GR_{WT} in the absence of Dex. The extraction efficiency of EGFP-GR reached a plateau of 90% at 90 min after cell lysis, same as HeLa cell in Fig. 3-5 (Fig. 4-4). FCS measurements were performed in microwells after 90 min cell lysis

and typical autocorrelation functions and fit residuals of EGFP, EGFP-GR_{WT} and mutants in the absence and the presence of Dex were shown in Fig. 4-5. The normalized CPPs of EGFP-GR_{WT}, EGFP-GR_{C421G}, EGFP-GR_{A458T} were higher than that of EGFP in the presence of Dex. On the other hand, in the absence of Dex, EGFP-GR_{WT} was similar to that of EGFP or some single-cell data was higher than that of EGFP (Fig. 4-6 A). The homodimeric fraction of EGFP-GR were calculated from the normalized CPPs using equation (4-7) (Fig. 4-6 B). Then, the concentration of homodimeric EGFP-GR was calculated using the homodimeric fraction and EGFP-GR concentration from FCS data. The data was fitted by the bimolecular reaction model (equation (4-1)) by the curve fitting based on the non-linear least square in the range from 0 to 50 nM, because of the overexpression of EGFP-GR in living cells (Fig. 4-6 C). The dissociation constant for homodimerization of EGFP-GR_{WT} was determined to be 137±37 nM and 419±120 nM in the presence and the absence of Dex (Fig. 4-7). The dissociation constant for homodimerization in presence Dex was lower than that in absence of Dex, suggesting that the homodimer formation may be induced by Dex. The dissociation constant for homodimerization of EGFP-GR_{WT} from U2OS cell was similar to that from HeLa cell in the presence of Dex. This indicated that there are negligible effects of endogenous GR for homodimerization of EGFP-GR_{WT} from HeLa cell. Moreover, the dissociation constant of mutants was determined to be 221±34 nM and 370±122 nM for DNA-binding deficient mutant (C421G) and homodimerization-deficient mutant (A458T) (Fig. 4-7). The dissociation constant of C421G mutant was lower than that of WT in the absence of Dex, indicating that DNA binding is not necessary for a homodimerization of GR. Moreover, the dissociation constant of A458T mutant was similar to that of WT in the absence of Dex. The point mutation of A458T inhibited the property of homodimerization of GR.

The diffusion constant of EGFP-GR_{WT} and mutants determined from the autocorrelation function of FCS measurements was lower than the theoretical diffusion constant calculated from the molecular weight of homodimeric EGFP-GR (240 kDa) (Fig. 4-8). These results

suggested that EGFP-GR_{WT} and mutants formed not only a homodimer but also a large-molecular-weight complex with endogenous interacting proteins. The average diffusion constant was compared between WT and mutants with and without Dex (Fig. 4-9). There are significant difference between WT in the absence of Dex and WT and mutants in the presence of Dex, indicating that the complex with endogenous interacting proteins is different before and after ligand binding. In contrast, a significant difference between WT and mutants with Dex was not observed. This suggested that complex formation is not dependent on the properties of DNA binding and homodimerization.

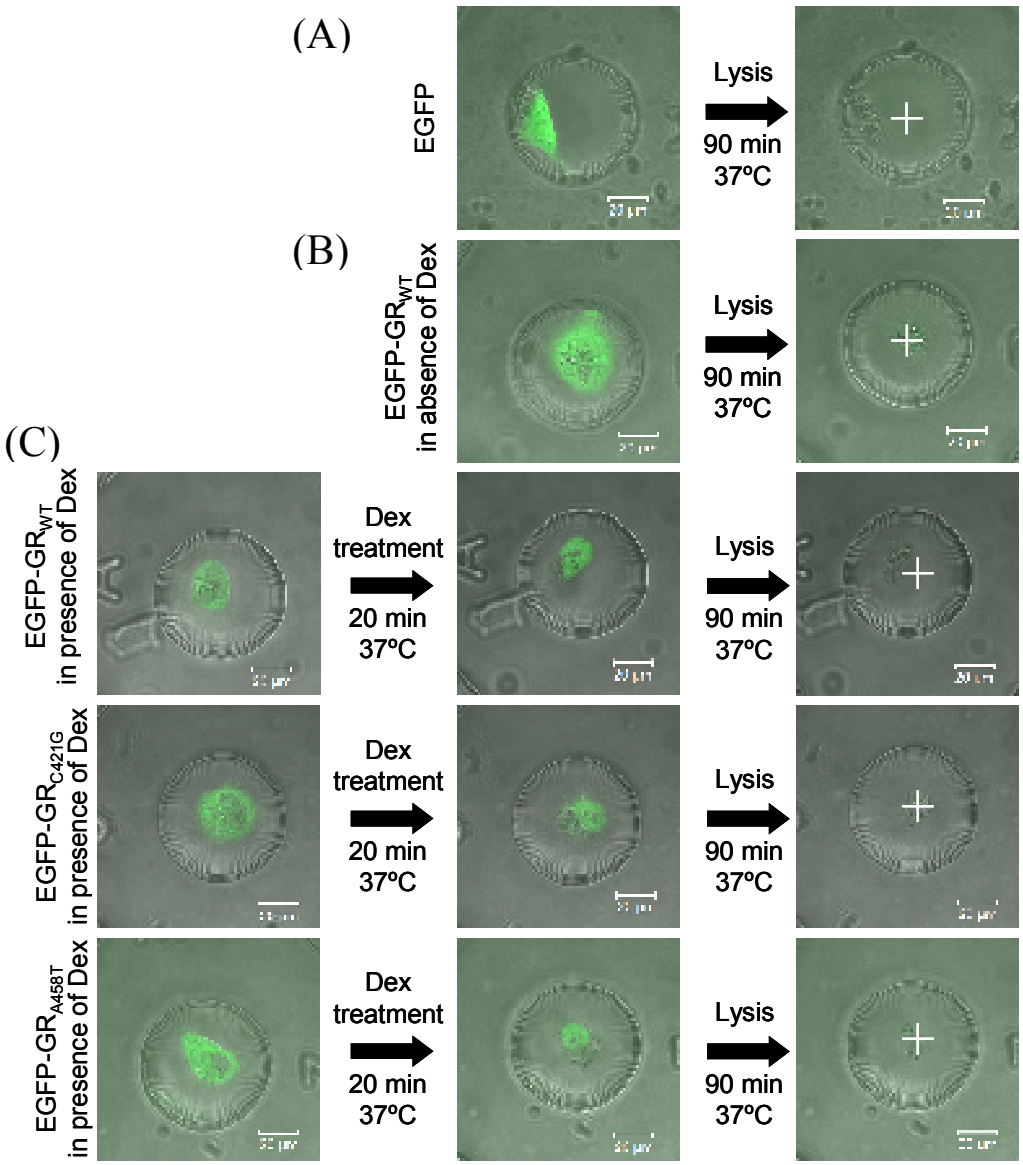

Fig. 4-3 Typical localization of EGFP-GR$_{WT}$ and mutants

(A) Typical images of EGFP before and after cell lysis. EGFP distributed homogenous in living U2OS cell. **(B)** Typical images of EGFP-GR$_{WT}$ without Dex treatment before and after cell lysis. EGFP-GR without Dex localized in cytoplasm. **(C)** Typical images of EGFP-GR$_{WT}$ and mutants with Dex treatment before and after cell lysis. EGFP-GR$_{WT}$ and mutants localized in nucleus after Dex treatment. White cross: FCS measurement position, Scale bar: 20 μm.

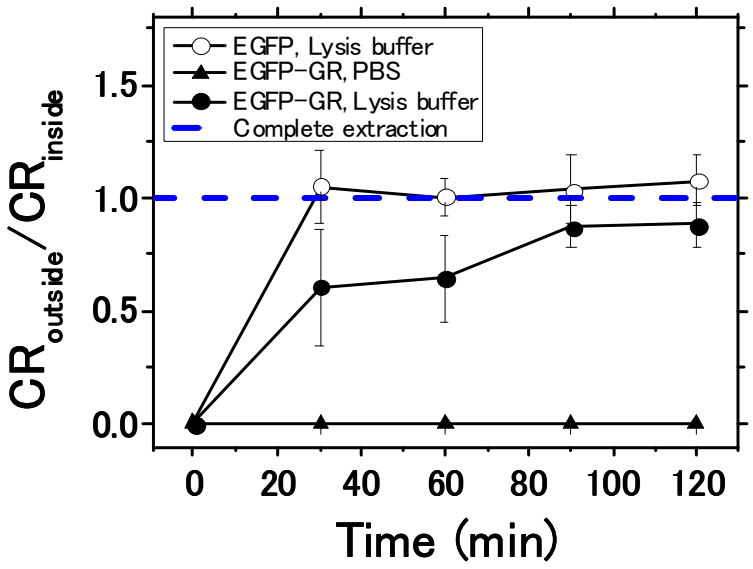

Fig. 4-4 The efficiency of EGFP-GR_{WT} extraction into lysis buffer from U2OS cell

The ratio of fluorescent intensity (Count rate: CR) between the inside and the outside of the cell was measured by FCS after cell lysis. When all EGFP and EGFP-GR_{WT} molecules were extracted from the cell, the ratio of CR at the inside of the cell to that at the outside of the cell reached to 1.0 (Blue dashed line). Open circles indicate the extraction of EGFP by lysis buffer as a positive control and filled triangles show the extraction of EGFP-GR_{WT} by PBS as a negative control. Filled circles show the extraction of EGFP-GR_{WT} by lysis buffer. These results suggested that 90 min lysis was an effective extraction time of EGFP-GR. Data number was 7, 5 and 13 for positive control, negative control and EGFP-GR_{WT} by lysis buffer, respectively.

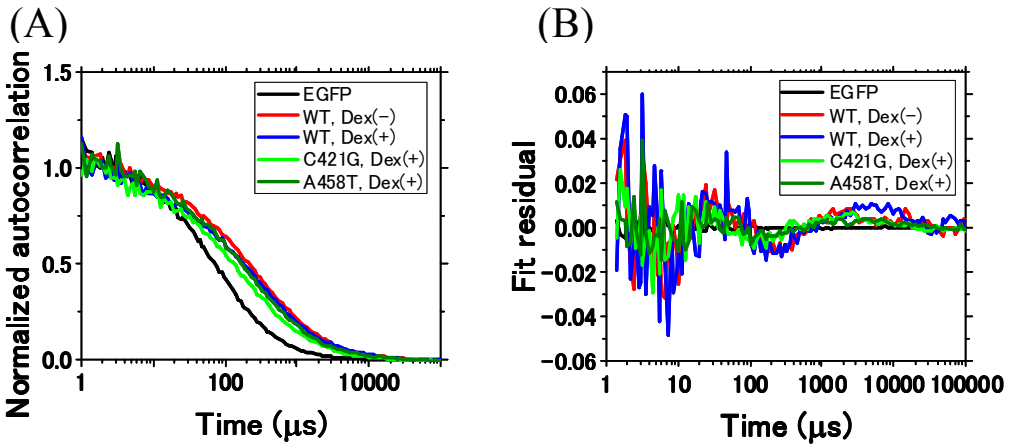

Fig. 4-5 Comparison of autocorrelation functions of WT and mutants with and without Dex

Typical normalized autocorrelation functions **(A)** and fit residuals **(B)** of EGFP and EGFP-GR_{WT}, EGFP-GR_{C421G} and EGFP-GR_{A458T} in the presence and the absence of Dex. Black solid line: EGFP, Red solid line: EGFP-GR_{WT} without Dex, Blue solid line: EGFP-GR_{WT} with Dex, Green solid line: EGFP-GR_{C421G} with Dex, Dark green solid line: EGFP-GR_{A458T} with Dex.

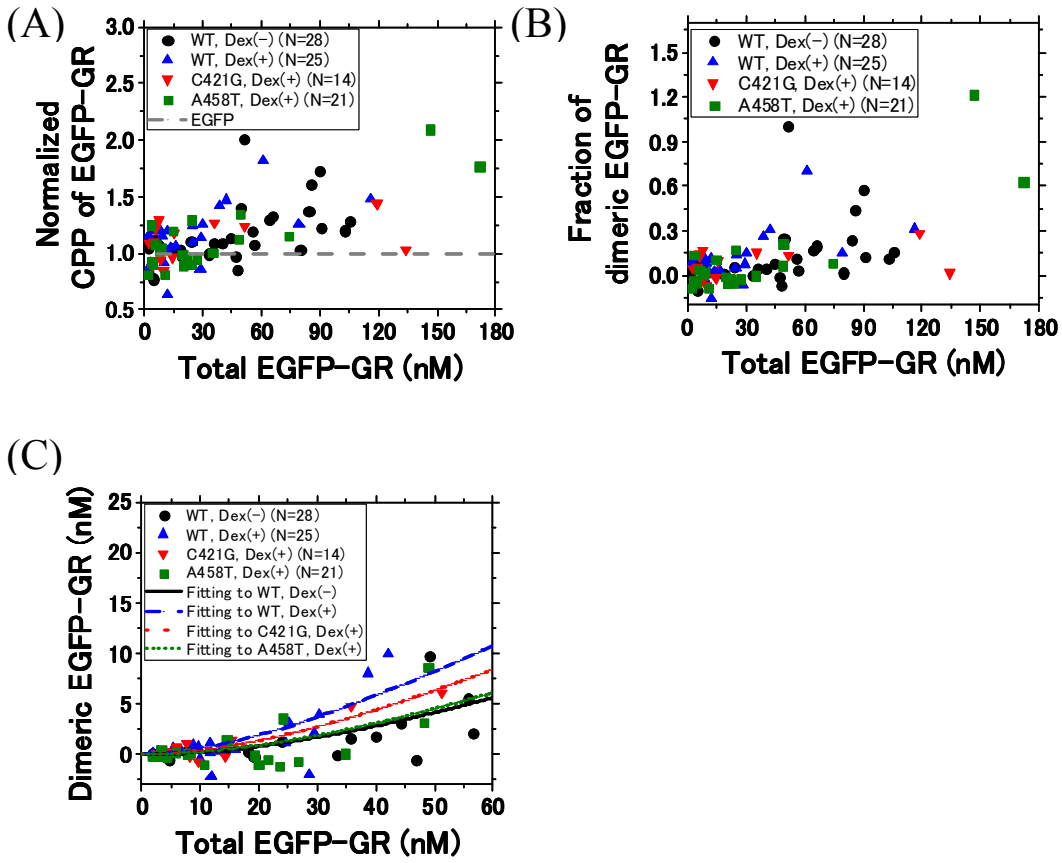

Fig. 4-6 Determination of dissociation constants for homodimerization from U2OS cells

(A) CPP of EGFP-GR normalized by CPP of EGFP. Gray dashed line: EGFP **(B)** Homodimeric fraction of EGFP-GR in the presence and the absence of Dex after cell lysis were calculated by equation (4-7) and normalized CPP of EGFP-GR. **(C)** Determination of the dissociation constant (K_d: 419±120 nM, 137±37 nM, 221±34 nM and 370±122 nM in EGFP-GR_{WT} without Dex, and EGFP-GR_{WT}, EGFP-GR_{C421G} and EGFP-GR_{A458T} with Dex, respectively) in EGFP-GR homodimerization by the non-linear least-squares fitting in the range from 0 to 50 nM. Black solid line: Fitting curve of EGFP-GR_{WT} without Dex, Blue dashed line: Fitting curve of EGFP-GR_{WT} with Dex, Red dotted line: Fitting curve of EGFP-GR_{C421G} with Dex, Dark green short-dotted line: Fitting curve of EGFP-GR_{A458T} with Dex. Filled black circle: EGFP-GR_{WT} without Dex (N = 28), Filled blue triangle: EGFP-GR_{WT} with Dex (N = 25), Filled red reverse triangle: EGFP-GR_{C421G} with Dex (N = 14), Filled dark green square: EGFP-GR_{A458T} with Dex (N = 21).

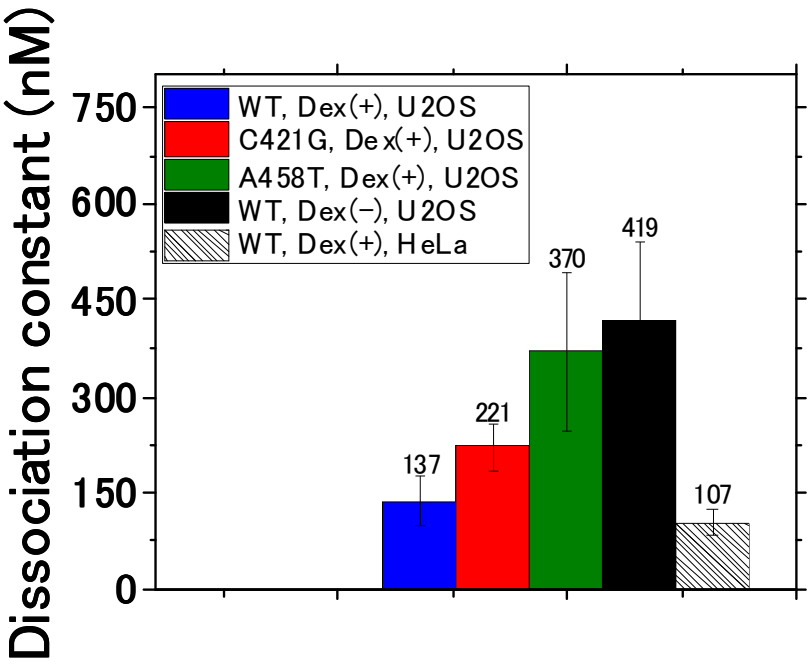

Fig. 4-7 Comparison of dissociation constants for homodimerization of WT and mutants from U2OS cell and WT from HeLa cell

The blue, red, dark green and black bar show the dissociation constant for homodimerization of WT, C421G and A458T with Dex and WT without Dex from U2OS cell. The shaded bar shows the dissociation constant for homodimerization of WT with Dex from HeLa cell determined at the chapter 3.

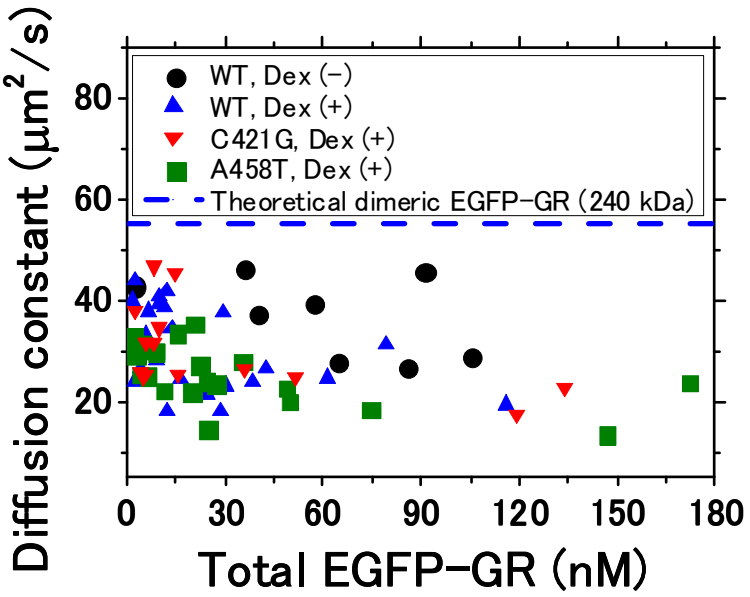

Fig. 4-8 Comparison of complex formation for EGFP-GR of WT and mutants with and without Dex

Diffusion constants of EGFP-GR of WT and mutants with and without Dex treatment. Filled black circle: EGFP-GR_{WT} without Dex (N = 28), Filled blue triangle: EGFP-GR_{WT} with Dex (N = 25), Filled red reverse triangle: EGFP-GR_{C421G} with Dex (N = 14), Filled dark green square: EGFP-GR_{A458T} with Dex (N = 21), Blue dashed line: Theoretical diffusion constant of homodimeric EGFP-GR calculated by molecular weight (240 kDa).

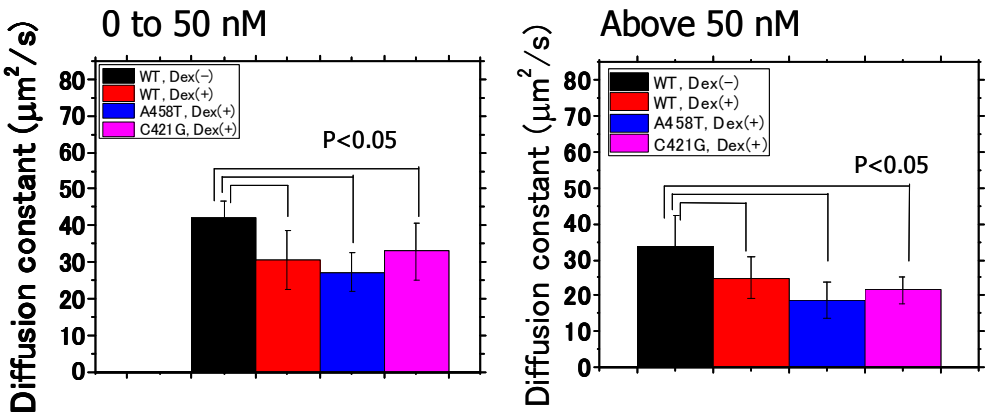

Fig. 4-9 Statistical difference of complex formation between EGFP-GRs of WT and mutants with and without Dex

The average and standard deviation of diffusion constant of EGFP-GR of WT and mutants with and without Dex in 0 to 50 nM concentration and above 50 nM concentration. Filled black bar: EGFP-GR_{WT} without Dex, Filled red bar: EGFP-GR_{WT} with Dex, Filled blue bar: EGFP-GR_{A458T} with Dex, Filled pink bar: EGFP-GR_{C421G} with Dex. There are significant difference between WT in the absence of Dex and WT and mutants in the presence of Dex. ($P<0.05$)

4.3.2 Determination of dissociation constant of EGFP-GR for homodimerization from U2OS cell using FCCS-microwell system

EGFP- or tandem dimer of mCherry-fused GR (EGFP-GR and mCh_2-GR) were transiently co-expressed in U2OS cells. FCCS measurement was combined with microwell system (FCCS-microwell system). The FCCS-microwell system determined the concentration of total EGFP-GR and mCh_2-GR from autocorrelation functions, and the concentration of heterodimeric EGFP-GR and mCh_2-GR from cross-correlation function. Using these parameters, the dissociation constant for homodimerization was determined by FCCS measurements of EGFP-GR and mCh_2-GR. Typical images of the U2OS cell expressing EGFP- or mCh_2-GR_{WT}, EGFP- or mCh_2-GR_{C421G} and EGFP- or mCh_2-GR_{A458T} (Fig. 4-10).

GR_{WT}, GR_{C421G} and GR_{A458T} localized in nucleus in the presence of Dex, but not localized in nucleus in the absence of Dex. After cell lysis, the fluorescent signal decreased in the cell, indicating that EGFP- or mCh_2-fused GR extracted from the cell by lysis buffer. FCCS measurements were performed in microwells after 90 min cell lysis and typical autocorrelation functions, cross-correlation function and their fit residuals were shown in Fig. 4-11. The cross-correlation function was clearly observed in all data. In contrast, cross-correlation function was not observed in the co-expression of EGFP and mCh_2 (data not shown). These data indicated that the heterodimer of EGFP-GR and mCh_2-GR formed. To determine the dissociation constant for homodimerization, the concentration of $[G_{free}]$ and $[R_{free}]$ was calculated by equations (4-26) and (4-27). The scatter plot analysis and linear fitting determined the dissociation constant for homodimerization of WT and mutants (Fig. 4-12). The dissociation constant for homodimerization was determined to be 468±24 nM in WT without Dex, and 157±22 nM, 219±32 nM and 382±51 nM in WT, C421G and A458T with Dex, respectively. These dissociation constants for homodimrization were summarized in Fig. 4-13. According to t-test, there are significant differences of WT and C421G mutant with Dex against WT without Dex, but not A458T with Dex. The similar value of dissociation constant for homodimerization was determined between FCS-microwell system and FCCS-microwell system. This indicated that FCS-microwell system determine the concentration of EGFP-GR and dissociation constant for homodimerization of WT and mutants precisely.

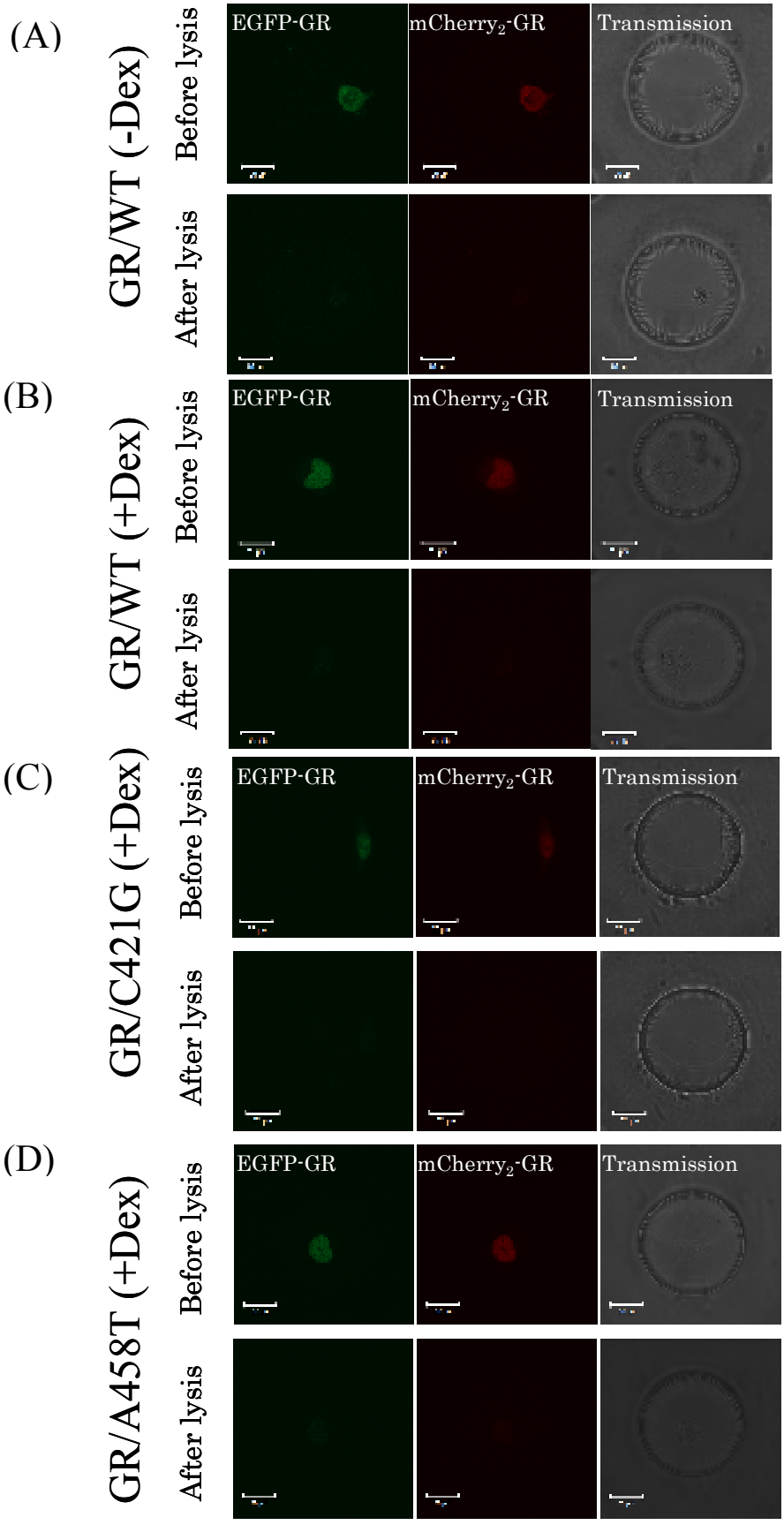
(A)
GR/WT (-Dex)
Before lysis
After lysis
EGFP-GR
mCherry2-GR
Transmission
(B)
GR/WT (+Dex)
Before lysis
After lysis
EGFP-GR
mCherry2-GR
Transmission
(C)
GR/C421G (+Dex)
Before lysis
After lysis
EGFP-GR
mCherry2-GR
Transmission
(D)
GR/A458T (+Dex)
Before lysis
After lysis
EGFP-GR
mCherry2-GR
Transmission

Fig. 4-10 Typical localization of GR_{WT} and mutants

Typical images of EGFP- or mCh2-GR before and after cell lysis. **(A)** WT without Dex. **(B)** WT with Dex. **(C)** C421G with Dex. **(D)** A458T with Dex. Scale bar: 20 μm.

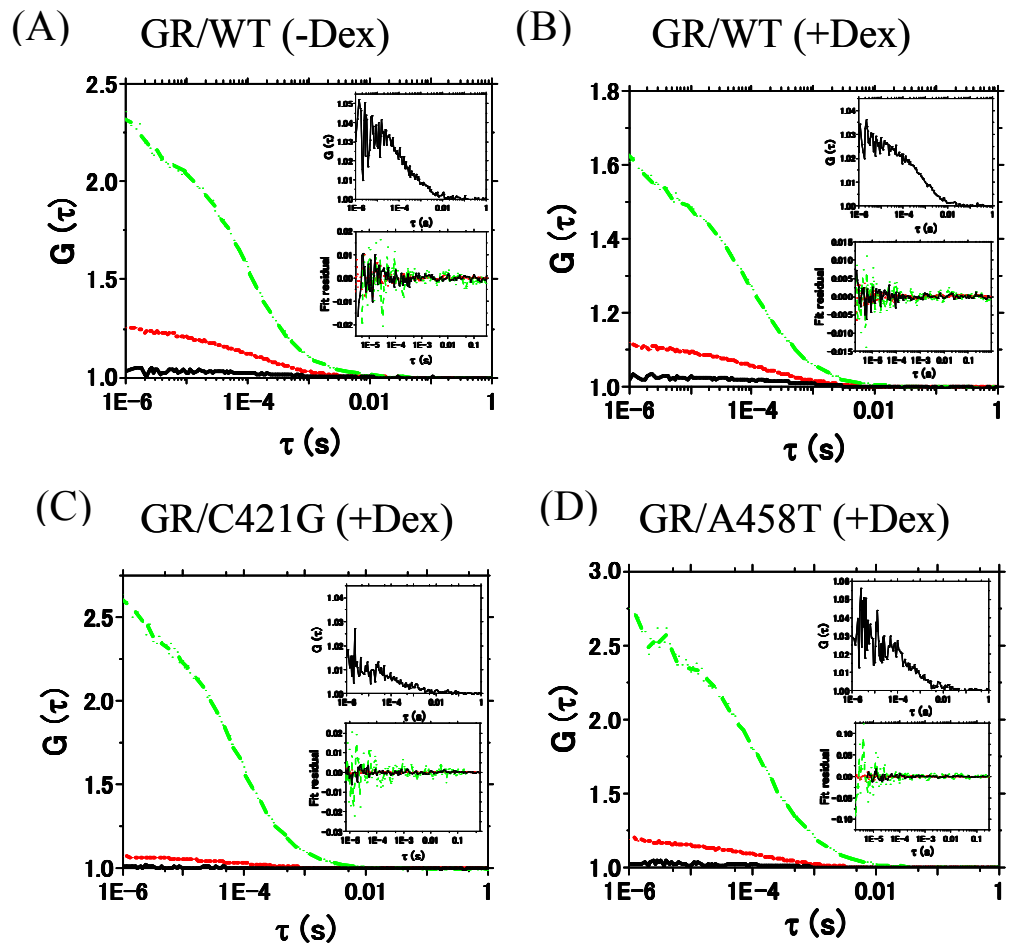

Fig. 4-11 FCCS measurements in microwell

Typical auto- and cross-correlation function of EGFP- or mCh_2-GR. The green dashed line, red dotted line and black solid line denotes the autocorrelation function of the EGFP-GR ($G_G(\tau)$), autocorrelation function of the mCh_2-GR ($G_R(\tau)$) and the cross-correlation function ($G_C(\tau)$), respectively. The insets show the enlarged cross-correlation function and fit residuals. **(A)** WT without Dex. **(B)** WT with Dex. **(C)** C421G with Dex. **(D)** A458T with Dex.

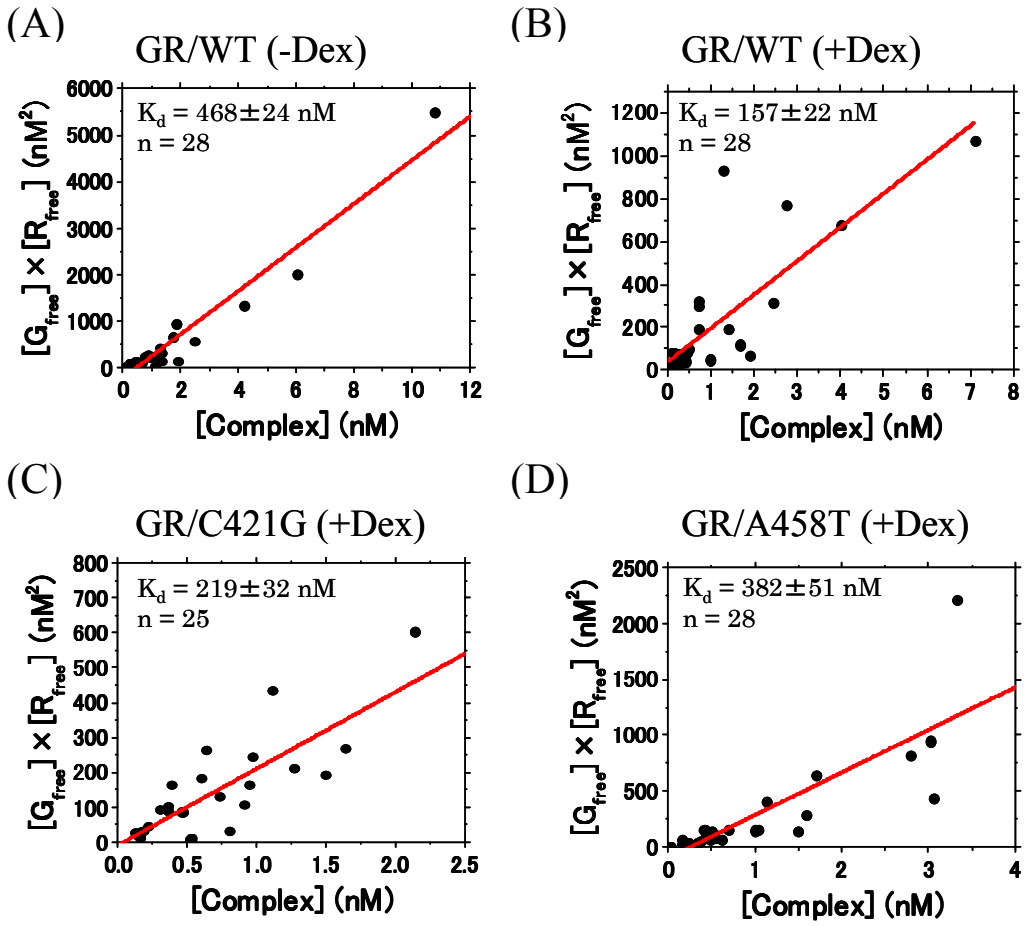

Fig. 4-12 Determination of dissociation constant for homodimerization of GR

The dissociation constant determined using scatter plot and linear fitting. The plots represent the product of concentration of the free EGFP-GR and mCh_2-GR against the concentration of the complex of EGFP-GR and mCh_2-GR. The solid red line shows the linear fitting. The slope indicates the dissociation constant for homodimerization. **(A)** WT without Dex (K_d: 468±23 nM). **(B)** WT with Dex (K_d: 157±22 nM). **(C)** C421G with Dex (K_d: 219±32 nM). **(D)** A458T with Dex (K_d: 382±52 nM).

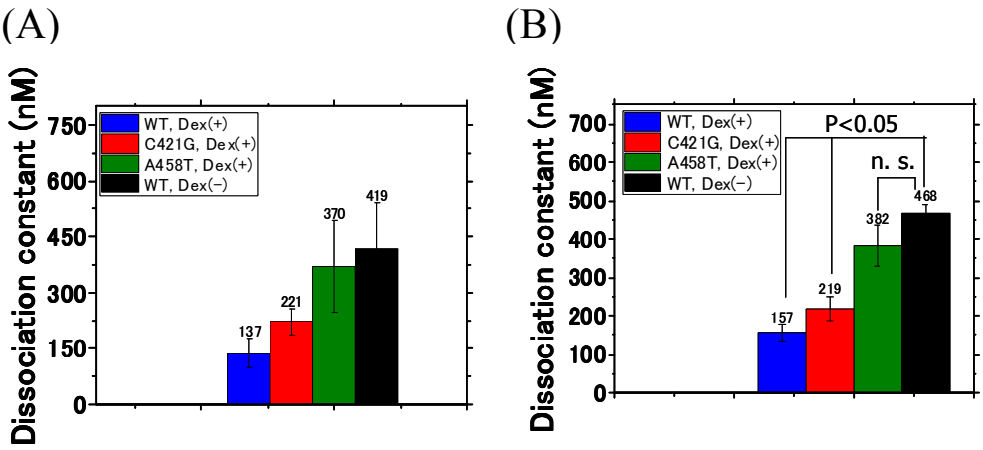

Fig. 4-13 Comparison of dissociation constant for homodimerization of GR between FCS-microwell system and FCCS-microwell system

(A) The dissociation constant for homodimerization determined using FCS-microwell system. **(B)** The dissociation constant for homodimerization determined using FCCS-microwell system. Blue bar: WT with Dex, Red bar: C421G with Dex, Green bar: A458T with Dex, Black bar: WT without Dex.

4.4 Discussion

The homodimerization of GR for WT was determined from HeLa cell in chapter 3. However, HeLa cells have the expression of endogenous GR. Therefore, GR formed pseudo dimer between EGFP-GR_{WT} and endogenous GR even if EGFP-GR_{WT} was overexpressed in HeLa cells. In this chapter, the homodimerization of GR for WT was determined in U2OS, which have no expression of endogenous GR. The dissociation constant for homodimerization of WT in the presence of Dex was determined to be 107±19 nM in HeLa cell and 137±37 nM in U2OS cell (Fig. 4-7). The homodimerization was similar between HeLa cell and U2OS cell, indicating that the effect of endogenous GR is negligible effect to determine the dissociation constant for homodimerization of GR.

Moreover, DNA-binding deficient mutant (C421G) and homodimerization deficient

mutant (A458T) was measured by FCS-microwell system. The dissociation constant for homodimerization of C421G mutant was lower than that of WT in the absence of Dex, but slightly higher than that of WT in the presence of Dex (Fig. 4-7). This suggests that the DNA binding of GR is not necessary for the homodimerization of GR. It is well-known that GR homodimerize via the surface of DNA-binding domain and A458T mutant inhibits homodimerization of GR. The dissociation constant for homodimerization of A458T mutant was similar to that of WT without Dex (Fig. 4-7), indicating that the homodimerization was inhibited by point mutation of A458T. If all molecules of EGFP-GR are monomeric states in living cell, the dissociation constant for homodimerization of GR should be infinite. However, the dissociation constant of A458T with Dex was 370 nM. It may be an effect of over-expression of A458T mutant, because homodimerization of A458T mutant was observed at high expression level of GR by immunorecipitation, FRET analysis and Number and Brightness analysis [18, 39].

Fluorescence cross-correlation spectroscopy (FCCS) determined easily the interaction between two-color-fluorescent molecules labeled particles, such as protein, DNA and so on. EGFP-fused GR and mCh_2-fused GR were co-expressed in U2OS cells and FCCS-microwell system was used to determine the dissociation constant for homodimrization of GR. The dissociation constant for homodimrization of WT in the absence of Dex and WT, C421G and A458T in the presence of Dex was similar between FCS-microwell system and FCCS-microwell system (Fig. 4-12). This result suggests that FCS-microwell system could determine the concentration of homodimeric GR and dissociation constant for homodimerization precisely.

FCS measurements determined the diffusion constant as well as concentration. The molecular size contributed diffusion constant. All data was lower than the theoretical diffusion constant calculated from molecular weight of homodimeric EGFP-GR (240 kDa) (Fig. 4-8). This suggests that EGFP-GR formed not only homodimer, but also large-molecular-weight complex with endogenous interacting proteins in U2OS cells, as well as HeLa cells. There are

no significant difference of complex formation between WT and mutants with Dex, suggesting that the complex formation are not dependent on the DNA binding and homodimerization of GR. In contrast, there are significant differences between WT in the absence of Dex and WT and mutants in the presence of Dex, indicating that the complex formation is different between unliganded GR and liganded GR. Before ligand binding, molecular chaperones, Hsp40, Hsp70 and Hsp90 interact with unligand GR [6, 7]. In contrast, liganded GR interacts with cofactors to regulate transcription of target genes [61-63].

Chapter 5

The relationship between homodimer and transcriptional activity of glucocorticoid receptor using FCS-microwell system

5.1 Introduction

The human glucocorticoid receptor α (GR) is a ligand-induced transcription factor which belongs to the nuclear receptor superfamily [1-3]. It is well-known that liganded GRs homodimerize and transactivate several target genes in the nucleus as described in chapter 1 [9-15].Therefore, its homodimerization property is essential for the regulation of the GR transactivation. The property of homodimerization and complex formation for WT and mutants was determined with and without Dex in the chapter 3 and 4. However, the relationship between the homodimer of GR and transcriptional activity still remains unclear. Recently, one report suggested that the ratio of monomers and homodimers of GR does not necessarily change the transcriptional activity determined by comparison of Number and Brightness analysis in living cells and quantitative real-time PCR using a whole cell lysate [18]. The quantitative real-time PCR method for transcriptional activity analysis is one of bulk measurements. It may be suggested that single-cell analysis of homodimer and transcriptional activity from same single cell is needed to understand the relationship between homodimer of GR and transcriptional activity.

FCS-microwell system is a simple method to determine the concentration of

homodimeric EGFP-GR and dissociation constant for homodimerization of EGFP-GR from two different cell line, HeLa and U2OS cell. A combination method of FCS-microwell system and transcriptional activity assay can reveal the relationship between the homodimer and transcriptional activity in single-cell level. Quantitative real-time PCR and luciferase assay have been widely used to determine the transcriptional activity [18, 39], but the components of PCR reaction or the chemical substrate, luciferin is necessary to determine the transcriptional activity. FCS-microwell system with quantitative real-time PCR or luciferase assay is difficult, because cell lysate in microwell can not be applied to PCR tube or luciferin can not be added into microwell after cell lysis. Therefore, fluorescent-protein reporter assay was selected [50-52]. The mouse-mammalian tumor virus (MMTV) promoter region is well characterized and widely used for transcriptional activity of GR [18, 53-55]. The five GREs were identified in this promoter region (one palindormic GRE and four half GREs).

In this chapter, FCS-microwell system was combined with fluorescent reporter assay and triple-color fluorescence correlation spectroscopy was performed in microwell after cell lysis to determine the concentration of homodimeric EGFP-GR and transcriptional activity from the same single cell.

5.2 Materials and methods

5.2.1 Constructs and chemicals

The expression vectors for EGFP-GR_{WT} and EGFP-GR_{A458T} were described previously [22, 36]. To determine the transcriptional activity, the vector encoded the mouse-mammalian tumor virus (MMTV) promoter region and fluorescent protein, mKO2 in downstream of MMTV promoter region (pMMTV-mKO2) was constructed. MMTV promoter region was amplified by PCR and forward primer with AseI and reverse primer with NheI. The vector encoded mKO2 and fragment of MMTV were digested by AseI and NheI sequentially. The linear DNA of mKO2 and digested MMTV were ligated by Ligation Mix (TAKARA).

Dex was used at a concentration of 0.5 μM in opti-MEM (GIBCO) for activation of GR. The components of the lysis buffer were 80% CelLytic M Cell Lysis Reagent (Sigma-Aldrich), 1% Protease Inhibitor Cocktail (Sigma-Aldrich), 10 mM $MgCl_2$, 0.1% SDS and 200 U/mL Benzonase nuclease (Sigma-Aldrich) for FCS-microwell system and 80% CelLytic M Cell Lysis Reagent, 1% Protease Inhibitor Cocktail for the FCCS measurements toward DNA binding affinity analysis.

5.2.2 Construction of Alexa647-labeled GRE

The perfect palindrome GRE (PpGRE), imperfect palindrome GRE (IpGRE) and half GRE (hGRE) were constructed. For PpGRE, 100 μM sense-oligonucleotide labeled by Alexa647 and 100 μM antisense-oligonucleotide was annealed at gradient decrease of temperature from 95 to 4°C. For IpGRE and hGRE, 100 mM Alexa647-labeled primer was annealed to template DNA and elongated by Klenow fragment. Then, the unreacting oligonucleotide was digested by exonuclease for 1 hour at 37 ºC. The Alexa647-labeled GREs was purified by spin column. The sequence of IpGRE and hGRE is originated from the MMTV promoter region.

(A) PpGRE

5'-Alexa647-TCGAGGGATCCGAATTCA**AGAACA**CTG**TGTTCT**CTC-3'
3'-AGCTCCCTAGGCTTAAGT**TCTTGT**GAC**ACAAGA**GAG-5'

(B) IpGRE

5'-Alexa647-TCGAGGGATCCGAATTC**AGAACA**GTT**TGTAAC**CAAAAACT-3'
3'-AGCTCCCTAGGCTTAAG**TCTTGT**CAA**ACATTG**GTTTTTGA-5'

(C) hGRE

5'-Alexa647-TCGAGGGATCCGAATTC**AGAACA**GGT**GCAAGG**ACTATTGA-3'
3'-AGCTCCCTAGGCTTAAG**TCTTGT**CCA**CGTTCC**TGATAACT-5'

Fig. 5-1 Sequence of perfect palindrome-, imperfect palindrome- and half-GRE

The palindrome GRE has two 6 nucleotides (Red letter) and 3 nucleotides as a spacer. In contrast, hGRE has one binding site of GR. **(A)** perfect palindrome GRE **(B)** imperfect palindrome GRE **(C)** half GRE.

5.2.3 Cell culture and transfection in microwells

U2OS cells were cultured in McCoy's 5A modified medium (GIBCO) supplemented with charcoal-stripped 10% FBS at 37 ºC with 5% CO_2. To culture the U2OS cells, the microwells on the PDMS chips were washed using a detergent water, which was then evaporated in a glass vacuum dryer to remove the water from the microwells. After evaporation, the cell culture medium containing the U2OS cell suspension was poured onto the PDMS chip in a 6-well plate dish and incubated for 4 hours at 37 ºC.

The subset of plasmid encoded 0.3 μg pEGFP, 0.7 μg empty vector, 4 μg pMMTV-mKO2 and 0.1 μg TagRFP675 or 1 μg pEGFP-GR, 4 μg pMMTV-mKO2 and 0.1 μg TagRFP675 were transfected to U2OS cells on 6-well plate dishes using ViaFact reagent (Promega). TagRFP675 is a transfection control to monitor the relative amount of transfected plasmid. After replacement of the culture medium on dishes with fresh medium, the plasmids were mixed with ViaFact in opti-MEM and added to the cell culture dishes. After 6 hours incubation at 37^{O}C with 5% CO_2, the medium on the dishes was changed to fresh one and the U2OS cells was incubated at 37^{O}C with 5% CO_2 for 18 hours. The transfected U2OS cells were treated 500 nM Dex 14 hours. After 14 hours treatment of Dex, the transfected U2OS cells were trypsinized and transferred to the microwells on the PDMS chips. The transfected U2OS cells were incubated with Dex on the microwell for 4 hours additionally. Total incubation time of Dex was 18 hours.

5.2.4 Single-cell method to detect the homodimer of GR

The PDMS chip was attached to a glass stick with double-sided tape (Nitoms, Tokyo, Japan) and pressed onto a coverslip in dexamethasone (Dex) with opti-MEM. After pressing the PDMS chip on coverslip, the position (a number and a letter) of the microwells in which single cell was cultured were noted down. The medium on the coverslip was changed to lysis buffer and the protein extracted from each cell was kept in the microwell after cell lysis,

following which FCS measurements were carried out in each microwell. The detailed method was described in the chapter 3.

5.2.5 LSM imaging and FCS measurements

LSM imaging and FCS measurements of EGFP or EGFP-GR, mKO2 and TagRFP675 were performed using an LSM510-ConfoCor2 (Carl Zeiss, Jena, Germany) equipped with an Ar ion laser, He-Ne laser water immersion objective (C-Apochromat, 40X, 1.2N.A., Corr, Carl Zeiss, Jena, Germany), photomultipliers for LSM imaging and avalanche photodiode detectors for FCS measurements (Fig. 5-2). EGFP, mKO2 and TagRFP675 were excited with 488 nm, 543 nm and 633 nm, respectively. The pinhole size was 140 μm for EGFP, 1000 μm for mKO2 and 280 μm for TagRFP675 in LSM imaging. The pinhole size was 70 μm for EGFP, 78 μm for mKO2 and 90 μm for TagRFP675 in FCS measurement. The fluorescent signal of EGFP, mKO2 and TagRFP675 was collected through band pass filter 500-530 nm, 565-615 nm and long pass filter 650 in LSM imaging, respectively. The fluorescent signal of EGFP, mKO2 and TagRFP675 was collected through band pass filter 505-550, 565-615 and long pass filter 650 in FCS measurement, respectively. The LSM imaging and FCS measurements were performed sequentially for EGFP/TagRFP675 and mKO2. The fluorescence was split by the dichroic mirror (635 nm). FCS measurements were performed 5 times with durations of 10 seconds.

For multi-color imaging and FCS measurements, cross talk signal in each detector is serious problem to quantify the concentration of fluorescent proteins. The cross talk signal was confirmed by triple-color FCS measurements with lysates containing each fluorescent protein. The counts per particle (CPP) from FCS was summarized in Table 5-1. If high CPP value is observed, the cross talk signal from other proteins flows into the detector. The high CPP value was determined by optimal setup for each fluorescent protein. This set of fluorescent proteins and FCS measurement method could determine the concentration of

EGFP, mKO2 and TagRFP675 with low cross-talk signal.

molecule	Channel name	Filter	543 nm (2%)	488 nm (1.5%), 633 nm (30%)
EGFP	EGFP ch	BP505-550	-	10.060
	mKO2 ch	BP560-610	0.008	-
	TagRFP675 ch	LP650	-	0.029
mKO2-CL1	EGFP ch	BP505-550	-	0.385
	mKO2 ch	BP560-610	8.264	-
	TagRFP675 ch	LP650	-	0.400
TagRFP675	EGFP ch	BP505-550	-	0.125
	mKO2 ch	BP560-610	0.062	-
	TagRFP675 ch	LP650	-	6.844

Table. 5-1 Confirmation of cross-talk signal toward triple-color FCS measurements

The each lysate containing single-fluorescent protein, EGFP, mKO2 or TagRFP675 was measured by triple-color FCS measurement. Orange column: Comparison of CPP in mKO2 channel, Blue column: Comparison of CPP in EGFP channel, Red column: Comparison of CPP in TagRFP675 channel.

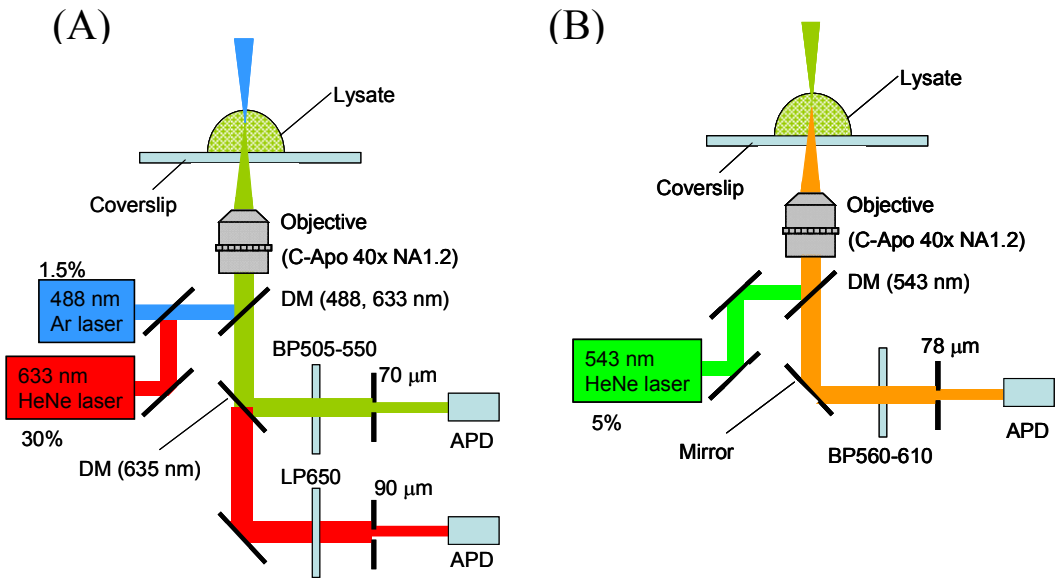

Fig. 5-2 Optical setup for triple-color FCS measurement

The continuous-wave Ar ion laser (488 nm) and He-Ne laser (543 nm and 633 nm) were used for the excitation of EGFP, mKO2 and TagRFP675, respectively. **(A)** Dichroic mirror represents 635 nm beam splitter. BP505-550 and LP650 represent band pass filter 505-550 nm and long pass filter 650 nm, respectively. The fluorescence was detected at 505-550 nm for EGFP and above 650 nm for TagRFP675. **(B)** The mKO2 was measured separately between EGFP/TagRFP675 and mKO2. BP560-610 represents long pass filter 560-610 nm. The fluorescence was detected at 560-610 nm for mKO2.

5.2.6 FCCS measurements toward DNA binding ability

EGFP, EGFP-GR_{WT} or EGFP-GR_{A458T} was transfected in the U2OS cells and the transfected cells were collected. The cell lysis was performed by appropriate lysis buffer volume, representing single cell lysis in microwell. The mixture of EGFP-GR lysate and Alexa647-labeled GRE was measured by FCCS.

FCCS measurements were performed using Confocor2 (Carl Zeiss, Jena, Germany) equipped with an Ar ion laser, He-Ne laser, water immersion objective (C-Apochromat, 40X,

1.2N.A., Corr, Carl Zeiss, Jena, Germany) and two avalanche photodiode detectors for FCCS measurements (Fig. 5-3). EGFP was excited at the 488 nm laser and Alexa647 was excited at the 633 nm laser. The pinhole diameter was adjusted to 70 μm for EGFP and 90 μm for Alexa647. The emission signals were split by a dichroic mirror (635 nm beam splitter) and detected at 505-550 nm for EGFP and above 650 nm for Alexa647 for FCCS measurements. FCCS measurements were performed 5 times with durations of 30 seconds.

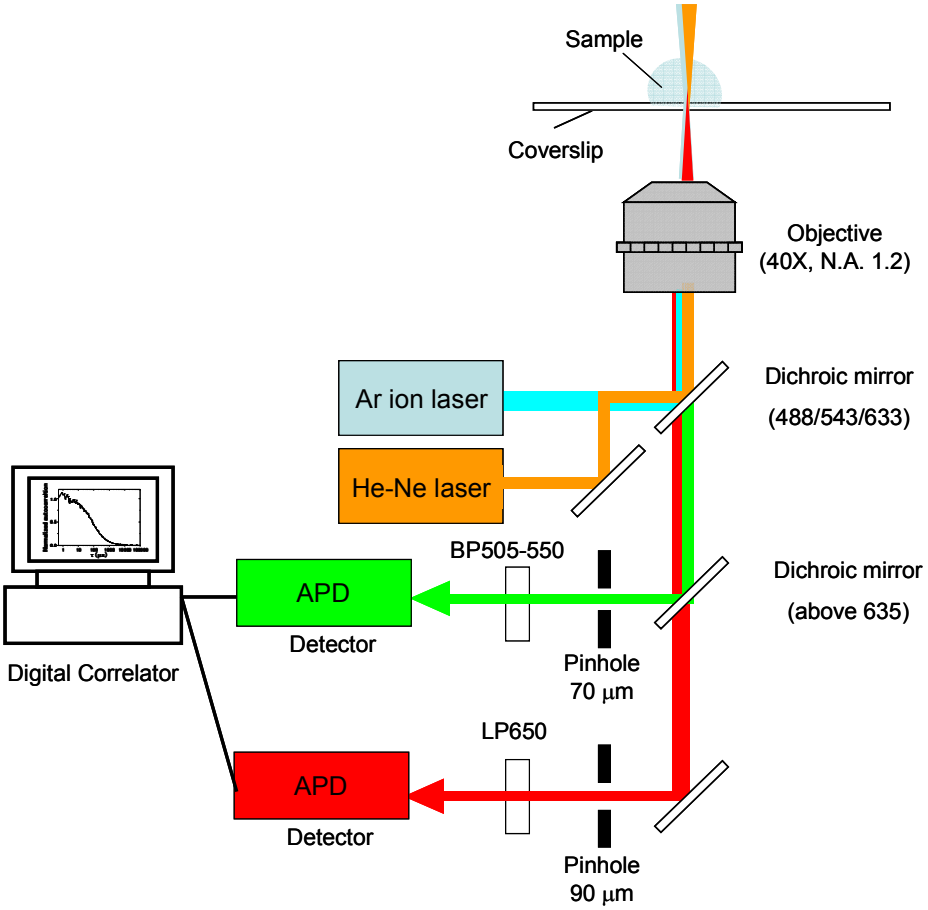

Fig. 5-3 Optical setup for FCCS measurement

The continuous-wave Ar ion laser (488 nm) and He-Ne laser (633 nm) were used for the excitation of EGFP and Alexa647, respectively. Dichroic mirror represents 635 nm beam splitter. BP505-550 and LP650 represent band pass filter 505-550 nm and long pass filter 650 nm, respectively. The fluorescence was detected at 505-550 nm for EGFP and above 650 nm for Alexa647.

5.2.7 Data analysis for the concentration of homodimer of EGFP-GR and transcriptional activity

Data obtained from triple-color FCS measurements were calculated with AIM software (Carl Zeiss, Jena, Germany). The autocorrelation function, $G_i(\tau)$ was defined as follows:

$$G_i(\tau) = \frac{\langle I_i(t) I_i(t+\tau) \rangle}{\langle I_i(t) \rangle^2} \quad \text{- (5-1)}$$

where i = EGFP-GR, mKO2 or TagRFP675 and τ shows the delay time, I is fluorescent intensity and $G_i(\tau)$ denotes the autocorrelation function, respectively. The obtained autocorrelation functions were fitted using a one-component model as follows:

$$G_i(\tau) = 1 + \left(1 + \frac{F_{i,\text{triplet}} e^{-\frac{\tau}{\tau_{i,\text{triplet}}}}}{1 - F_{i,\text{triplet}}} \right) \cdot \frac{1}{N_i} \left(1 + \frac{\tau}{\tau_{i,D}} \right)^{-1} \cdot \left(1 + \frac{1}{{s_i}^2} \frac{\tau}{\tau_{i,D}} \right)^{-\frac{1}{2}} \quad \text{- (5-2)}$$

where i = EGFP-GR, mKO2 or TagRFP675 and F_{triplet} is the average fraction of triplet state molecules, τ_{triplet} is the average relaxation time and τ_D is the average diffusion time of molecules. The diffusion constant of EGFP-GR was calculated from the diffusion constant of a standard molecule, rhodamine 6G (D_{R6G}; 414 μm^2/s [31]) and the ratio of diffusion times τ_{R6G} and τ_D. N is the average number of fluorescent molecules in the effective observation volume ($V_{i,\text{eff}}$) defined by 3D Gaussian volume elements with lateral radius $w_{i,0}$ and axial radius $z_{i,0}$. s_i shows the structure parameter representing the ratio of $w_{i,0}$ to $z_{i,0}$ ($s_i = z_{i,0}/ w_{i,0}$). $w_{i,0}$ and $z_{i,0}$ were determined by calibration measurement of R6G (D_{R6G}; 414 μm^2/s [31]) for EGFP and mKO2 detector, and Alexa647 (D_{Alexa647}; 430 μm^2/s [56]) for TagRFP675 detector.

$$w_{i,0} = \sqrt{4D_i \cdot \tau_i} \quad \text{-(5-3)}$$

$$s_i = \frac{z_{i,0}}{w_{i,0}} \quad \text{-(5-4)}$$

.

The effective observation volume was calculated using the following equation.

$$V_{i,\mathrm{eff}} = \pi^{\frac{3}{2}} \cdot w_{i,0}^2 \cdot z_{i,0} \quad \text{-(5-5)}$$

To remove the effect of background fluorescence on the obtained N_{meas}, the corrected N (N_{corr}) was calculated as follows [32, 33]:

$$N_{i,\mathrm{corr}} = \frac{N_{i,\mathrm{meas}} \cdot (I_{i,\mathrm{meas}} - I_{i,\mathrm{B}})^2}{(I_{i,\mathrm{meas}})^2} \quad \text{-(5-6)}$$

where i = EGFP-GR, mKO2 and TagRFP675. $N_{i,\mathrm{meas}}$ is the number of molecules obtained from FCS measurements, $I_{i,\mathrm{meas}}$ is the measured average fluorescent intensity and $I_{i,\mathrm{B}}$ is the background average fluorescent intensity from FCS measurement of a non-transfected HeLa cell lysate.

The concentration of fluorescent molecules ([$C_{i,\mathrm{corr}}$]) was calculated from the effective observation volume ($V_{i,\mathrm{eff}}$), corrected number of molecules ($N_{i,\mathrm{corr}}$) and Avogadro's number ($\mathrm{N_A}$) as given below.

$$\left[C_{i,\mathrm{corr}}\right] = \frac{N_{i,\mathrm{corr}}}{V_{i,\mathrm{eff}} \cdot \mathrm{N_A}} \quad \text{-(5-7)}$$

To obtain the concentration of monomeric and homodimeric GR, [M] and [D], the monomeric fraction F_{m} and homodimeric fraction F_{d} (F_{m}+F_{d} = 1) of EGFP-GR were calculated using equations (5-8), (5-9) and (5-10). FCS measurement can be used to obtain the apparent number of molecules and brightness, which is defined as the counts per particle (CPP). When monomeric and homodimeric EGFP-GR are contained in the lysate, the apparent CPP ($CPP_{\mathrm{EGFP\text{-}GR,app}}$) is obtained as shown by the following equation [38].

$$CPP_{\text{EGFP-GR, app}} = \frac{F_{\text{m}} \cdot \eta_{\text{m}}^{2} + F_{\text{d}} \cdot \eta_{\text{d}}^{2}}{F_{\text{m}} \cdot \eta_{\text{m}} + F_{\text{d}} \cdot \eta_{\text{d}}} \quad \text{-(5-8)}$$

where η_{m} and η_{d} are the CPP of monomeric and homodimeric EGFP-GR, respectively. If the CPP of the tandem dimer of EGFP is twice that of EGFP (Fig. 3-2), the CPP of homodimeric EGFP-GR (η_{d}) will be twice the CPP of monomeric EGFP-GR (η_{m}), which is the same as that of EGFP (CPP_{EGFP}).

$$\eta_m = CPP_{\text{EGFP}} \quad \text{-(5-9)}$$

$$\eta_d = 2 \cdot CPP_{\text{EGFP}} \quad \text{-(5-10)}$$

By using equations (5-8), (5-9) and (5-10), the fractions of monomeric and homodimeric EGFP-GR (F_{m} and F_{d}) were shown as equations (5-11) and (5-12).

$$F_m = \frac{4 - 2R}{3 - R} \quad \text{-(5-11)}$$

$$F_d = \frac{R - 1}{3 - R} \quad \text{-(5-12)}$$

where,

$$R = \frac{CPP_{\text{EGFP-GR, app}}}{CPP_{\text{EGFP}}} \quad \text{-(5-13)}$$

5.2.8 FCCS data analysis and determination of dissociation constant between EGFP-GR and Alexa647-labeled GRE

Data acquired from FCCS were calculated with AIM software (Carl Zeiss, Jena, Germany). The autocorrelation functions from green and red channels, $G_{\text{G}}(\tau)$, $G_{\text{R}}(\tau)$ and the

cross-correlation function $G_C(\tau)$ were calculated as follows:

$$G_G(\tau) = \frac{\langle I_G(t) I_G(t+\tau) \rangle}{\langle I_G(t) \rangle^2} \quad \text{-(5-14)}$$

$$G_R(\tau) = \frac{\langle I_R(t) I_R(t+\tau) \rangle}{\langle I_R(t) \rangle^2} \quad \text{-(5-15)}$$

$$G_C(\tau) = \frac{\langle I_G(t) I_R(t+\tau) \rangle}{\langle I_G(t) \rangle \cdot \langle I_R(t) \rangle} \quad \text{-(5-16)}$$

where τ denotes the delay time, I_G is the fluorescent intensity of the green channel, I_R is the fluorescent intensity of the red channel and $G_G(\tau)$, $G_R(\tau)$ and $G_C(\tau)$ denote the autocorrelation functions of green, red and cross-correlation function, respectively. The acquired auto- and cross-correlation functions were fitted using one-component model as follows:

$$G_{auto}(\tau) = 1 + \left(1 + \frac{F_{triplet} e^{-\frac{\tau}{\tau_{triplet}}}}{1 - F_{triplet}} \right) \cdot \frac{1}{N} \left(1 + \frac{\tau}{\tau_D} \right)^{-1} \cdot \left(1 + \frac{1}{s^2} \frac{\tau}{\tau_D} \right)^{-\frac{1}{2}} \quad \text{-(5-17)}$$

$$G_{cross}(\tau) = 1 + \frac{1}{N} \left(1 + \frac{\tau}{\tau_D} \right)^{-1} \cdot \left(1 + \frac{1}{s^2} \frac{\tau}{\tau_D} \right)^{-\frac{1}{2}} \quad \text{-(5-18)}$$

where $F_{triplet}$ is the average fraction of triplet state molecules, $\tau_{triplet}$ is the average relaxation time and τ_D is the average diffusion time of molecules. N is the average number of fluorescent particles in the effective observation volume defined by lateral radius w_0 and axial radius z_0 of the confocal volume element, and s is the structural parameter ($s = z_0/w_0$). The values of $w_{0,i}$ and $z_{0,i}$ (i = G or R) are determined from the diffusion constant of the rhodamine 6G (R6G, D_{R6G}: 414 μm^2/s [31]) and Alexa 647 ($D_{Alexa647}$: 330 μm^2/s [56]) used as standard

fluorescent dyes, respectively.

$$w_{0,i} = \sqrt{4D \cdot \tau_{\mathrm{D},i}} \qquad \text{-(5-19)}$$

$$s_i = \frac{z_{0,i}}{w_{0,i}} \qquad \text{-(5-20)}$$

The effective volume ($V_{\mathrm{eff},i}$) are calculated as following:

$$V_{\mathrm{eff},i} = \pi^{\frac{3}{2}} \cdot w_{0,i}^2 \cdot z_{0,i} \qquad \text{-(5-21)}$$

$$V_{\mathrm{eff,C}} = \left(\frac{\pi}{2}\right)^{\frac{3}{2}} \cdot (\omega_{0,\mathrm{G}}^2 + \omega_{0,\mathrm{R}}^2)(z_{0,\mathrm{G}}^2 + z_{0,\mathrm{R}}^2)^{\frac{1}{2}} \qquad \text{-(5-22)}$$

The average number of green fluorescent particles (N_{G}), red fluorescent particles (N_{R}) and particles that have both green and red fluorescence (N_{C}) are give by

$$N_{\mathrm{G}} = \frac{1}{G_{\mathrm{G}}(0) - 1} \qquad \text{-(5-23)}$$

$$N_{\mathrm{R}} = \frac{1}{G_{\mathrm{R}}(0) - 1} \qquad \text{-(5-24)}$$

$$N_{\mathrm{C}} = \frac{G_{\mathrm{C}}(0) - 1}{(G_{\mathrm{G}}(0) - 1) \cdot (G_{\mathrm{R}}(0) - 1)} \qquad \text{-(5-25)}$$

To remove the effect of background fluorescence on the obtained N_{meas}, the corrected N (N_{corr}) was calculated as follows [32, 33]:

$$N_{i,\mathrm{corr}} = \frac{N_{i,\mathrm{meas}} \cdot (I_{i,\mathrm{meas}} - I_{i,\mathrm{B}})^2}{(I_{i,\mathrm{meas}})^2} \qquad \text{-(5-26)}$$

Where $N_{i,\mathrm{meas}}$ is the average numbers of green or red fluorescent particles obtained from each autocorrelation function and fitting analysis (i = G or R). $I_{i,\mathrm{meas}}$ is the average intensity of green or red fluorescent particles during FCCS measurement (i = G or R). $I_{i,\mathrm{B}}$ was the average background intensity of green or red fluorescence obtained from FCCS

measurements of non-transfected U2OS cell lysate (i = G or R). To use the corrected number of molecules for green and red particles from equation (5-26), the apparent number of cross was corrected as following equation:

$$N_{\mathrm{C,corr}} = (G_{\mathrm{C,corr}}(0) - 1) \cdot N_{\mathrm{G,corr}} \cdot N_{\mathrm{R,corr}} \quad \text{-(5-27)}$$

where,

$$(G_{\mathrm{C,corr}}(0) - 1) = (G_{\mathrm{C,meas}}(0) - 1) \cdot \frac{I_{\mathrm{G,meas}} \cdot I_{\mathrm{R,meas}}}{\left(I_{\mathrm{G,meas}} - I_{\mathrm{G,B}}\right) \cdot \left(I_{\mathrm{R,meas}} - I_{\mathrm{R,B}}\right)} \quad \text{-(5-28)}$$

The concentration of each fluorescent protein was calculated with the use of N_A (Avogadro's number) as give below:

$$\left[C_{i,\mathrm{corr}}\right] = \frac{N_{i,\mathrm{corr}}}{V_{i,\mathrm{eff}} \cdot \mathrm{N_A}} \quad \text{-(5-29)}$$

$$\left[C_{\mathrm{C,corr}}\right] = \frac{N_{\mathrm{C,corr}}}{V_{\mathrm{C,eff}} \cdot \mathrm{N_A}} \quad \text{-(5-30)}$$

where, i = G or R

The dissociation constant for EGFP-GR binding to Alexa647-labeled GRE was determined using following equation:

$$K_{\mathrm{d}} = \frac{\left[G_{\mathrm{free}}\right] \cdot \left[R_{\mathrm{free}}\right]}{\left[Complex\right]} \quad \text{-(5-31)}$$

The $[G_{\mathrm{free}}]$ and $[R_{\mathrm{free}}]$ were calculated following equations

$$\left[G_{\mathrm{free}}\right] = \left[C_{\mathrm{G,corr}}\right] - \left[C_{\mathrm{C,corr}}\right] \quad \text{-(5-32)}$$

$$\left[R_{\mathrm{free}}\right] = \left[C_{\mathrm{R,corr}}\right] - \left[C_{\mathrm{C,corr}}\right] \quad \text{-(5-33)}$$

$$\left[Complex\right] = \left[C_{\mathrm{C,corr}}\right] \quad \text{-(5-34)}$$

The concentrations of the unbound EGFP or Alexa647-labeled GRE, $[G_{\mathrm{free}}]$ or $[R_{\mathrm{free}}]$ were

calculated by the subtraction of the concentration of the complex [*Complex*] from the total concentration of the EGFP or Alexa647-GRE, [$C_{G,\mathrm{corr}}$] or [$C_{R,\mathrm{corr}}$].

5.3 Results

5.3.1 The relationship between for homodimer of GR and transcriptional activity

EGFP, EGFP-fused GR_{WT} or GR_{A458T} (A458T: Homodimerization deficient mutant) were transiently expressed in U2OS cells. EGFP-GR_{WT} and EGFP-GR_{A458T} localized in nucleus with Dex, but not EGFP and EGFP-GR_{WT} without Dex treatment (Fig. 5-4). To quantify the transcriptional activity, GRE responsive fluorescent reporter plasmid and TagRFP675 as a transfection control were co-transfected with EGFP and EGFP-GRs into U2OS cells. The fluorescent intensity of mKO2 was detected in case of WT and A458T with Dex (Fig. 5-4). Triple-color FCS measurements were performed after 90 min cell lysis and the autocorrelation functions and fit residuals of mKO2, TagRFP675 and EGFP or EGFP-GRs with and without Dex were shown in Fig. 5-5. To determine the relationship between the homodimer of GR and transcriptional activity, the concentration of homodimeric EGFP-GR, mKO2 and TagRFP675 was measured from same single cells expressing the different concentration of EGFP-GR_{WT} and EGFP-GR_{A458T}. The scatter plot of transcriptional activity against the concentration of homodimeric EGFP-GR was shown in Fig. 5-6. EGFP-GR_{WT} without Dex shows low and constant transcriptional activity in the whole range of concentration of homodimeric EGFP-GR. In contrast, EGFP-GR_{WT} and EGFP-GR_{A458T} with Dex show the increase of transcriptional activity with the increase of concentration of homodimeric EGFP-GR. To obtain the correlation value of linear relationship, linear fitting was performed. The correlation value of WT and A458T with Dex was 0.59 and 0.6, while WT without Dex was -0.23. These results indicated that there are positive relationship between the concentration of homodimeric EGFP-GR and transcriptional activity in the

presence of Dex for WT and A458T. These results also suggested that the homodimeric EGFP-GR activated Dex is important to regulate the transcription activity.

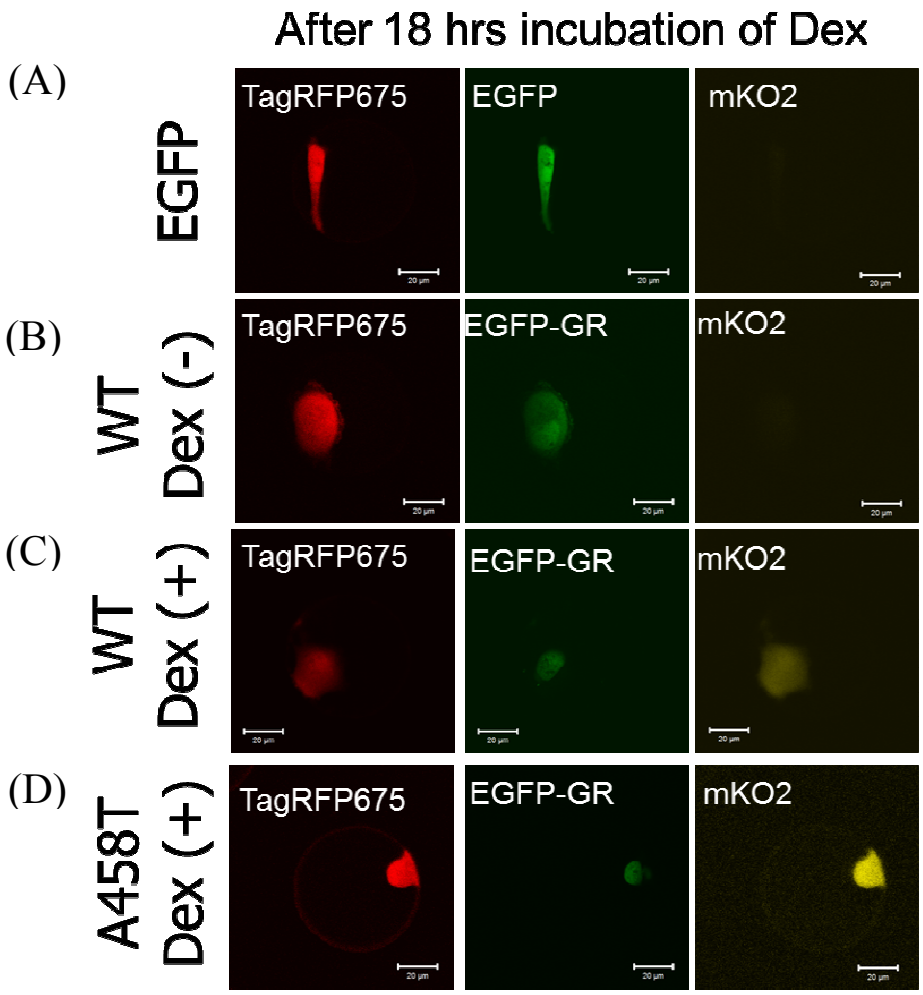

Fig. 5-4 Comparison of expression of mKO2

Typical images of EGFP-GR, mKO2 and TagRFP675 after 18 hours activation of Dex. **(A)** EGFP without Dex. **(B)** EGFP-GR_{WT} without Dex. **(C)** EGFP-GR_{WT} with Dex. **(D)** EGFP-GR_{A458T} with Dex. Scale bar: 20 μm.

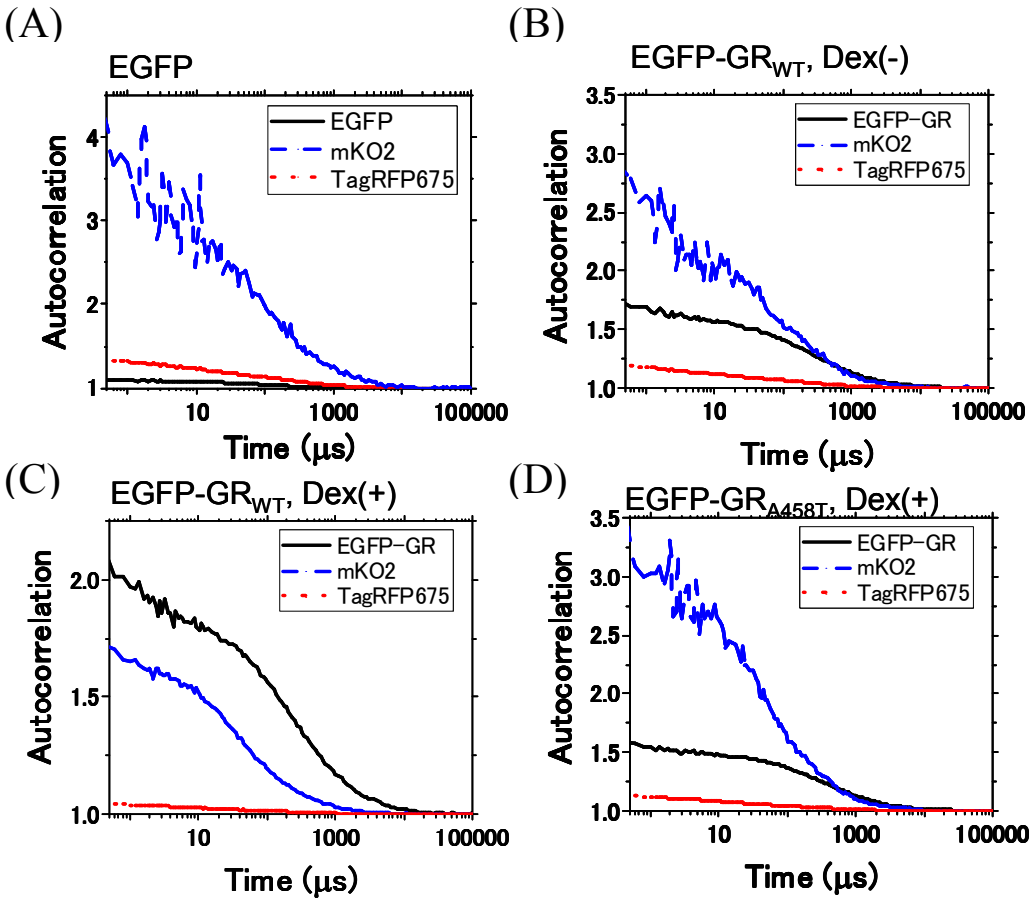

Fig. 5-5 Triple-color FCS measurements for homodimerization of GR and transcriptional activity

Typical autocorrelation functions of mKO2 and TagRFP675 in EGFP or EGFP-GRs. **(A)** EGFP, **(B)** EGFP-GR$_{WT}$ without Dex. **(C)** EGFP-GR$_{WT}$ with Dex. **(D)** EGFP-GR$_{A458T}$ with Dex. Black solid line: autocorrelation function of EGFP or EGFP-GRs, Blue dashed line: autocorrelation function of mKO2, Red dotted line: autocorrelation function of TagRFP675.

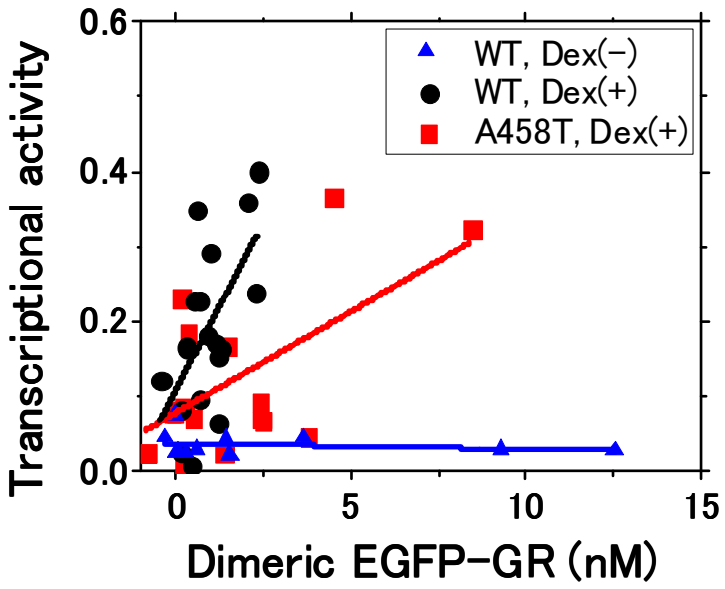

Fig. 5-6 Relationship between the concentration of homodimeric EGFP-GR and transcriptional activity

The scatter plot of transcriptional activity against the concentration of homodimeric EGFP-GR. The linear fitting revealed the correlation value of 0.59, 0.6 and -0.23 for WT with Dex, A458T with Dex and WT without Dex. Black circle: WT with Dex, Red square: A458T with Dex, Blue triangle: WT without Dex. Black line: Linear fitting for WT with Dex, Red line: Linear fitting for A458T with Dex, Blue line: Linear fitting for WT without Dex.

5.3.2 Comparison of DNA binding affinity between WT and homodimerization deficient mutant

The positive relationship between the concentration of homodimeric EGFP-GR and transcriptional activity was observed in the presence of Dex, but not in the absence of Dex (Fig. 5-6). However, the slope of linear fitting was different between WT and A458T in the presence of Dex (Fig. 5-6). To address this difference, DNA-binding affinity was compared with WT and A458T. The mixture of EGFP-GR lysate and Alexa647-labeled GRE (Alexa647-GRE) solution was measured by FCCS to determine the dissociation constant for

DNA binding. The perfect palindrome GRE (PpGRE), imperfect palindrome GRE in MMTV (IpGRE) and half GRE in MMTV (hGRE) were used. Typical auto- and cross-correlation functions for PpGRE, IpGRE and hGRE was shown in Fig. 5-7, 5-8 and 5-9. The cross-correlation functions were normalized by Alexa647-GRE to compare the cross-correlation functions between EGFP, EGFP-GR_{WT}, EGFP-GR_{A458T}. The cross-correlation functions between Alexa647-GRE and EGFP-GR_{WT} or EGFP-GR_{A458T} were observed in PpGRE, IpGRE and hGRE, compared with EGFP (Fig. 5-10). These indicated that EGFP-GR_{WT} and EGFP-GR_{A458T} interact with Alexa647-GRE. The dissociation constants for DNA binding of GR_{WT} and GR_{A458T} were determined using a scatter plot and linear least-squares fitting in PpGRE, IpGRE and hGRE, respectively (Fig. 5-11). For IpGRE and hGRE, the similar dissociation constants were determined between WT and A458T (IpGRE: WT (K_d: 2253±160 nM), A458T (K_d: 2115±12.5 nM) and hGRE: WT (K_d: 1286±156 nM), A458T (K_d: 1299±79.9 nM)). However, a difference of dissociation constant was observed in PpGRE (WT (K_d: 196±25.1 nM), A458T (K_d: 309±8.86 nM)). Moreover, the scatter plot of WT in PpGRE was not linear relationship. This suggested that GR_{WT} binds to perfect palindrome GRE by different mechanism from A458T and WT in IpGRE and hGRE.

To show the difference of DNA binding between WT and A458T, the dissociation constants were determined from single data point (Fig. 5-12). The apparent dissociation constant of WT increased and reached a similar value of A458T with the increase of relative concentration of PpGRE or IpGRE. In contrast, the apparent dissociation constant of A458T was similar value with the increase of the relative concentration of PpGRE or IpGRE (Fig. 5-12 A and B). This may suggest that the increase of apparent dissociation constant for DNA binding is dependent on homodimerization of GR. To reveal the relationship between DNA binding and homodimerization of GR, the apparent dissociation constants of WT and A458T was compared in hGRE. For hGRE, the increase of apparent dissociation constant of WT was not observed and the apparent dissociation constant of WT was similar value to that of A458T.

These results indicated that WT have two pathways to bind to palindrome GRE as monomer and homodimer in which homodimer bound to GRE with relatively higher affinity than monomer of GR.

This concluded that apparent dissociation constant of WT for DNA binding is at least stronger than that of A458T mutant, because the apparent dissociation constant of WT was low compared with that of A458T in low relative concentration of GRE and similar to that of A458T in high relative concentration of GRE. Therefore, the difference of slope in Fig. 5-6, at least, was originated from the difference of DNA binding affinity between WT and A458T.

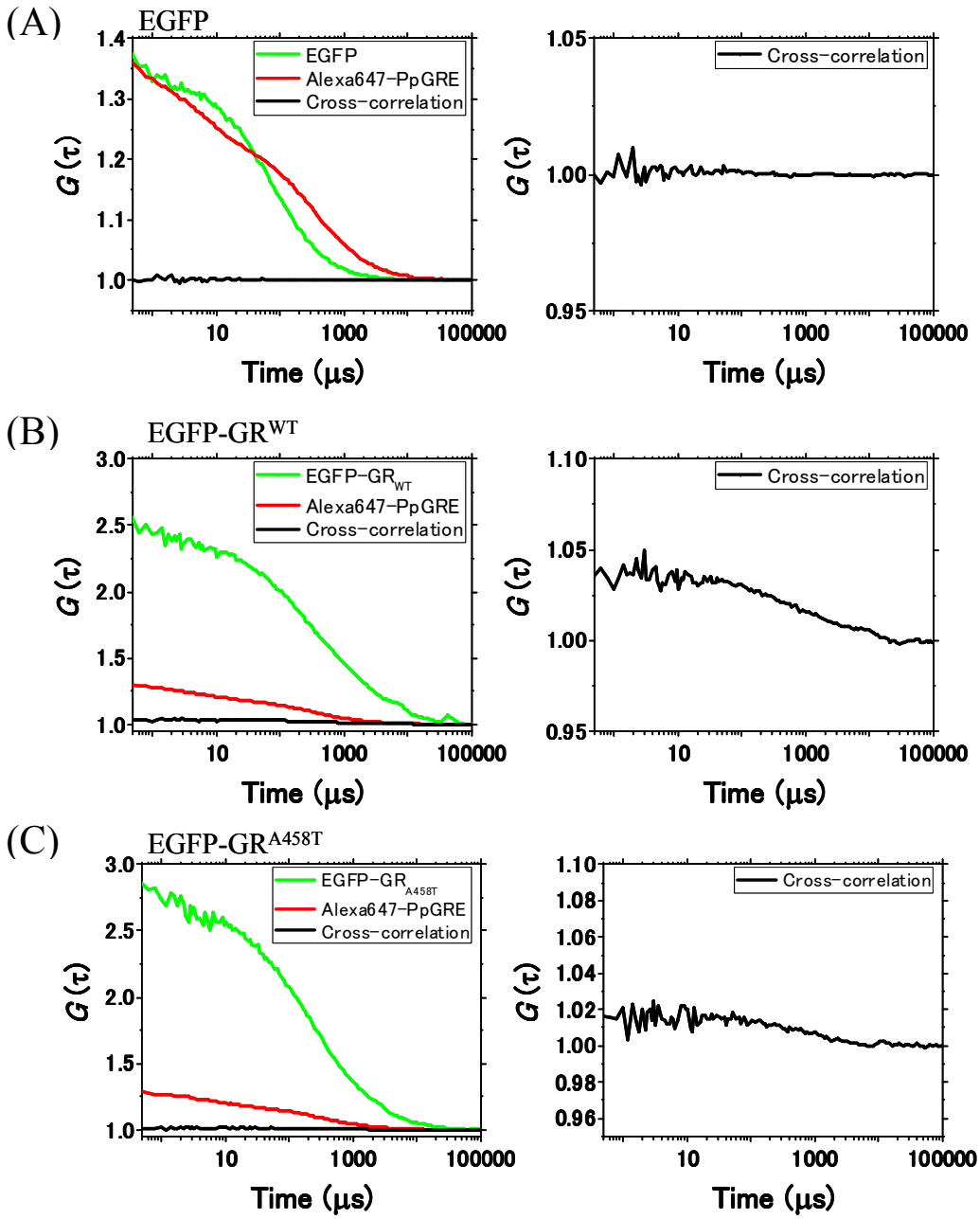

Fig. 5-7 Typical auto- and cross-correlation functions of EGFP, EGFP-GR$_{WT}$ and EGFP-GR$_{A458T}$ for DNA-binding to perfect palindrome GRE (PpGRE)

The mixture of EGFP or EGFP-GRs with PpGRE was measured using FCCS. Green solid line: Autocorrelation function of EGFP or EGFP-GRs, Red solid line: Autocorrelation function of Alexa647-PpGRE, Black solid line: Cross-correlation function between EGFP or EGFP-GRs and Alexa647-PpGRE. The light graphs show the enlarged cross-correlation functions. **(A)** EGFP. **(B)** EGFP-GR$_{WT}$. **(C)** EGFP-GR$_{A458T}$.

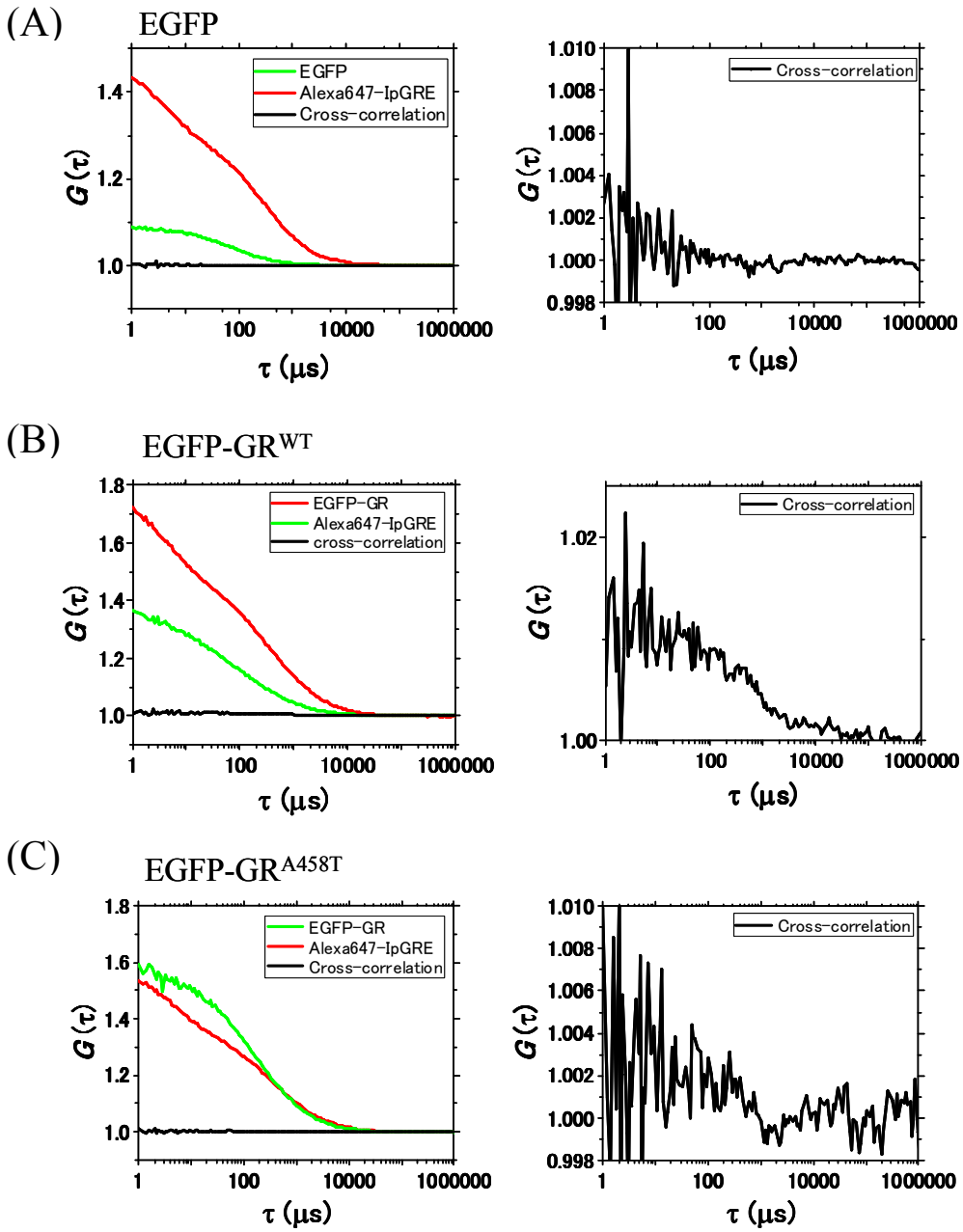

Fig. 5-8 Typical auto- and cross-correlation functions of EGFP, EGFP-GR$_{WT}$ and EGFP-GR$_{A458T}$ for DNA-binding to imperfect palindrome GRE (IpGRE)

The mixture of EGFP or EGFP-GRs with IpGRE was measured using FCCS. Green solid line: Autocorrelation function of EGFP or EGFP-GRs, Red solid line: Autocorrelation function of Alexa647-IpGRE, Black solid line: Cross-correlation function between EGFP or EGFP-GRs and Alexa647-IpGRE. The light graphs show the enlarged one for cross-correlation functions. **(A)** EGFP. **(B)** EGFP-GR$_{WT}$. **(C)** EGFP-GR$_{A458T}$.

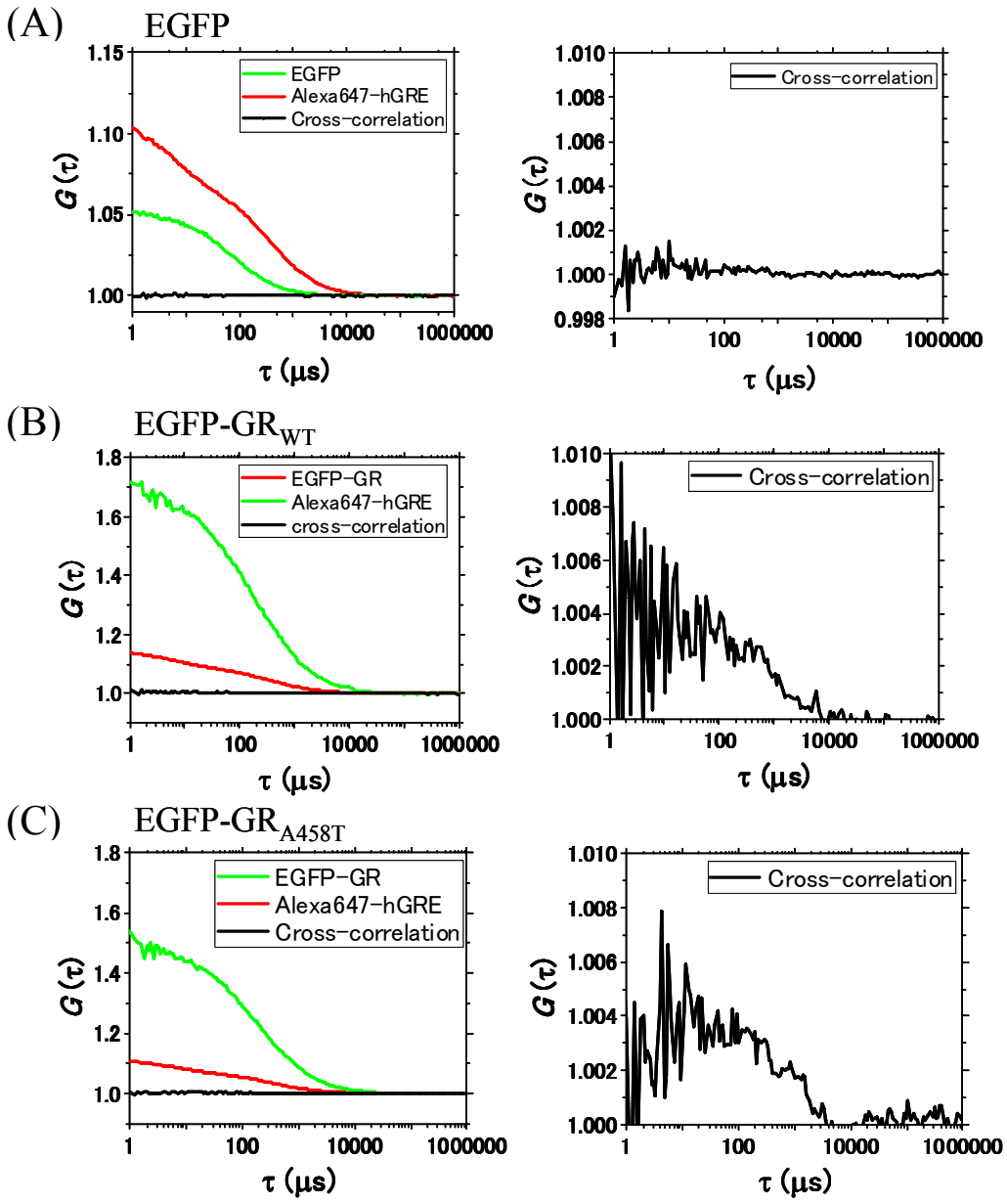

Fig. 5-9 Typical auto- and cross-correlation functions of EGFP, EGFP-GR$_{WT}$ and EGFP-GR$_{A458T}$ for DNA-binding to half GRE (hGRE)

The mixture of EGFP or EGFP-GRs with hGRE was measured using FCCS. Green solid line: Autocorrelation function of EGFP or EGFP-GRs, Red solid line: Autocorrelation function of Alexa647-hGRE, Black solid line: Cross-correlation function between EGFP or EGFP-GRs and Alexa647-hGRE. The light graphs show the enlarged one for cross-correlation functions. **(A)** EGFP. **(B)** EGFP-GR$_{WT}$. **(C)** EGFP-GR$_{A458T}$.

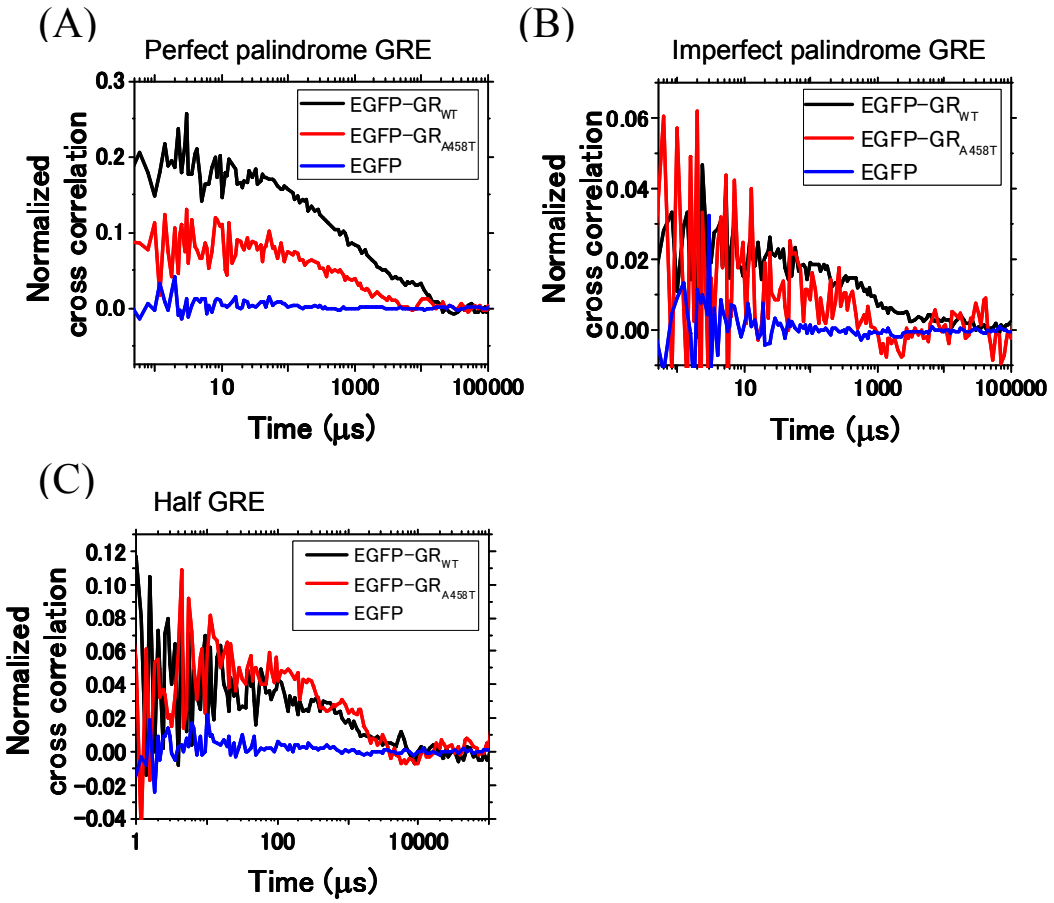

Fig. 5-10 Comparison of normalized cross-correlation functions between EGFP, EGFP-GR$_{WT}$ and EGFP-GR$_{A458T}$

The cross-correlation functions were normalized by the number of molecules of Alexa647-GRE to compare the cross-correlation functions between EGFP, EGFP-GR$_{WT}$ and EGFP-GR$_{A458T}$. Blue solid line: Normalized cross-correlation function of EGFP, Black solid line: Normalized cross-correlation function of EGFP-GR$_{WT}$, Red solid line: Normalized cross-correlation function of EGFP-GR$_{A458T}$. **(A)** Perfect palindrome GRE (PpGRE). **(B)** Imperfect palindrome GRE (IpGRE). **(C)** Half GRE (hGRE).

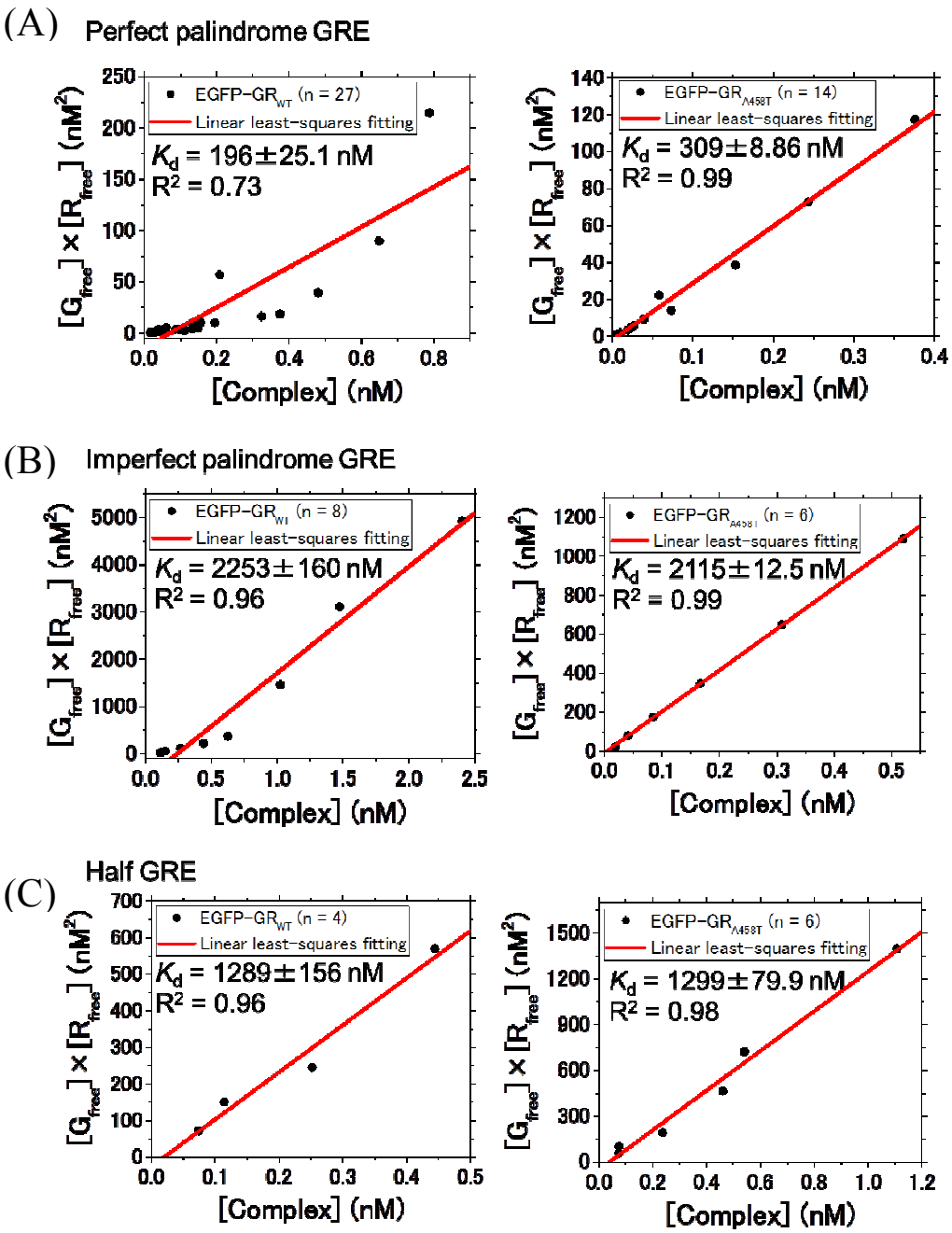

Fig. 5-11 Determination of dissociation constant for DNA binding of GR

The dissociation constant determined using scatter plot and linear fitting. The plots represent the product of concentration of the free EGFP-GR and Alexa647-GRE against the concentration of the complex of EGFP-GR and Alexa647-GRE. The solid red line shows the linear fitting. The slope indicates the dissociation constant for DNA-binding of GR. Left and light graphs show the EGFP-GR$_{WT}$ and EGFP-GR$_{A458T}$, respectively. **(A)** Perfect palindrome

GRE: WT (K_d: 196±25.1 nM), A458T (K_d: 309±8.86 nM). **(B)** Imperfect palindrome GRE: WT (K_d: 2253±160 nM), A458T (K_d: 2115±12.5 nM). **(C)** Half palindrome GRE: WT (K_d: 1286±156 nM), A458T (K_d: 1299±79.9 nM).

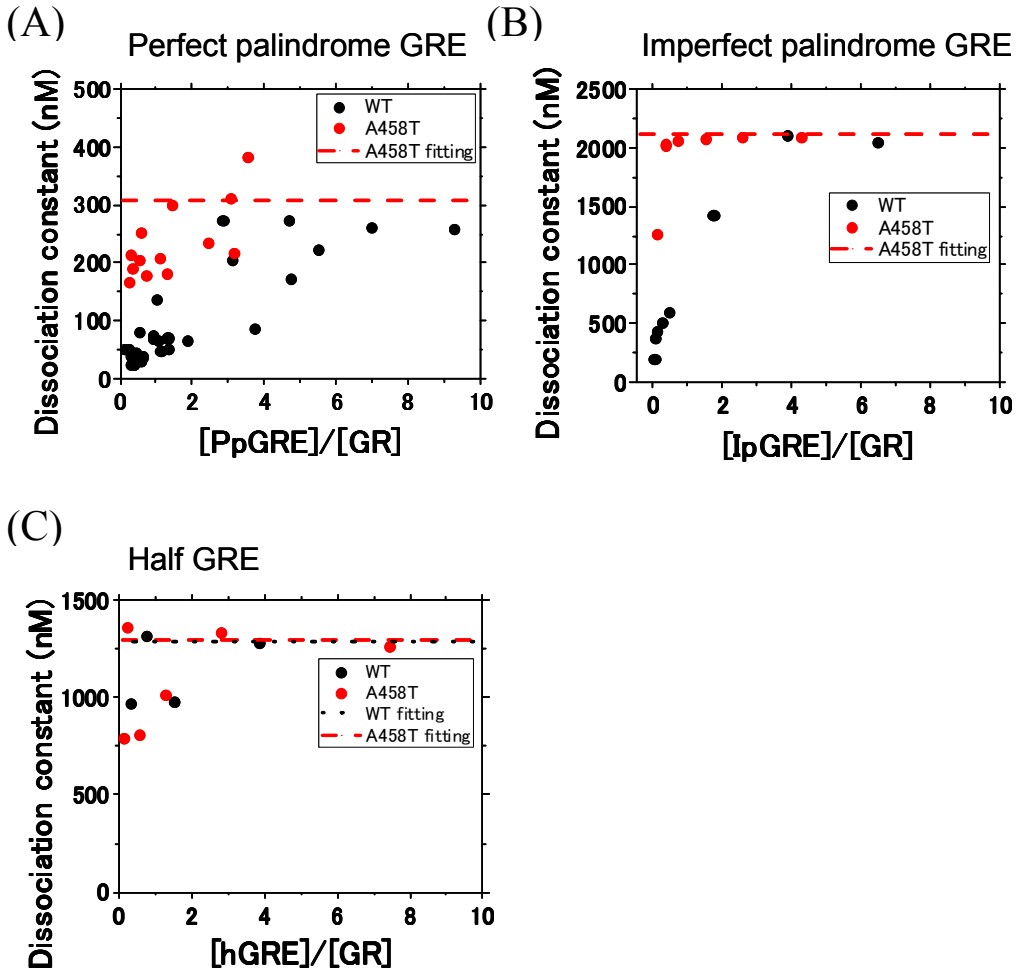

Fig. 5-12 Comparison of the dissociation constant for DNA binding of EGFP-GR between WT and A458T from single data

The apparent dissociation constant for DNA binding of GR was calculated from single data in Perfect palindrome GRE (PpGRE), Imperfect palindrome GRE (IpGRE) and Half GRE (hGRE). Black filled circle: EGFP-GR_{WT}, Red filled circle: EGFP-GR_{A458T}. **(A)** PpGRE. Red dashed line: Fitting result of A458T in Fig. 5-11 A. **(B)** IpGRE. Red dashed line: Fitting result of A458T in Fig. 5-11 B. **(C)** hGRE. Black dotted line: Fitting result of WT, Red dashed line: Fitting result of A458T in Fig. 5-11 C.

5.4 Discussion

The dissociation constant for homodimerization of EGFP-GR with and without Dex was determined using FCS-microwell system in the chapter 3 and 4. In this chapter, FCS-microwell system combined with fluorescent reporter assay was constructed to determine the homodimeric EGFP-GR and transcriptional activity in single-cell level. The fluorescent report plasmid was transfected with EGFP-GR_{WT} or EGFP-GR_{A458T} into U2OS cells which have no endogenous expression of GR. To quantify the concentration of EGFP-GR, mKO2 for transcriptional activity and TagRFP675 as transfection control, triple-color FCS measurements of EGFP-GR, mKO2 and TagRFP675 were carried out. For multi-color imaging and FCS measurements, there are serious problem of cross-talk signal of detectors. However, this set of fluorescent proteins and FCS measurement method had low cross-talk signal into each detector (Table. 5-1). This method will be effective to multi-color imaging and FCS measurement.

In this chapter, FCS-microwell system combined with triple-color FCS revealed the positive relationship between the concentration of homodimeric GR and transcriptional activity in the presence of Dex, but not in the absence of Dex (Fig. 5-6). The homodimerization of GR induced by Dex may be important for transcriptional activity of target genes. Recently, it was suggested that the ratio of monomers and dimers of GR does not necessarily change the transcriptional activity determined by comparison of Number and Brightness analysis in living cells and quantitative real-time PCR using a whole cell lysate [18]. This may be caused by average process between cells in bulk measurements, such as quantitative real-time PCR. Therefore, our results indicate that single-cell measurement is effective to understand the relationship between homodimer of GR and transcriptional activity.

The Pearson's correlation value was 0.59 and 0.6 in WT and A458T, respectively. These values show the moderate positive relationship between the concentration of homodimeric

EGFP-GR and transcriptional activity for WT and A458T. The phosphorylation of Serine 203 and 211 increased GR transcriptional activity [57-61]. Moreover, the phosphorylated GR interacts with coregulator such as GRIP1, MED14 for regulation of transcriptional activity [61-63]. The moderate positive relationship may be caused by the difference of expression level of cofactor and degree of phosphorylation of GR between single cells.

Moreover, the slope of linear fitting for WT was larger than that of A458T (Fig. 5-6). This means that the transcriptional activity of A458T is lower than that of WT in same concentration of homodimeric GR. The apparent dissociation constant for DNA binding of GR_{WT} was at least lower than that of GR_{A458T} (Fig. 5-12). This indicated that the low transcriptional activity of A458T was caused by the low DNA binding affinity of A458T compared with WT.

The apparent dissociation constant increased and reached to similar value of GR_{A458T} with the increase of relative concentration of Alexa647-GRE with EGFP-GR_{WT} in perfect palindrome GRE (PpGRE) and imperfect palindrome GRE (IpGRE), but not half GRE (hGRE). There may be DNA binding mechanism of monomeric and homodimeric GR_{WT} to PpGRE and IpGRE. It was reported that DNA binding affinity of homodimeric GR_{WT} was stronger than that of monomeric GR_{WT} [17]. Therefore, the homodimeric GR_{WT} preferentially binds to PpGRE and IpGRE in low relative concentration of GRE with GR. In contrast, monomeric GR_{WT} preferentially binds to PpGRE and IpGRE in high relative concentration of GRE with GR.

It this thesis, FCS-microwell system determined the concentration of homodimeric EGFP-GR in microwell and the relationship between this concentration and transcriptional activity. Therefore, homodimerization of GR may be different between in microwell and in single-living cell. In the future, the homodimerization of GR should be determined in living cell to address the relationship between homodimerization of GR in microwell and in single-living cell.

Chapter 6

Concluding Remarks

In this thesis, the measurement system combined with fluorescence correlation spectroscopy (FCS) and microwells (FCS-microwell system) was constructed and the dissociation constant for homodimerization of GR and the relationship between homodimer of GR and transcriptional activity were studied using FCS-microwell system. FCS quantifies the concentration of fluorescent molecules. The microwell system provides a stable condition to isolate single cell. Therefore, the FCS-microwell system can determine the concentration of fluorescent molecules from single cell.

In chapter 2, the feasibility of FCS-microwell system toward single-cell measurements was described. As a result, FCS-microwell system can quantify the concentration of EGFP-fused functional proteins in the range from 0.17 nM to 1741 nM in microwell (6.4 nM to 65.6 μM in the cell).

In chapter 3 and 4, EGFP-fused glucocorticoid receptor (EGFP-GR) was transiently transfected into HeLa cells or U2OS cells to determine the dissociation constant for homodimerization of GR using FCS-microwell system. The dissociation constant for homodimerization of WT in the presence of Dex was lower than that of WT in the absence of Dex, indicating that Dex induces the homodimerization of GR. Similar dissociation constant of WT in the presence of Dex was determined between different cell lines, HeLa cell and U2OS cell. This means that the endogenous GR have low effect to homodimerization of EGFP-GR in HeLa cell. Moreover it have been suggested that the homodimerization of GR

occurs following DNA binding, but not prior to DNA binding. In this thesis, DNA binding deficient mutant in the presence of Dex shows the lower dissociation constant for homodimerization of GR than that of WT in the absence of Dex, indicating that the homodimerization of GR also occurs prior to DNA binding. The homodimerization deficient mutant shows the similar dissociation constant to WT in the absence of Dex. These results concluded that FCS-microwell system successfully determine the concentration of homodimeric GR and dissociation constant for homodimerization of GR. Moreover, the diffusion constant analysis suggests that EGFP-GR forms not only homodimer but also large complex with endogenous interacting proteins.

In chapter 5, FCS-microwell system with triple-color FCS measurements revealed the positive relationship between the concentration of homodimeric GR and transcriptional activity in the presence of Dex, but not in the absence of Dex. This indicates that the homodimerization induced by Dex was essential process for transcriptional activity. It have been identified that monomeric GR have functions for transrepression. In the future, FCS-microwell system combined with fluorescent reporter assay for transrepression could determine the relationship between the concentration of monomeric GR and transrepression to understand for transrepression mechanisms of GR.

FCS is a powerful tool to determine the dynamics and interaction of biomolecules *in vitro* and *in vivo* system. The FCS-microwell system is simple method to determine the absolute number of molecules of fluorescent protein fused functional proteins in single cell. FCS-microwell system should be shed new light to single-cell biology and nuclear receptor.

References

[1] Kadmiel M. and Cidlowski J. A., Glucocorticoid Receptor Signaling in Health and Disease, Trends Pharmacol. Sci., 34, 518-530 (2013).

[2] Cain D. W. and Cidlowski J. A., Specificity and sensitivity of glucocorticoid signaling in health and disease, Best Pract. Res. Clin. Endocrinol. Metab., 29, 545-556 (2015).

[3] Kumar R., Volk D. E., Li J., Gorenstein D. G., Thompson E. B., TATA box binding protein induces structure in the recombinant glucocorticoid receptor AF1 domain, Proc. Natl. Acad. USA, 101, 16425-16430 (2004).

[4] Kumar R. and Thompson E. B., Gene regulation by the glucocorticoid receptor: structure: function relationship, J. Steroid Biochem. Mol. Biol., 94, 383-394 (2005).

[5] Revollo J. R. and Cidlowski J. A., Mechanisms generating diversity in glucocorticoid receptor signaling., Ann. NY Acad. Sci., 1179, 167-178 (2009).

[6] Cheung J. and Smith D. F., Molecular chaperone interactions with steroid receptors: an update, Mol. Endocrinol., 14, 939-946 (2000).

[7] Morishima Y., Kanelakis K. C., Murphy P. J. M., Lowe E. R., Jenkins G. J., Osawa Y., Sunahara R. K. and Pratt W. B., The Hsp90 Cochaperone p23 is the Limiting Component of the Multiprotein Hsp90/Hsp70-based Chaperone System *in Vivo* Where it Acts to Stabilize the Client Protein-Hsp90 Complex., J. Biol. Chem., 278, 48754-48763 (2003).

[8] Heitzer M. D., Wolf I. M., Sanchez E. R., Witchel S. F. and Defranco D. B., Glucocorticoid receptor physiology, Rev. Endocr. Metab. Disord., 8, 321-330 (2007).

[9] Vandevyver S., Dejager L. and Libert C., on the trail of the glucocorticoid receptor: into the nucleus and back., Traffic, 13, 364-374 (2012).

[10] McNally J. G., Muller W. G., Walker D., Wolford R. and Hager G. L., The glucocorticoid receptor: Rapid exchange with regulatory sites in living cells, Science, 287, 1262-1265 (2000).

[11] De Bosscher K. and Haegeman G., Minireview: Latest perspectives on Antiinflammatory Actions of Glucocorticoids, Mol. Endocrinol., 23, 281-291 (2009).

[12] Silverman M. N., Mukhopadhyay P., Belyavskaya E., Tonelli L. H., Revenis B. D., Doran J. H., Ballard B. E., Tam J., Pacher P. and Sternberg E. M., Glucocorticoid receptor dimerization is required for proper recovery of LPS-induced inflammation, sickness behavior and metabolism in mice, Mol. Psychiatry, 18, 1006-1017 (2013).

[13] Surjit M., Ganti K. P., Mukherji A., Ye T., Hua G., Metzger D., Li M. and Chambon P., Widespread Negative Response Elements Mediate Direct Repression by Agonist-Liganded Glucocorticoid Receptor, Cell, 145, 224-241 (2011).

[14] Bain D. L., Yang Q., Connaghan K. D., Robblee, J. P., Miura M. T., Degala G. D., Lambert J. R. and Maluf N. K. J., Glucocorticoid Receptor–DNA Interactions: Binding Energetics Are the Primary Determinant of Sequence-Specific Transcriptional Activity, Mol. Biol., 422, 18-32 (2012).

[15] Kassel O. and Herrlich P., Crosstalk between the glucocorticoid receptor and other transcription factors: Molecular aspects, Mol. Cell Endocrinol., 275, 13-29 (2007).

[16] Luisi B. F., Xu W. X., Otwinowski Z., Freedman L. P., Yamamoto K. R. and Sigler P. B. Crystallographic Analysis of the Interaction of the Glucocorticoid Receptor with DNA, Nature, 352, 497-505 (1991).

[17] Drouin J., Sun Y. L., Tremblay S., Lavender P., Schmidt T. J., de Lean A. and Nemert M., Homodimer Formation Is Rate-Limiting for High Affinity DNA Binding by Glucocorticoid Receptor, Mol. Endocrinol., 6, 1299-1309 (1992).

[18] Presman D M., Ogara M. F., Stortz M., Alvarez L. D., Pooley J. R., Schiltz R. L., Grøntved L., Johnson T. A., Mittelstadt P. R., Ashwell J. D., Ganesan S., Burton G., Levi V., Hager G. L. and Pecci A., Live Cell Imaging Unveils Multiple Domain Requirements for *In Vivo* Dimerization of the Glucocorticoid Receptor, PLOS Biol., 12, e1001813 (2014).

[19] Kinjo M., Sakata H. and Mikuni S., First Steps for Fluorescence Correlation Spectroscopy of Living Cells, Live Cell Imaging-A Laboratory Manual, (Goldman R., Swedlow J. and Spector D., eds.) 229-238, Cold Spring Harbor Press (2010).

[20] Ries J. and Schwille P., Fluorescence Correlation Spectroscopy, Bioassays, 34, 361-368 (2012)

[21] Kinjo M.,Detection of asymmetric PCR products in homogenous solution by fluorescence correlation spectroscopy, Biotechniques, 25, 706-712, 714-715 (1998).

[22] Mikuni S., Tamura M. and Kinjo M., Analysis of Intranuclear Binding Process of Glucocorticoid Receptor using Fluorescence Correlation Spectroscopy, FEBS Lett., 581, 389-393 (2007).

[23] Vukojević V., Papadopoulos D. K., Terenius L., Gehring W. J. and Rigler R., Quantitative Study of Synthetic Hox Transcription Factor-DNA Interactions in Live Cells, Proc. Natl. Acad. Sci. USA, 107, 4093-4098 (2010).

[24] Oasa S., Sasaki A., Yamamoto J., Mikuni S. and Kinjo M., Homodimerization of glucocorticoid receptor from single cells investigated using fluorescence correlation spectroscopy and microwells, FEBS Lett., 589, 2171-2178 (2015).

[25] Sasaki A., Sakata H. and Kinjo M., Single-cell Quantitative Analysis of DNA Incorporation and Protein Expression in Microwells, Curr. Pharm. Biotech., 11, 117-121 (2011).

[26] Bacia K., Kim S. A. and Schwille P., Fluorescence cross-correlation spectroscopy in living cells, Nature Methods, 3, 83-89 (2006).

[27] Sun F., Mikuni S. and Kinjo M., Monitoring the caspase cascade in single apoptotic cells using a three-color fluorescent protein substrate, Biochem. Biophys. Res. Commun., 404, 706-710 (2011).

[28] Mikuni S., Kodama K., Kohira N., Maki H., Munetomo M., Maenaka K. and Kinjo M., Screening for FtsZ Dimerization Inhibitors Using Fluorescence Cross-Correlation Spectroscopy and Surface Resonance Plasmon Analysis, PLOS One, 10, e130933 (2015).

[29] Tiwari M., Mikuni S., Muto H. and Kinjo M., Determination of dissociation constant of the NFκB p50/p65 heterodimer using fluorescence cross-correlation spectroscopy in the living cell, Biochem. Biophys. Res. Commun., 436, 430-435 (2013).

[30] Foo Y. H., Naredi-Rainer N., Lamb D. C., Ahmed S. and Wholand T., Factors affecting the quantification of biomolecular interactions by fluorescence crosscorrelation spectroscopy, Biophys J., 102, 1174-1183 (2012).

[31] Müller C. B., Loman A., Pacheco V., Koberling F., Willbold D., Richtering W. and Enderlein J., Precise Measurement of Diffusion by Multi-color Dual-focus Fluorescence Correlation Spectroscopy, Europhys. Lett., 83, 460001 (2008).

[32] Thompson, N. L., Fluorescence Correlation Spectroscopy, in Topics in Fluorescence Spectroscopy, vol. 1. (Lakowicz, J. R., ed.), Plenum Press, New York, NY, 337-378 (1991).

[33] Glauner H., Ruttekolk I. R., Hansen K., Steemers B., Chung Y. D., Becker F., Hannus S. and Brock R., Simultaneous Detection of Intracellular Target and Off-target Binding of Small Molecule Cancer Drugs at Nanomolar Concentrations, Br. J. Pharmacol., 160, 958-970 (2010).

[34] Segard-Manurel I., Rajkowski K., Jibard N., Schweizer-Groyer G., Baulieu E. E. and Cadepond F., Glucocorticosteroid Receptor Dimerization Investigated by Analysis of Receptor Binding to Glucocorticosteroid Responsive Elements Using a Monomer-Dimer Equilibrium Model, Biochemistry, 35, 1634-1642 (1996).

[35] Robblee J. P., Miura M. T. and Bain D. L., Glucocorticoid Receptor-Promoter Interactions: Energetic Dissection Suggests a Framework for Specificity of Steroid Receptor-Mediated Gene Regulation, Biochemistry, 51, 4463-4472 (2012).

[36] Mikuni S., Pack C., Tamura M. and Kinjo M., Diffusion Analysis of Glucocorticoid Receptor and Antagonist Effect in Living Cell Nucleus, Exp. and Mol. Path., 82, 163-168 (2007).

[37] Pack C., Saito K., Tamura M. and Kinjo M., Microenvironment and effect of energy depletion in the nucleus analyzed by mobility of multiple oligomeric EGFPs, Biophys. J., 91, 3921-3936 (2006).

[38] Chen Y., Wei L. N. and Mùller J. D., Probing Protein Oligomerization in Living Cells with Fluorescence Fluctuation Spectroscopy, Proc. Natl. Acad. Sci. USA, 100, 15492-15497 (2003).

[39] Robertson S., Rohwer J. M., Hapgood J. P. and Louw A., Impact of Glucocorticoid Receptor Density on Ligand-Independent Dimerization, Cooperative Ligand-Binding and Basal Priming of Transactivation: A Cell Culture Model, PLOS One, 8, e64831 (2013).

[40] Driver P. M., Kilby M. D., Bujalska I., Walker E. A., Hewison M. and Stewart P. M., Expression of 11β-Hydroxysteroid Dehydrogenase Isozymes and Corticosteroid Hormone Receptors in Primary Cultures of Human Trophoblast and Placental Bed Biopsies, Mol. Hum. Reprod., 7, 357-363 (2001).

[41] McEwan I., Wright A. P. H. and Gustafsson J. A., Mechanism of Gene Expression by the Glucocorticoid Receptor: Role of Protein-Protein Interactions, Bioessays, 19, 153-160 (1996).

[42] Tsai S. Y., Carlstedt-Duke J., Weigel N. L., Dahlman K., Gustafsson J. A., Tsai M. J. and O'Malley B. W., Molecular-interactions of steroid-hormone receptor with its enhancer element-evidence for receptor dimer formation, Cell, 55, 361-369 (1988).

[43] Kim B. and Little J. W., Dimerization of a specific DNA-binding protein on the DNA, Science, 255, 203-206 (1992).

[44] Kohler J. J., Metallo S. J., Schneider T. L. and Schepartz A., DNA specificity enhanced by sequential binding of protein monomers, Proc. Natl. Acad. Sci. USA, 96, 11735-11739 (1999).

[45] Presman D. M., Alvarez L. D., Levi V., Eduardo S., Digman M. A., Marti M. A., Veleiro A. S., Burton G. and Pecci A., Insights on glucocorticoid receptor activity modulation through the biding of rigid steroids, PLOS One, 5, e13279 (2010).

[46] Wrange O., Eriksson P. and Perlmann T., The purified activated glucocorticoid receptor is a homodimer, J. Biol. Chem., 264, 5253-5259 (1989).

[47] Cairns W., Cairns C., pongratz I., Poellinger L. and Okret S., Assembly of a glucocorticoid receptor complex prior to DNA-binding enhances its specific interaction with a glucocorticoid response element, J. Biol. Chem., 266, 11221-11226 (1991).

[48] Robertson S., Allie-Reid F., Vanden Berghe W., Visser K., Binder A., Africander D., Vismer M., De Bosscher K., Hapgood J., Haegeman G. and Louw A., Abrogation of glucocorticoid receptor dimerization correlates with dissociated glucocorticoid behavior of compound A, J. Biol. Chem., 285, 8061-8075 (2010).

[49] Weber P. A., Chang Hou-Chien, Spaeth K. E., Nitsche J. M. and Nicholson B. J., The Permeability of Gap Junction Channels to Probes of Different Size Is Dependent on Connexin Composition and Permeant-Pore Affinities, Biophys. J., 87, 958-973 (2004).

[50] Gorelick D. A. and Halpern M. E., Visualization of Estrogen Receptor Transcriptional Activity in Zebrafish, Endocrinology, 152, 2690-2703 (2011).

[51] Moro E., Ozhan-Kizil G., Mongera A., Beis D., Wierzbicki C., Young R. M., Bournele D., Domenichini A., Valdivia L. E., Lum L., Chen C., Amatruda J. F., Tiso N., Weidinger G. and Argenton F., *In vivo* Wnt signaling tracing through a transgenic biosensor fish reveals novel activity domains, Dev. Biol., 366, 327-340 (2012).

[52] Benato F., Colletti E., Skobo T., Moro E., Colombo L., Argenton F. and Valle L. D., A living biosensor model to dynamically trace glucocorticoid transcriptional activity during development and adult life in zebrafish, Mol. and Cellular Endocrinol., 392, 60-72 (2014).

[53] Varmus H. E., Bishop J. M., Nowinski R. C. and Sarkar N. H., Mammary tumour viru specific nucleotide sequences in mouse DNA, Nature, 238, 189-191 (1972).

[54] Beato M., Gene Regulation by Steroid Hormones, Cell Rev., 56, 335-344 (1989).

[55] Belikov S., Gelius B. and Wrange O., Hormone-induced nucleosome positioning in the MMTV promoter is reversible, EMBO J., 20, 2802-2811 (2001).

[56] Kapusta P., Application Note., Berlin PicoQuant GmbH, Absolute diffusion coefficients: compilation of reference data for FCS calibration, Available at http://www.picoquant.com/technotes/appnote_diffusion_coefficients.pdf.

[57] Krstic M. D., Rogatsky I., Yamamoto K. R. and Garabedian M. J., Mitogen-activated and cyclin-dependent protein kinases selectively and differentially modulate transcriptional enhancement, Mol. Cell Biol., 17, 3947-3954 (1997).

[58] Webster J. C., Jewell C. M., Bodwell J. E., Munck A., Sar M. and Cidlowski J. A., Mouse glucocorticoid receptor phosphyorylation status infuluences multiple functions of the receptor protein, J. Biol. Chem., 272, 9287-9293 (1997).

[59] Miller A. L., Webb M. S., Copik A. J., Wang Y., Johnson B. H., Kumar R. and Thompson E. B., p38 Mitogen-activated protein kinase (MAPK) is a key mediator in glucocorticoid-induced apoptosis of lymphoid cells: correlation between p38 MAPK activation and site-specific phosphrylation of the human glucocorticoid receptor at serine 211, Mol. Endocrinol., 19, 1569-1583 (2005).

[60] Blind R. D. and Garabedian M. J., Differential recruitment of glucocorticoid receptor phosphor-isoforms to glucocorticoid-induced genes, J. Steroid Biochem. Mol. Biol., 109, 150-157 (2008).

[61] Chen W., Dang T., Blind R. D., Wang Z., Cavasotto C. N., Hittelman A. B., Rogatsky I., Logan S. K. and Garabedian M. J., Glucocorticoid receptor phosphorylation differentially affects target gene expression, Mol. Endocrinol., 22, 1754-1766 (2008).

[62] Avenant C., Kotitschke A. and Hapgood J. P., Glucocorticoid receptor phosphorylation modulates transcription efficacy through GRIP-1 recruitment, Biochemistry, 49, 972-985 (2010).

[63] Garza A. M., Khan S. H. and Kumar R., Site-specific phosphorylation induces functionally active conformation in the intrinsically disordered N-terminal activation function (AF-1) domain of the glucocorticoid receptor, Mol. Cell Biol., 30, 220-230 (2010).

Acknowledgements

This thesis would not have been possible without the help and support of colleagues, family and friends.

First, I would like to thank my supervisor Prof. Masataka Kinjo for giving the opportunity to investigate glucocorticoid receptor using FCS-microwell system and providing supports. This work would not have been possible without his guidance and encouragement. Thank you for my scientific development.

My special words of thanks should go to Dr. Akira Sasaki in National Institute of Advanced Industrial Science and Technology (AIST). His valuable advices and supports made possible to construct FCS-microwell system and apply this system to the measurements of glucocorticoid receptor (GR).

I would like to thank Dr. Mikuni Shintaro for the effective support and discussion to all GR measurements. His constant guidance, cooperation, effective advice and support have kept me going ahead. Without his guidance, it was impossible to investigate the relationship between homodimer of GR and transcriptional activity.

I would like to express the gratitude to Dr. Akira Kitamura, Dr. Johtaro Yamamoto for all scientific discussions and valuable comments for all my works. Dr. Akira Kitamura gave me helpful discussions and encouraged me to keep my going ahead in many times. Dr. Johtaro Yamamoto gave me suggestions about data analysis, especially determination of dissociation constant for homodimerization of GR.

No words will suffice to explain the immense help, cooperation and fortitude by current and previous members of the laboratory of Molecular Cell Dynamics.

Finally, I thank my family for the great financial support and kind encouragement.